# nabc/sff

# 1 NAB and libsff

## 1.1 A little history

The NAB language compiler *nab2c* (which converts NAB source code to C, for subsequent compilation) was written in the 1990's by Tom Macke. The original design idea was to create a "molecular awk": a scripting language for manipulation of (macro-)molecules that would be primarily used to create short scripts to carry out molecular manipulations. It was quickly realized that manipulations like force field minimization would be useful, and the Amber-compatible molecular mechanics routines were added by David Case as *sff*, a "simple force field".

Over the years, *sff* evolved to keep pace with (and in many cases drive) Amber developments involving implicit force fields, including generalized Born, Poisson-Boltzmann and RISM approaches. In keeping with its original motivation, *sff* concentrated on implicit solvation, leaving explicit solvent and periodic simulations to the main Amber programs *sander* and *pmemd*. The *sff* routines were parallelized using both openmp and MPI, and second derivatives of the generalized Born model were added by Russ Brown.[1] Apart from the lack of a GPU implementation, the routines in *sff* are the most general and efficient ones in the Amber package. In particular, *sff* excels at generalized Born simulations on large systems, benefitting from an advanced nonbonded list builder, and from the hierarchical charge partition model described in Section 1.6.

As a first step, we have prepared sample files in `$AMBERHOME/AmberTools/test/nabc`, which illustrate how to use most of the *sff* functionality directly from a stand-alone C driver. The *Makefile* in this directory can guide you through running several sample calculations. Looking at the code, and its comments, along with the header file (`$AMBERHOME/include/sff.h`) should go a long way towards allowing direct integration into C codes, without any reference to the NAB compiler. The rest of this chapter has documentation for *libsff*.

## 1.2 Basic molecular mechanics routines

```
int readparm( molecule m, string parmfile );
int mme_init( molecule mol, string aexp, string aexp2, point xyz_ref[], string filename );
int mm_options( string opts );
float mme( point xyz[], point grad[], int iter );
float mme_rattle( point xyz[], point grad[], int iter );
int conjgrad( float x[], int n, float fret, float func(), float rmsgrad,
        float dfpred, int maxiter );
int md( int n, int maxstep, point xyz[], point f[], float v[], float func );
int getxv( string filename, int natom, float start_time, float x[], float v[] );
int putxv( string filename, string title, int natom, float start_time,
        float x[], float v[] );
void mm_set_checkpoint( string filename );
```

readparm reads an AMBER parameter-topology file, created by tleap or with other AMBER programs, and sets up a data structure which we call a "parmstruct". This is part of the molecule, but is not directly accessible (yet) to nab programs. You would use this command as an alternative to getpdb_prm(). You need to be sure that the molecule used in the readparm() call has been created by calling getpdb() with a PDB file that has been created by tleap itself (i.e., that has exactly the Amber atoms in the correct order). As noted above, the readparm() routine is primarily intended for cases where getpdb_prm() fails (i.e., when you need to run *tleap* by hand).

setxyz_from_mol() copies the atomic coordinates of mol to the array xyz. setmol_from_xyz() replaces the atomic coordinates of mol with the contents of xyz. Both return the number of atoms copied with a 0 indicating an error occurred.

The getxv() and putxv() routines read and write non-periodic Amber-style restart files. Velocities are read if present.

The getxyz() and putxyz() routines are used in conjunction with the mm_set_checkpoint() routine to write checkpoint or restart files. The coordinates are written at higher precision than to an AMBER restart file, i.e., with sufficiently high precision to restart even a Newton-Raphson minimization where the error in coordinates may be on the order of$10^{-12}$ . The checkpoint files are written at iteration intervals that are specified by the *nchk* or *nchk2* parameters to the mm_options() routine (see below). The checkpoint file names are determined by the filename string that is passed to mm_set_checkpoint(). If filename contains one or more %d format specifiers, then the file name will be a modification of filename wherein the leftmost %d of filename is replaced by the iteration count. If filename contains no %d format specifier, then the file name will be filename with the iteration count appended on the right.

The mme_init() function must be called after mm_options() and before calls to mme(). It sets up parameters for future force field evaluations, and takes as input an nab molecule. The string aexp is an atom expression that indicates which atoms are to be allowed to move in minimization or dynamics: atoms that do not match aexp will have their positions in the gradient vector set to zero. A NULL atom expression will allow all atoms to move. The second string, aexp2 identifies atoms whose positions are to be restrained to the positions in the array xyz_ref. The strength of this restraint will be given by the wcons variable set in mm_options(). A NULL value for aexp2 will cause all atoms to be constrained. The last parameter to mme_init() is a file name without extension for the output trajectory file. This should be NULL if no output file is desired. NAB writes trajectories in the *netCDF* format, which can be read by *cpptraj*, and either analyzed, or converted to another format. The default netCDF extension of .nc is automatically added to the file name.

mm_options() is used to set parameters, and must be called before mme_init(); if you change options through a call to mm_options() without a subsequent call to mme_init() you may get incorrect calculations with no error messages. Beware. The opts string contains keyword/value pairs of the form keyword=value separated by white space or commas. Allowed values are shown in the following table.

| *keyword* | *default* | *meaning* |
|---|---|---|
| ntpr | 10 | Frequency of printing of the energy and its components. |
| e_debug | 0 | If nonzero printout additional components of the energy. |
| gb_debug | 0 | If nonzero printout information about Born first derivatives. |
| gb2_debug | 0 | If nonzero printout information about Born second derivatives. |
| nchk | 10000 | Frequency of writing checkpoint file during first derivative calculation, i.e., in the mme() routine. |
| nchk2 | 10000 | Frequency of writing checkpoint file during second derivative calculation, i.e., in the mme2() routine. |
| nsnb | 25 | Frequency at which the non-bonded list is updated. |
| nscm | 0 | If > 0, remove translational and rotational center-of-mass (COM) motion after every nscm steps. For Langevin dynamics (gamma_ln>0) without HCP (hcp=0), the position of the COM is reset to zero every nscm steps, but the velocities are not affected. With HCP (hcp>0) COM translation and rotation are also removed, with or without Langevin dynamics. It is strongly recommended that this option be used whenever HCP is used. |
| cut | 8.0 | Non-bonded cutoff, in angstroms. This parameter is ignored if hcp > 0. |
| wcons | 0.0 | Restraint weight for keeping atoms close to their positions in xyz_ref (see *mme_init*). |
| dim | 3 | Number of spatial dimensions; supported values are 3 and 4. |

| *keyword* | *default* | *meaning* |
|---|---|---|
| k4d | 1.0 | Force constant for squeezing out the fourth dimensional coordinate, if dim=4. If this is nonzero, a penalty function will be added to the bounds-violation energy, which is equal to 0.5 * *k4d* * *w* * *w*, where *w* is the value of the fourth dimensional coordinate. |
| dt | 0.001 | Time step, ps. |
| t | 0.0 | Initial time, ps. |
| rattle | 0 | If set to 1, bond lengths will be constrained to their equilibrium values, for dynamics; if set to 2, bonds to hydrogens will be constrained; default is not to include such constraints. Note: if you want to use rattle (effectively "shake") for minimization, you do not need to set this parameter; rather, pass the mme_rattle() function to *conjgrad()*. |
| tautp | 999999. | Temperature coupling parameter, in ps. The time constant determines the strength of the weak-coupling ("Berendsen") temperature bath.[2] Set *tautp* to a very large value (e.g. 9999999.) in order to turn off coupling and revert to Newtonian dynamics. This variable only has an effect if *gamma_ln* remains at its default value of zero; if *gamma_ln* is not zero, Langevin dynamics is assumed, as discussed below. |
| gamma_ln | 0.0 | Collision frequency for Langevin dynamics, in $ps^{-1}$ . Values in the range 2-5$ps^{-1}$ often give acceptable temperature control, while allowing transitions to take place.[3] Values near 50$ps^{-1}$ correspond to the collision frequency for liquid water, and may be useful if rough physical time scales for motion are desired. The so-called BBK integrator is used here.[4] |
| temp0 | 300.0 | Target temperature, K. |
| vlimit | 20.0 | Maximum absolute value of any component of the velocity vector. |
| ntpr_md | 10 | Printing frequency for dynamics information to stdout. |
| ntwx | 0 | Frequency for dumping coordinates to traj_file. |
| zerov | 0 | If nonzero, then the initial velocities will be set to zero. |
| tempi | 0.0 | If *zerov*=0 and *tempi*>0, then the initial velocities will be randomly chosen for this temperature. If both *zerov* and *tempi* are zero, the velocities passed into the md() function will be used as the initial velocities; this combination is useful to continue an existing trajectory. |
| genmass | 10.0 | The general mass to use for MD if individual masses are not read from a prmtop file; value in amu. |
| diel | C | Code for the dielectric model. "C" gives a dielectric constant of 1; "R" makes the dielectric constant equal to distance in angstroms; "RL" uses the sigmoidal function of Ramstein & Lavery, PNAS **85**, 7231 (1988); "RL94" is the same thing, but speeded up assuming one is using the Cornell *et al* force field; "R94" is a distance-dependent dielectric, again with speedups that assume the Cornell *et al.* force field. |
| dielc | 1.0 | This is the dielectric constant used for *non-GB* simulations. It is implemented in routine mme_init() by scaling all of the charges by sqrt(dielc). This means that you need to set this (if desired) in mm_options() before calling mme_init(). |

| *keyword* | *default* | *meaning* |
|---|---|---|
| gb | 0 | If set to 0 then GB is off. Setting gb=1 turns on the Hawkins, Cramer, Truhlar (HCT) form of pairwise generalized Born model for solvation. See ref [5] for details of the implementation; this is equivalent to the *igb=1* option in *sander* and *pmemd*. Set diel to "C" if you use this option. Setting gb=2 turns on the Onufriev, Bashford, Case (OBC) variant of GB,[6, 7] with $\alpha$=0.8, $\beta$=0.0 and $\gamma$=2.909. This is equivalent to the *igb=2* option in *sander* and *pmemd*. Setting gb=5 just changes the values of $\alpha$, $\beta$ and $\gamma$ to 1.0, 0.8, and 4.85, respectively, corresponding to the *igb=5* option in *sander*. Setting gb=7 turns on the GB Neck variant of GB,[8] corresponding to the *igb=7* option in *sander* and *pmemd*. Setting gb=8 turns on the updated GB Neck variant of GB, corresponding to the *igb=8* option in *sander* and *pmemd*. |
| rgbmax | 999.0 | A maximum value for considering pairs of atoms to contribute to the calculation of the effective Born radii. The default value means that there is effectively no cutoff. Calculations will be sped up by using smaller values, say around 15. Å or so. This parameter is ignored if hcp > 0. |
| gbsa | 0 | If set to 1, add a surface-area dependent energy equal to surfen*SASA, where surften is discussed below, and SASA is an approximate surface area term. NAB uses the "LCPO" approximation developed by Weiser, Shenkin, and Still.[9] |
| surften | 0.005 | Surface tension (see *gbsa*, above) in kcal/mol/Å$^2$. |
| epsext | 78.5 | Exterior dielectric for generalized Born; interior dielectric is always 1. |
| kappa | 0.0 | Inverse of the Debye-Hueckel length, if gb is turned on, in Å$^{-1}$. This parameter is related to the ionic strength as $\kappa = [8\pi\beta I/\varepsilon]^{1/2}$, where $I$ is the ionic strength (same as the salt concentration for a 1-1 salt). For $T$=298.15 and $\varepsilon$=78.5, $\kappa = (0.10806I)^{1/2}$, where $I$ is in [M]. |
| ipb | 0 | Switch to compute electrostatic solvation free energy. If set to 0 then PBSA is off. This is equivalent to the ipb option in *pbsa*. Possible values: **0**, **1**, **2**, and **4**. See PBSA chapter for more information. |
| inp | 2 | Option to select different methods to compute non-polar solvation free energy. This is equivalent to the inp option in *pbsa*. Possible values: **0**, **1**, and **2**. See PBSA chapter for more information. |
| epsin | 1.0 | Sets the dielectric constant of the solute region. The solute region is defined to be the solvent excluded volume. |
| epsout | 80.0 | Sets the implicit solvent dielectric constant. The solvent region is defined to be the space not occupied the solute region. Thus, only two dielectric regions are allowed in the current release. |
| smoothopt | 1 | Instructs PB how to set up dielectric values for finite-difference grid edges that are located across the solute/solvent dielectric boundary. |
| istrng | 0.0 | Sets the ionic strength (in mM) for the PB equation. |
| radiopt | 1 | Option to set up atomic radii. This is equivalent to the radiopt option in *pbsa*. Possible values: **0**, and **1**. See PBSA chapter for more information. |

| *keyword* | *default* | *meaning* |
|---|---|---|
| dprob | 1.4 | Solvent probe radius for molecular surface used to define the dielectric boundary between solute and solvent. If set 0.0, it would be later assigned to the value of sprob. |
| iprob | 2.0 | Mobile ion probe radius for ion accessible surface used to define the Stern layer. |
| npbopt | 0 | Option to select the linear or the full nonlinear PB equation.<br>= **0** Linear PB equation is solved.<br>= **1** Nonlinear PB equation is solved. |
| solvopt | 1 | Option to select iterative solvers. This is equivalent to the solvopt option in *pbsa*. Possible values: **1**, **2**, **3**, **4**, **5**, and **6**. See PBSA chapter for more information. |
| accept | 0.001 | Sets the iteration convergence criterion (relative to the initial residue). |
| maxitn | 100 | Sets the maximum number of iterations for the finite difference solvers, default to 100. |
| fillratio | 2.0 | The ratio between the longest dimension of the rectangular finite-difference grid and that of the solute. |
| space | 0.5 | Sets the grid spacing for the finite difference solver. |
| nfocus | 2 | Set how many successive FD calculations will be used to perform an electrostatic focussing calculation on a molecule. Possible values: **1** and **2**. |
| fscale | 8 | Set the ratio between the coarse and fine grid spacings in an electrostatic focussing calculation. |
| bcopt | 5 | Boundary condition options. This is equivalent to the bcopt option in *pbsa*. Possible values: **1**, **5**, **6**, and **10**. See PBSA chapter for more information. |
| eneopt | 2 | Option to compute total electrostatic energy and forces. This is equivalent to the eneopt option in *pbsa*. Possible values: **1**, and **2**. See PBSA chapter for more information. |
| dbfopt | n/a | This keyword is phased out in this release. |
| frcopt | 0 | Option to compute and output electrostatic forces to a file named force.dat in the working directory. This is equivalent to the frcopt option in *pbsa*. Possible values: **0**, **1**, **2**, and **3**. See PBSA chapter for more information. |
| cutnb | 0.0 | Atom-based cutoff distance for van der Waals interactions, and pairwise Coulombic interactions when ENEOPT = 2. When ENEOPT = 1, this is the cutoff distance used for van der Waals interactions only. |
| sprob | 0.557 | Solvent probe radius for solvent accessible surface area (SASA) used to compute the dispersion term. |
| npbverb | 0 | This turns on verbose mode in PB when set to 1. |
| arcres | 0.25 | gives the resolution (in the unit of Å) of dots used to represent solvent accessible arcs. |
| maxarcdot | 1500 | 1500 actually means automatically determine number of arc dots required for solvent accessible surface, might grow too large to fit machines with less available memory. Please assign it to 4000~7000 and see if it fits into your computers. |
| npbgrid | 1 | How many step do pbsa wait to re-calculate the geometry in a simulation, npbgrid = 1 is required to do trajectory evaluation. npbgrid is recommended to be 100 if “conjgrad” is used. |

| *keyword* | *default* | *meaning* |
|---|---|---|
| irism | 0 | Use 3D-RISM.<br>**= 0** Off.<br>**= 1** On. |
| xvvfile | n/a | .xvv file which describes bulk solvent properties. Required for 3D-RISM calculations. Produced by rism1d. |
| guvfile | n/a | Root name for solute-solvent 3D pair distribution function, $G^{\mathrm{UV}}(\mathbf{R})$. This will produce one file for each solvent atom type for each frame requested. |
| huvfile | n/a | Rootname for solute-solvent 3D total correlation function, $H^{\mathrm{UV}}(\mathbf{R})$. This will produce one file for each solvent atom type for each frame requested. |
| cuvfile | n/a | Rootname for solute-solvent 3D total correlation function, $C^{\mathrm{UV}}(\mathbf{R})$. This will produce one file for each solvent atom type for each frame requested. |
| quvfile | n/a | Rootname for solvent 3D charge density distribution [$e$/Å]. This will produce one file with contributions from each solvent atom type for each frame requested. |
| chgdist | n/a | Rootname for solvent 3D charge distribution [$e$]. This will produce one file with contributions from each solvent atom type for each frame requested. |
| uuvfile | n/a | Rootname for solute-solvent 3D potential energy, $U^{\mathrm{UV}}(\mathbf{R})$. This will produce one file for each solvent atom type for each frame requested. |
| asympfile | n/a | Rootname for solute-solvent 3D long range real-space asymptotics for $C$ and $H$. This will produce one file for $C$ and $H$ for each frame requested. |
| exchemfile | n/a | Root name for 3D excess chemical potential distribution files. |
| solvenefile | n/a | Root name for 3D solvation energy distribution files. |
| entropyfile | n/a | Root name for 3D solvation entropy distribution files. |
| potUVfile | n/a | Root name for 3D solute-solvent potential energy distribution files. |
| molReconstruct | 1 | For any thermodynamic distributions requested, also out the molecular reconstruction (see section **??**). |
| volfmt | dx | Output format for volumetric data.<br>**= mrc** (default) MRC format.<br>**= ccp4** CCP4 format.<br>**= dx** DX format.<br>**= xyzv** XYZV format. |

| *keyword* | *default* | *meaning* |
|---|---|---|
| closure | KH | Comma separate list of closure approximations.<br>**= HNC** Hyper-netted chain equation (HNC).<br>**= KH** Kovalenko-Hirata (KH).<br>**= PSEn** Partial series expansion of order *n* where "n" is a positive integer.<br>If more than one closure is provided, the 3D-RISM solver will use the closures in order to obtain a solution for the last closure in the list when no previous solutions are available. The solution for the last closure in the list is used for all output. |
| closureorder | 1 | (Deprecated) Order for PSE-n closure if closure is specified as "PSE" or "PSEN" (no integers). |
| solvcut | buffer | Cut-off distance for solvent-solute potential and force calculations. `solvcut` must be explicitly set if buffer$< 0$. For minimization it is recommended to not use a cut-off (e.g. solvcut=`9999`). |
| buffer | 14 | Minimum distance in Å between the solute and the edge of the solvent box.<br>**< 0** Use fixed box size (`ng3` and `solvbox`).<br>**>= 0** Buffer distance. |
| grdspc | 0.5 | Linear grid spacing in x-, y- and z-dimensions [Å]. May be specified as single number if all dimensions have the same value. E.g., 'grdspc=0.5' is equivalent to 'grdspc=0.5,0.5,0.5'. |
| ng | n/a | Sets the number of grid points for a fixed size solvation box. May be specified as single integer if all dimensions have the same value. E.g., 'ng=64' is equivalent to 'ng=64,64,64'. |
| solvbox | n/a | Sets the size in Å of the fixed size solvation box. May be specified as single number if all dimensions have the same value. E.g., 'solvbox=32.0' is equivalent to 'solvbox=32.0,32.0,32.0'. |

| *keyword* | *default* | *meaning* |
|---|---|---|
| tolerance | 1e-5 | A list of maximum residual values for solution convergence. When used in combination with a list of closures it is possible to define different tolerances for each of the closures. This can be useful for difficult to converge calculations (see §**??**). For the sake of efficiency, it is best to use as high a tolerance as possible for all but the last closure. For minimization a tolerance of 1e-11 or lower is recommended. Three formats of list are possible.<br>`one tolerance` All closures but the last use a tolerance of 1. The last tolerance in the list is used by the last closure. In practice this, is the most efficient.<br>`two tolerances` All closures but the last use the first tolerance in the list. The last tolerance in the list is used by the last closure.<br>*n* `tolerances` Tolerances from the list are assigned to the closure list in order. |
| **ljTolerance** | -1 | Determines the Lennard-Jones cutoff distance based on the desired accuracy of the calculation. See §**??** for details on how this affects numerical accuracy and how this interacts with `tolerance`, `buffer`, and `solvbox`. |
| **asympKSpaceTolerance** | -1 | Determines the reciprocal space long range asymptotics cutoff distance based on the desired accuracy of the calculation. See §**??** for details on how this affects numerical accuracy. Possible values are<br>$< 0$ `asympKSpaceTolerance=tolerance/10`,<br>`0` no cutoff, and<br>$> 0$ given value determines the maximum error in the reciprocal-space long range asymptotics calculations. |
| **treeDCF** | 1 | Use direct sum or the treecode approximation to calculate the direct correlation function long-range asymptotic correction.<br>**0** Use direct sum.<br>**1** Use treecode approximation. |
| **treeTCF** | 1 | Use direct sum or the treecode approximation to calculate the total correlation function long-range asymptotic correction.<br>**0** Use direct sum.<br>**1** Use treecode approximation. |

| *keyword* | *default* | *meaning* |
|---|---|---|
| **treeCoulomb** | 0 | Use direct sum or the treecode approximation to calculate the Coulomb potential energy.<br><br>**0** Use direct sum.<br><br>**1** Use treecode approximation. |
| **treeDCFMAC** | 0.1 | Treecode multipole acceptance criterion for the direct correlation function long-range asymptotic correction. |
| **treeTCFMAC** | 0.1 | Treecode multipole acceptance criterion for the total correlation function long-range asymptotic correction. |
| **treeCoulombMAC** | 0.1 | Treecode multipole acceptance criterion for the Coulomb potential energy. |
| **treeDCFOrder** | 2 | Treecode Taylor series order for the direct correlation function long-range asymptotic correction. |
| **treeTCFOrder** | 2 | Treecode Taylor series order for the total correlation function long-range asymptotic correction. Note that the Taylor expansion used does not converge exactly to the TCF long-range asymptotic correction, so a very high order will not necessarily increase accuracy. |
| **treeCoulombOrder** | 2 | Treecode Taylor series order for the Coulomb potential energy. |
| **treeDCFN0** | 500 | Maximum number of grid points contained within the treecode leaf clusters for the direct correlation function long-range asymptotic correction. This sets the depth of the hierarchical octtree. |
| **treeTCFN0** | 500 | Maximum number of grid points contained within the treecode leaf clusters for the total correlation function long-range asymptotic correction. This sets the depth of the hierarchical octtree. |
| **treeCoulombN0** | 500 | Maximum number of grid points contained within the treecode leaf clusters for the Coulomb potential energy. This sets the depth of the hierarchical octtree. |
| mdiis_del | 0.7 | "Step size" in MDIIS. |
| mdiis_nvec | 5 | Number of vectors used by the MDIIS method. Higher values for this parameter can greatly increase memory requirements but may also accelerate convergence. |
| mdiis_restart | 10 | If the current residual is `mdiis_restart` times larger than the smallest residual in memory, then the MDIIS procedure is restarted using the lowest residual solution stored in memory. Increasing this number can sometimes help convergence. |
| mdiis_method | 2 | Specify implementation of the MDIIS routine.<br><br>**= 0** Original reference implementation.<br><br>**= 1** BLAS optimized.<br><br>**= 2** BLAS and memory optimized. |
| maxstep | 10000 | Maximum number of iterations allowed to converge on a solution. |

| *keyword* | *default* | *meaning* |
|---|---|---|
| npropagate | 5 | Number of previous solutions propagated forward to create an initial guess for this solute atom configuration.<br>**= 0** Do not use any previous solutions<br>**= 1..5** Values greater than 0 but less than 4 or 5 will use less system memory but may introduce artifacts to the solution (e.g., energy drift). |
| centering | 1 | Controls how the solute is centered/re-centered in the solvent box. (See Subsection **??**.)<br>**= -4** Center-of-geometry with grid-point rounding. Center on first step only.<br>**= -3** Center-of-mass with grid-point rounding. Center on first step only.<br>**= -2** Center-of-geometry. Center on first step only.<br>**= -1** Center-of-mass. Center on first step only.<br>**= 0** No centering. Dangerous.<br>**= 1** Center-of-mass. Center on every step. Recommended for molecular dynamics.<br>**= 2** Center-of-geometry. Center on every step. Recommended for minimization.<br>**= 3** Center-of-mass with grid-point rounding.<br>**= 4** Center-of-geometry with grid-point rounding. |
| zerofrc | 1 | Redistribute solvent forces across the solute such that the net solvation force on the solute is zero.<br>**= 0** Unmodified forces.<br>**= 1** Zero net force. |
| apply_rism_force | 1 | Calculate and use solvation forces from 3D-RISM. Not calculating these forces can save computation time and is useful for trajectory post-processing.<br>**= 0** Do not calculate forces.<br>**= 1** Calculate forces. |
| ntwrism | 0 | Indicates that solvent density grid should be written to file every `ntwrism` iterations.<br>**= 0** No files written.<br>**>= 1** Output every ntwrism time steps. |

| *keyword* | *default* | *meaning* |
|---|---|---|
| ntprism | 0 | Indicates that 3D-RISM thermodynamic output should be written to file every `ntprism` iterations.<br>**= 0** No files written.<br>**>= 1** Output every ntwrism time steps. |
| polarDecomp | 0 | Decompose the solvation free energy into polar and non-polar contributions. This is only useful if ntprism$\neq$ 0 and adds about 80% to the total calculation time.<br>**= 0** No decomposition.<br>**= 1** Decomposition is performed. |
| entropicDecomp | 0 | Decomposes solvation free energy into energy and entropy components. Also performs temperature derivatives of other calculated quantities. Note that this typically requires 80% more computation time and requires a .xvv file version 1.000 or higher (see §**??** and **??**).<br>**= 0** No entropic decomposition.<br>**= 1** Entropic decomposition. |
| gf | 0 | Compute the Gaussian fluctuation excess chemical potential functional (see §**??**). |
| pcpluscorrection | 0 | Compute the PC+/3D-RISM excess chemical potential functional (see §**??**). |
| uccoeff | 0,0,0,0 | Compute the UC excess chemical potential functional with the provided coefficients (see §**??**). *a* and *b* are the coefficients for the original UC functional, though using the closure excess chemical potential functional. *a1* and *b1* are optional and provide temperature dependence to the correction (UCT in [10]). |
| verbose | 0 | Indicates level of diagnostic detail about the calculation written to the log file.<br>**= 0** No output.<br>**= 1** Print the number of iterations required to converge.<br>**= 2** Print details for each iteration and information about what FCE is doing every progress iterations. |
| progress | 1 | Display progress of the 3D-RISM solution every `progress` iterations. 0 indicates this information will not be displayed. Only used if `verbose` $>$ 1. |
| static_arrays | 1 | If set to 1, do not allocate dynamic arrays for each call to the mme() and mme2() functions. The default value of 1 reduces computation time by avoiding array allocation. |

| *keyword* | *default* | *meaning* |
|---|---|---|
| blocksize | 8 | The granularity with which loop iterations are assigned to OpenMP threads or MPI processes. For MPI, a blocksize as small as 1 results in better load balancing during parallel execution. For OpenMP, blocksize should not be smaller than the number of floating-point numbers that fit into one cache line in order to avoid performance degradation through 'false sharing'. For ScaLAPACK, the optimum blocksize is not know, although a value of 1 is probably too small. |
| hcp | 0 | Use the GB-HCP model:<br>**= 0** No GB-HCP.<br>**= 1** 1-charge approximation.<br>**= 2** 2-charge approximation.<br>**= 4** 2-charge based on optimal point charge approximation (recommended for GB-HCP).<br>See Section 1.6 for detailed instructions on using the GB-HCP. It is strongly recommended that the NSCM option above be used whenever GB-HCP is used. |
| dhcp | 0.25 | Adjusts the separation between the charges used to approximate uncharged components for hcp=4. dhcp is empirically determined so that the RMS error in force, compared to GB without further approximation, is minimized. Our testing on various structures suggests that the optimal value for dhcp can be found within the range of 0.1 and 0.4. See Section 1.6 for details. |
| hcp_h1 | 15 | GB-HCP level 1 threshold distance. The recommended level 1 threshold distance for amino acids is 15A. For structures with nucleic acids the recommended level 1 threshold distance is 21A. |
| hcp_h2 | 50 | GB-HCP level 2 threshold distance. The recommended level 2 threshold distance for proteins is 50A. For structures with nucleic acids the recommended level 2 threshold distance is 90A. |
| hcp_h3 | 150 | GB-HCP level 3 threshold distance. The recommended level 3 threshold distance for amino acids is 150A. For structures with nucleic acids the recommended level 1 threshold distance is 169A. |

The mme() function takes a coordinate set and returns the energy in the function value and the gradient of the energy in grad. The input parameter *iter* is used to control printing (see the *ntpr* variable) and non-bonded updates (see *nsnb*). The mme_rattle() function has the same interface, but constrains the bond lengths and returns a corrected gradient. If you want to minimize with constrained bond lengths, pass *mme_rattle* and not *mme* to the *conjgrad* routine.

The conjgrad() function will carry out conjugate gradient minimization of the function func that depends upon n parameters, whose initial values are in the x array. The function func must be of the form func( x[], g[], iter ), where x contains the input values, and the function value is returned through the function call, and its gradient with respect to x through the g array. The iteration number is passed through iter, which func can use for whatever purpose it wants; a typical use would just be to determine when to print results. The input parameter dfpred is the expected drop in the function value on the first iteration; generally only a rough estimate is needed. The minimization will

proceed until maxiter steps have been performed, or until the root-mean-square of the components of the gradient is less than rmsgrad. The value of the function at the end of the minimization is returned in the variable fret. conjgrad can return a variety of exit codes:

| *Return codes for conjgrad routine* | |
|---|---|
| >0 | minimization converged; gives number of final iteration |
| -1 | bad line search; probably an error in the relation of the function to its gradient (perhaps from round-off if you push too hard on the minimization). |
| -2 | search direction was uphill |
| -3 | exceeded the maximum number of iterations |
| -4 | could not further reduce function value |

Finally, the md function will run maxstep steps of molecular dynamics, using func as the force field (this would typically be set to a function like mme.) The number of dynamical variables is given as input parameter n: this would be 3 times the number of atoms for ordinary cases, but might be different for other force fields or functions. The arrays x[], f[] and v[] hold the coordinates, gradient of the potential, and velocities, respectively, and are updated as the simulation progresses. The method of temperature regulation (if any) is specified by the variables *tautp* and *gamma_ln* that are set in *mm_options()*.

**Note:** In versions of NAB up to 4.5.2, there was an additional input variable to md() called *minv* that reserved space for the inverse of the masses of the particles; this has now been removed. This change is not backwards compatible: you must modify existing NAB scripts that call md() to remove this variable.

## 1.3 NetCDF read/write routines

NAB has several routines for reading/writing Amber NetCDF trajectory and restart files. All of the routines except netcdfGetNextFrame() return a 1 on error, 0 on success. The netcdfGetNextFrame() routine returns 0 on error, 1 on success to make it easier to use in loops. For an example of how to use NetCDF files in NAB see the NAB script in **'$AMBERHOME/AmberTools/test/nab/tnetcdf.nab'**.

### 1.3.1 struct AmberNetcdf

An AmberNetcdf struct must be used to interface with the netcdf commands in NAB (except netcdfWriteRestart()). It contains many fields, but the following are the ones commonly needed by users:

**temp0** Temperature of current frame (if temperature is present).

**restartTime** Simulation time if NetCDF restart.

**isNCrestart** 0 if trajectory, 1 if restart.

**ncframe** Number of frames in the file.

**currentFrame** Current frame number.

**ncatom** Number of atoms.

**ncatom3** Number of coordinates (ncatom * 3).

**velocityVID** If not -1, velocity information is present.

**TempVID** If not -1, temperature information is present.

In order to use it, you must include nab_netcdf.h and declare it as a struct, e.g.:

```
#include "nab_netcdf.h"
struct AmberNetcdf NC;
```

### 1.3.2 netcdfClose

```
int netcdfClose(struct AmberNetcdf NC)
```

Close NetCDF file associated with **NC**.

### 1.3.3 netcdfCreate

```
int netcdfCreate(struct AmberNetcdf NC, string filename, int natom, int isBox)
NC AmberNetcdf struct to set up.
filename Name of file to create.
natom Number of atoms in file.
isBox 0 = No box coordinates, 1 = Has box coordinates.
```

Create NetCDF trajectory file and associate with struct **NC**. For writing NetCDF restarts, use netcdfWriteRestart().

### 1.3.4 netcdfDebug

```
int netcdfDebug(struct AmberNetcdf NC)
```

Print debug information for NetCDF file associated with **NC**.

### 1.3.5 netcdfGetFrame

```
int netcdfGetFrame(struct AmberNetcdf NC, int set, float X[], float box[])
NC AmberNetcdf struct, previously set up and opened.
set Frame number to read.
X Array to store coordinates (dimension NC.ncatom3).
box Array of dimension 6 to store box coordinates if present (X Y Z
    ALPHA BETA GAMMA); can be NULL.
```

Get coordinates at frame **set** (starting from 0).

### 1.3.6 netcdfGetNextFrame

```
int netcdfGetNextFrame(struct AmberNetcdf NC, float X[], float box[])
NC AmberNetcdf struct, previously set up and opened.
X Array to store coordinates (dimension NC.ncatom3).
box Array of size 6 to store box coordinates if present (X Y Z ALPHA
    BETA GAMMA); can be NULL.
```

Get the coordinates at frame **NC.currentFrame** and increment **NC.currentFrame** by one. Unlike the other netcdf routines, this returns 1 on success and 0 on error to make it easy to use in loops.

### 1.3.7 netcdfGetVelocity

```
int netcdfGetVelocity(struct AmberNetcdf NC, int set, float V[])
NC AmberNetcdf struct, previously set up and opened.
set Frame number to read.
V Array to store velocities (dimension NC.ncatom3).
```

Get velocities at frame **set** (starting from 0).

### 1.3.8 netcdfInfo

```
int netcdfInfo(struct AmberNetcdf NC)
```

Print information for **NC**, including file type, presence of velocity/box/temperature info, and number of atoms, coordinates, and frames present.

### 1.3.9 netcdfLoad

```
int netcdfLoad(struct AmberNetcdf NC, string filename)
NC AmberNetcdf struct to set up.
filename Name of NetCDF file to load.
```

Load NetCDF file filename and set up the AmberNetcdf structure **NC** for reading. The file type is automatically detected.

### 1.3.10 netcdfWriteFrame

```
int netcdfWriteFrame(struct AmberNetcdf NC, int set, float X[], float box[])
NC AmberNetcdf struct, previously set up and opened.
set Frame number to write.
X Array of coordinates to write (dimension NC.ncatom3).
box Array of size 6 of box coordinates to write (X Y Z ALPHA BETA
    GAMMA); can be NULL.
```

Write to NetCDF trajectory at frame **set** (starting from 0). NOTE: This routine is for writing NetCDF trajectories only; to write NetCDF restarts use netcdfWriteRestart().

### 1.3.11 netcdfWriteNextFrame

```
int netcdfWriteNextFrame(struct AmberNetcdf NC, float X[], float box[])
NC AmberNetcdf struct, previously set up and opened.
X Array of coordinates to write (dimension NC.ncatom3).
box Array of size 6 of box coordinates to write (X Y Z ALPHA BETA
    GAMMA); can be NULL.
```

Write coordinates to frame **NC.currentFrame** and increment **NC.currentFrame** by one. NOTE: This routine is for writing NetCDF trajectories only; to write NetCDF restarts use netcdfWriteRestart().

### 1.3.12 netcdfWriteRestart

```
int netcdfWriteRestart(string filename, int natom, float X[], float V[],
                       float box[], float time, float temperature)
```

**filename** Name of NetCDF restart file to create.

**natom** Number of atoms in netcdf restart file.

**X** Array of coordinates to write (dimension natom*3).

**V** Array of velocities to write (dimension natom*3); can be NULL.

**box** Array of size 6 of box coordinates to write (X Y Z ALPHA BETA GAMMA); can be NULL.

**time** Restart time in ps.

**temperature** Restart temperature; if < 0 no temperature will be written.

## 1.4 Second derivatives and normal modes

Russ Brown has contributed codes that compute analytically the second derivatives of the Amber functions, including the generalized Born terms.[1] This capability resides in the three functions described here.

```
int newton( float x[], int n, float fret, float func1(), float func2(), float rms,
        float nradd, int maxiter );
float nmode( float x[], int n, float func(), int eigp, int ntrun, float eta, float hrmax, int ioseen );
```

These routines construct and manipulate a Hessian (second derivative matrix), allowing one (for now) to carry out Newton-Raphson minimization and normal mode calculations. The mme2() routine takes as input a *3*natom* vector of coordinates x[], and returns a gradient vector g[], a Hessian matrix, stored columnwise in a *3*natom x 3*natom* vector h[], and the masses of the system, in a vector m[] of length *natom*. The iteration variable iter is just used to control printing. At present, these routines only work for *gb* = 0 or 1.

Users cannot call mme2() directly, but will pass this as an argument to one of the next two routines.

The newton() routine takes a input coordinates x[] and a size parameter n (must be set to *3*natom*). It performs Newton-Raphson optimization until the root-mean-square of the gradient vector is less than rms, or until maxiter steps have been taken. For now, the input function func1() must be mme() and func2() must be mme2(). The value nradd will be added to the diagonal of the Hessian before the step equations are solved; this is generally set to zero, but can be set something else under particular circumstances, which we do not discuss here.[11]

Generally, you only want to try Newton-Raphson minimization (which can be very expensive) after you have optimized structures with conjgrad() to an rms gradient of 10 -3 or so. In most cases, it should only take a small number of iterations then to go down to an rms gradient of about 10 -12 or so, which is somewhere near the precision limit.

Once a good minimum has been found, you can use the nmode() function to compute normal/Langevin modes and thermochemical parameters. The first three arguments are the same as for newton(), the next two integers give the number of eigenvectors to compute and the type of run, respectively. The last three arguments (only used for Langevin modes) are the viscosity in centipoise, the value for the hydrodynamic radius, and the type of hydrodynamic interactions. Several techniques are available for diagonalizing the Hessian depending on the number of modes required and the amount of memory available.

In all cases the modes are written to an Amber-compatible "vecs" file for normal modes or "lmodevecs" file for Langevin modes. There are currently no nab routines that use this format. The Langevin modes will also generate an output file called "lmode" that can be read by the Amber module *lmanal*.

`ntrun`
- **0:** The dsyev routine is used to diagonalize the Hessian
- **1:** The dsyevd routine is used to diagonalize the Hessian

**2:** The ARPACK package (shift invert technique) is used to obtain a small number of eigenvalues

**3:** The Langevin modes are computed with the viscosity and hydrodynamic radius provided

`hrmax` Hydrodynamic radius for the atom with largest area exposed to solvent. If a file named "expfile" is provided then the relative exposed areas are read from this file. If "expfile" is not present all atoms are assigned a hydrodynamic radius of hrmax or 0.2 for the hydrogen atoms. The "expfile" can be generated with the ms (molecular surface) program.

`ioseen` **0:** Stokes Law is used for the hydrodynamic interaction

**1:** Oseen interaction included

**2:** Rotne-Prager correction included

Here is a typical calling sequence:

```
molecule m;
float x[4000], fret;

m = getpdb_prm( "mymolecule.pdb", "leaprc.protein.ff14SB", "", 0 );
mm_options( "cut=999., ntpr=50, nsnb=99999, diel=C, gb=1, dielc=1.0" );
mme_init( m, NULL, "::Z", x, NULL);
setxyz_from_mol( m, NULL, x );

//  conjugate gradient minimization
conjgrad(x, 3*m.natoms, fret, mme, 0.1, 0.001, 2000 );

//  Newton-Raphson minimization\fP
mm_options( "ntpr=1" );
newton( x, 3*m.natoms, fret, mme, mme2, 0.00000001, 0.0, 6 );

// get the normal modes:
nmode( x, 3*m.natoms, mme2, 0, 0, 0.0, 0.0, 0);
```

## 1.5 Low-MODe (LMOD) optimization methods

István Kolossváry has contributed functions, which implement the LMOD methods for minimization, conformational searching, and flexible docking.[12–15] The centerpiece of LMOD is a conformational search algorithm based on eigenvector following of low-frequency vibrational modes. It has been applied to a spectrum of computational chemistry domains including protein loop optimization and flexible active site docking. The search method is implemented without explicit computation of a Hessian matrix and utilizes the Arnoldi package (ARPACK, *http://www.caam.rice.edu/software/ARPACK/*) for computing the low-frequency modes. LMOD optimization can be thought of as an advanced minimization method. LMOD can not only energy minimize a molecular structure in the local sense, but can generate a series of very low energy conformations. The LMOD capability resides in a single, top-level calling function *lmod()*, which uses fast local minimization techniques, collectively termed XMIN that can also be accessed directly through the function *xmin()*.

There are now **four "real-life" examples** of carrying out LMOD searches: look in *$AMBERHOME/AmberTools/examples/nab/lmod_**. Each directory has a README file that give more information.

### 1.5.1 LMOD conformational searching

The LMOD conformational search procedure is based on gentle, but very effective structural perturbations applied to molecular systems in order to explore their conformational space. LMOD perturbations are derived from low-frequency vibrational modes representing large-amplitude, concerted atomic movements. Unlike essential dynamics where such low modes are derived from long molecular dynamics simulations, LMOD calculates the modes directly and utilizes them to improve Monte Carlo sampling.

LMOD has been developed primarily for macromolecules, with its main focus on protein loop optimization. However, it can be applied to any kind of molecular systems, including complexes and flexible docking where it has found widespread use. The LMOD procedure starts with an initial molecular model, which is energy minimized. The minimized structure is then subjected to an ARPACK calculation to find a user-specified number of low-mode eigenvectors of the Hessian matrix. The Hessian matrix is never computed; ARPACK makes only implicit reference to it through its product with a series of vectors. Hv, where v is an arbitrary unit vector, is calculated via a finite-difference formula as follows,

$$Hv = [\nabla(x_{min} + h) - \nabla(x_{min})]/h \tag{1.1}$$

where $x_{min}$ is the coordinate vector at the energy minimized conformation and $h$ denotes machine precision. The computational cost of Eq. 1 requires a single gradient calculation at the energy minimum point and one additional gradient calculation for each new vector. Note that $\bigtriangledown x$ is never 0, because minimization is stopped at a finite gradient RMS, which is typically set to 0.1-1.0 kcal/mol-Å in most calculations.

The low-mode eigenvectors of the Hessian matrix are stored and can be re-used throughout the LMOD search. Note that although ARPACK is very fast in relative terms, a single ARPACK calculation may take up to a few hours on an absolute CPU time scale with a large protein structure. Therefore, it would be impractical to recalculate the low-mode eigenvectors for each new structure. Visual inspection of the low-frequency vibrational modes of different, randomly generated conformations of protein molecules showed very similar, collective motions clearly suggesting that low-modes of one particular conformation were transferable to other conformations for LMOD use. This important finding implies that the time limiting factor in LMOD optimization, even for relatively small molecules, is energy minimization, not the eigenvector calculation. This is the reason for employing XMIN for local minimization instead of NAB's standard minimization techniques.

### 1.5.2 LMOD procedure

Given the energy-minimized structure of an initial protein model, protein- ligand complex, or any other molecular system and its low-mode Hessian eigenvectors, LMOD proceeds as follows. For each of the first n low-modes repeat steps 1-3 until convergence:

1. Perturb the energy-minimized starting structure by moving along the ith (i =1-n) Hessian eigenvector in either of the two opposite directions to a certain distance. The 3N-dimensional (N is equal to the number of atoms) travel distance along the eigenvector is scaled to move the fastest moving atom of the selected mode in 3-dimensional space to a randomly chosen distance between a user-specified minimum and maximum value.
   *Note*: A single LMOD move inherently involves excessive bond stretching and bond angle bending in Cartesian space. Therefore the primarily torsional trajectory drawn by the low-modes of vibration on the PES is severely contaminated by this naive, linear approximation and, therefore, the actual Cartesian LMOD trajectory often misses its target by climbing walls rather than crossing over into neighboring valleys at not too high altitudes. The current implementation of LMOD employs a so-called ZIG-ZAG algorithm, which consists of a series of alternating short LMOD moves along the low-mode eigenvector (ZIG) followed by a few steps of minimization (ZAG), which has been found to relax excessive stretches and bends more than reversing the torsional move. Therefore, it is expected that such a ZIG- ZAG trajectory will eventually be dominated by concerted torsional movements and will carry the molecule over the energy barrier in a way that is not too different from finding a saddle point and crossing over into the next valley like passing through a mountain pass.
   *Barrier crossing check:* The LMOD algorithm checks barrier crossing by evaluating the following criterion: IF the current endpoint of the zigzag trajectory is lower than the energy of the starting structure, OR, the endpoint is at least lower than it was in the previous ZIG-ZAG iteration step AND the molecule has also moved farther away from the starting structure in terms of all-atom superposition RMS than at the previous position THEN it is assumed that the LMOD ZIG-ZAG trajectory has crossed an energy barrier.

2. Energy-minimize the perturbed structure at the endpoint of the ZIG- ZAG trajectory.

| *Parameter list for xmin()* | | |
|---|---|---|
| *keyword* | *default* | *meaning* |
| func | N/A | The name of the function that computes the function value and gradient of the objective function to be minimized. *func()* must have the following argument list: `float func( float x[], float g[], int i)` where `x[]` is the vector of the iterate, `g[]` is the gradient and `i` is currently ignored except when `func = mme` where `i` is handled internally. |
| natm | N/A | Number of atoms. **NOTE:** if `func` is other than `mme`, `natm` is used to pass the total number of variables of the objective function to be minimized. However, `natm` retains its original meaning in case `func` is a user-defined energy function for 3-dimensional (molecular) structure optimization. Make sure that the meaning of `natm` is compatible with the setting of `mol_struct_opt` below. |
| x[] | N/A | Coordinate vector. User has to allocate memory in calling program and fill x[] with initial coordinates using, e.g., the setxyz_from_mol function (see sample program below). Array size = 3*natm. |
| g[] | N/A | Gradient vector. User has to allocate memory in calling program. Array size = 3*natm. |
| ene | N/A | On output, ene stores the minimized energy. |
| grms_out | N/A | On output, grms_out stores the gradient RMS achieved by XMIN. |

Table 1.2: *Arguments for xmin().*

3. Save the new minimum-energy structure and return to step 1. Note that LMOD saves only low-energy structures within a user-specified energy window above the then current global minimum of the ongoing search.

After exploring the modes of a single structure, LMOD goes on to the next starting structure, which is selected from the set of previously found low- energy structures. The selection is based on either the Metropolis criterion, or simply the than lowest energy structure is used. LMOD terminates when the user-defined number of steps has been completed or when the user-defined number of low-energy conformations has been collected.

Note that for flexible docking calculations LMOD applies explicit translations and rotations of the ligand(s) on top of the low-mode perturbations.

### 1.5.3 XMIN

```
float xmin( float func(), int natm, float x[], float g[],
                  float ene, float grms_out, struct xmod_opt xo);
```

At a glance: The *xmin()* function minimizes the energy of a molecular structure with initial coordinates given in the x[] array. On output, *xmin()* returns the minimized energy as the function value and the coordinates in x[] will be updated to the minimum-energy conformation. The arguments to xmin() are described in Table 1.2; the parameters in the xmin_opt structure are described in Table 1.3; these should be preceded by "`xo.`", since they are members of an *xmod_opt* struct with that name; see the sample program below to see how this works.

There are three types of minimizers that can be used, specified by the *method* parameter:

`method`

***1:*** PRCG Polak-Ribiere conjugate gradient method, similar to the *conjgrad()* function [17].

***2:*** L-BFGS Limited-memory Broyden-Fletcher-Goldfarb-Shanno quasi-Newton algorithm [18]. L-BFGS is 2-3 times faster than PRCG mainly, because it requires significantly fewer line search steps than PRCG.

***3:*** lbfgs-TNCG L-BFGS preconditioned truncated Newton conjugate gradient algorithm [17, 19]. Sophisticated technique that can minimize molecular structures to lower energy and gradient

| ***Parameter list for xmin_opt*** | | |
|---|---|---|
| *keyword* | *default* | *meaning* |
| mol_struct_opt | 1 | *1*= 3-dimensional molecular structure optimization. Any other value means general function optimization. |
| maxiter | 1000 | Maximum number of iteration steps allowed for XMIN. A value of zero means single point energy calculation, no minimization. |
| grms_tol | 0.05 | Gradient RMS threshold below which XMIN should minimize the input structure. |
| method | 3 | Minimization algorithm. See text for description. |
| numdiff | 1 | Finite difference method used in TNCG for approximating the product of the Hessian matrix and some vector in the conjugate gradient iteration (the same approximation is used in LMOD, see Eq. 1.1 in section 1.5.1). 1= Forward difference. 2=Central difference. |
| m_lbfgs | 3 | Size of the L-BFGS memory used in either L-BFGS minimization or L-BFGS preconditioning for TNCG. The value zero turns off preconditioning. It usually makes little sense to set the value $>$10. |
| print_level | 0 | Amount of debugging printout. 0= No output. 1= Minimization details. 2= Minimization (including conjugate gradient iteration in case of TNCG) and line search details. If *print_level* $>$ 2, print minimization output every *print_level* steps |
| iter | N/A | Output parameter. The total number of iteration steps completed by XMIN. |
| xmin_time | N/A | Output parameter. CPU time in seconds used by XMIN. |
| ls_method | 2 | *1*= modified Armijo [16](not recommended, primarily used for testing). *2*= Wolfe (after J. J. More' and D. J. Thuente). |
| ls_maxiter | 20 | Maximum number of line search steps per single minimization step. |
| ls_maxatmov | 0.5 | Maximum (co-ordinate) movement per degree of freedom allowed in line search, range $>$ *0*. |
| beta_armijo | 0.5 | Armijo beta parameter, range (0, 1). *Only change it if you know what you are doing.* |
| c_armijo | 0.4 | Armijo c parameter, range (0, 0.5). *Only change it if you know what you are doing.* |
| mu_armijo | 1.0 | Armijo mu parameter, range [0, 2). *Only change it if you know what you are doing.* |
| ftol_wolfe | 0.0001 | Wolfe ftol parameter, range (0, 0.5). *Only change it if you know what you are doing.* |
| gtol_wolfe | 0.9 | Wolfe gtol parameter, range (ftol_wolfe, 1). *Only change it if you know what you are doing.* |
| ls_iter | N/A | Output parameter. The total number of line search steps completed by XMIN. |
| error_flag | N/A | Output parameter. A nonzero value indicates an error. In case of an error XMIN will always print a descriptive error message. |

Table 1.3: *Options for xmin_opt.*

than PRCG and L-BFGS and requires an order of magnitude fewer minimization steps, but L-BFGS can sometimes be faster in terms of total CPU time.

**4:** Debugging option; printing analytical and numerical derivatives for comparison. Almost all failures with *xmin* can be attributed to inaccurate analytical derivatives, e.g., when SCF hasn't converged with a quantum based Hamiltonian.

NOTE: The xmin routine can be utilized for minimizing arbitrary, user-defined objective functions. The function must be defined in a user NAB program or in any other user library that is linked in. The name of the function is passed to *xmin()* via the *func* argument.

### 1.5.4 Sample XMIN program

The following sample program, which is based on the test program txmin.nab, reads a molecular structure from a PDB file, minimizes it, and saves the minimized structure in another PDB file.

```
//   XMIN reverse communication external minimization package.
//   Written by Istvan Kolossvary.

#include "xmin_opt.h"

// M A I N  P R O G R A M  to carry out XMIN minimization on a molecule:

struct xmin_opt xo;

molecule mol;
int natm;
float xyz[ dynamic ], grad[ dynamic ];
float energy, grms;
point dummy;

    xmin_opt_init( xo );  //  set up defaults (shown here)

    // xo.mol_struct_opt = 1;
    // xo.maxiter        = 1000;
    // xo.grms_tol       = 0.05;
    // xo.method         = 3;
    // xo.numdiff        = 1;
    // xo.m_lbfgs        = 3;
    //    xo.ls_method   = 2;
    //    xo.ls_maxiter  = 20;
    //    xo.maxatmov    = 0.5;
    //    xo.beta_armijo = 0.5;
    //    xo.c_armijo    = 0.4;
    //    xo.mu_armijo   = 1.0;
    //    xo.ftol_wolfe  = 0.0001;
    //    xo.gtol_wolfe  = 0.9;
    // xo.print_level    = 0;

    xo.maxiter     = 10;  //  non-defaults are here
    xo.grms_tol    = 0.001;
    xo.method      = 3;
    xo.ls_maxatmov = 0.15;
    xo.print_level = 2;

    mol = getpdb( "gbrna.pdb" );
    readparm( mol, "gbrna.prmtop" );
    natm = mol.natoms;
```

```
    allocate xyz[ 3*natm ]; allocate grad[ 3*natm ];
    setxyz_from_mol( mol, NULL, xyz );

    mm_options( "ntpr=1, gb=1, kappa=0.10395, rgbmax=99., cut=99.0, diel=C ");
    mme_init( mol, NULL, "::ZZZ", dummy, NULL );

    energy = mme( xyz, grad, 0 );
    energy = xmin( mme, natm, xyz, grad, energy, grms, xo );

// E N D  M A I N
```

The corresponding screen output should look similar to this. Note that this is fairly technical, debugging information; normally print_level is set to zero.

```
Reading parm file (gbrna.prmtop)
title:
PDB 5DNB, Dickerson decamer
old prmtop format => using old algorithm for GB parms
      mm_options:  ntpr=99
      mm_options:  gb=1
      mm_options:  kappa=0.10395
      mm_options:  rgbmax=99.
      mm_options:  cut=99.0
      mm_options:  diel=C
    iter    Total    bad         vdW     elect.     cons.   genBorn   frms

ff:   0  -4107.50    906.22   -192.79   -137.96      0.00  -4682.97 1.93e+01


-------------------------------------------------------------------

 MIN:                          It=    0  E=   -4107.50 ( 19.289)
  CG:   It=    3 (  0.310)  :-)
  LS: step= 0.94735  it= 1  info= 1
 MIN:                          It=    1  E=   -4423.34 (  5.719)
  CG:   It=    4 (  0.499)  :-)
  LS: step= 0.91413  it= 1  info= 1
 MIN:                          It=    2  E=   -4499.43 (  2.674)
  CG:   It=    9 (  0.498)  :-)
  LS: step= 0.86829  it= 1  info= 1
 MIN:                          It=    3  E=   -4531.20 (  1.543)
  CG:   It=    8 (  0.499)  :-)
  LS: step= 0.95556  it= 1  info= 1
 MIN:                          It=    4  E=   -4547.59 (  1.111)
  CG:   It=    9 (  0.491)  :-)
  LS: step= 0.77247  it= 1  info= 1
 MIN:                          It=    5  E=   -4556.35 (  1.068)
  CG:   It=    8 (  0.361)  :-)
  LS: step= 0.75150  it= 1  info= 1
 MIN:                          It=    6  E=   -4562.95 (  1.042)
  CG:   It=    8 (  0.273)  :-)
  LS: step= 0.79565  it= 1  info= 1
 MIN:                          It=    7  E=   -4568.59 (  0.997)
  CG:   It=    5 (  0.401)  :-)
  LS: step= 0.86051  it= 1  info= 1
 MIN:                          It=    8  E=   -4572.93 (  0.786)
  CG:   It=    4 (  0.335)  :-)
  LS: step= 0.88096  it= 1  info= 1
 MIN:                          It=    9  E=   -4575.25 (  0.551)
```

```
  CG:   It=   64 (  0.475)  :-)
  LS: step= 0.95860  it= 1  info= 1
 MIN:                          It=   10  E=   -4579.19 (  0.515)
-------------------------------------------------------------

 FIN:             :-)                    E=   -4579.19 (  0.515)
```

The first few lines are typical NAB output from mm_init() and mme(). The output below the horizontal line comes from XMIN. The MIN/CG/LS blocks contain the following pieces of information. The MIN: line shows the current iteration count, energy and gradient RMS (in parentheses). The CG: line shows the CG iteration count and the residual in parentheses. The happy face :-) means convergence whereas :-( indicates that CG iteration encountered negative curvature and had to abort. The latter situation is not a serious problem, minimization can continue. This is just a safeguard against uphill moves. The LS: line shows line search information. "step" is the relative step with respect to the initial guess of the line search step. "it" tells the number of line search steps taken and "info" is an error code. "info" = 1 means that line searching converged with respect to sufficient decrease and curvature criteria whereas a non- zero value indicates an error condition. Again, an error in line searching doesn't mean that minimization necessarily failed, it just cannot proceed any further because of some numerical dead end. The FIN: line shows the final result with a happy face :-) if either the grms_tol criterion has been met or when the number of iteration steps reached the maxiter value.

### 1.5.5 LMOD

```
float lmod( int natm, float x[], float g[], float ene, float conflib[],
       float lmod_traj[], int lig_start[], int lig_end[], int lig_cent[],
       float tr_min[], float tr_max[], float rot_min[], float rot_max[],
       struct xmin_opt, struct xmin_opt, struct lmod_opt);
```

At a glance: The *lmod()* function is similar to *xmin()* in that it optimizes the energy of a molecular structure with initial coordinates given in the x[] array. However, the optimization goes beyond local minimization, it is a sophisticated conformational search procedure. On output, *lmod()* returns the global minimum energy of the LMOD conformational search as the function value and the coordinates in x[] will be updated to the global minimum-energy conformation. Moreover, a set of the best low-energy conformations is also returned in the array conflib[]. Coordinates, energy, and gradient are in NAB units. The parameters are given in the table below; items above the line are passed as parameters; the rest of the parameters are all preceded by "`lo.`", because they are members of an *lmod_opt* struct with that name; see the sample program below to see how this works.

Also note that *xmin()*'s *xmin_opt* struct is passed to *lmod()* as well. *lmod()* changes the default values of some of the "`xo.`" parameters via the call to *lmod_opt_int()* relative to a call to *xmin_opt_init()*, which means that in a more complex NAB program with multiple calls to *xmin()* and *lmod()*; make sure to always initialize and set user parameters for each and every XMIN and LMOD search via, respectively calling *xmin_opt_init()* and *lmod_opt_init()* just before the calls to *xmin()* and *lmod()*.

| *keyword* | *default* | *meaning* |
|---|---|---|
| natm | | Number of atoms. |
| x[] | | Coordinate vector. User has to allocate memory in calling program and fill x[] with initial coordinates using, e.g., the setxyz_from_mol function (see sample program below). Array size = 3*natm. |
| g[] | | Gradient vector. User has to allocate memory in calling program. Array size = 3*natm. |
| ene | | On output, ene stores the global minimum energy. |
| conflib[] | | User allocated storage array where LMOD stores low-energy conformations. Array size = 3*natm*nconf. |

| *keyword* | *default* | *meaning* |
|---|---|---|
| lmod_traj[] | | User allocated storage array where LMOD stores snapshots of the pseudo trajectory drawn by LMOD on the potential energy surface. Array size = 3*natom * (nconf + 1). |
| lig_start[] | N/A | The serial number(s) of the first/last atom(s) of the ligand(s). The number(s) should correspond to the numbering in the NAB input files. Note that the ligand(s) can be anywhere in the atom list, however, a single ligand must have continuous numbering between the corresponding lig_start and lig_end values. The arrays should be allocated in the calling program. Array size = nlig, but in case nlig=0 there is no need for allocating memory. |
| lig_end[] | N/A | See above. |
| lig_cent[] | N/A | Similar array in all respects to lig_start/end, but the serial number(s) define the center of rotation. The value zero means that the center of rotation will be the geometric center of gravity of the ligand. |
| tr_min[] | N/A | The range of random translation/rotation applied to individual ligand(s). Rotation is carried out about the origin defined by the corresponding lig_cent value(s). The angle is given in +/- degrees and the distance in angstroms. The particular angles and distances are randomly chosen from their respective ranges. The arrays should be allocated in the calling program. Array size = *nlig*, but in case *nlig=0* there is no need to allocate memory. |
| tr_max[] | | See tr_min[], above. |
| rot_min[] | | See tr_min[], above. |
| rot_max[] | | See tr_min[], above. |
| niter | 10 | The number of LMOD iterations. Note that a single LMOD iteration involves a number of different computations (see section 1.5.2.). A value of zero results in a single local minimization; like a call to xmin. |
| nmod | 5 | The total number of low-frequency modes computed by LMOD every time such computation is requested. |
| minim_grms | 0.1 | The gradient RMS convergence criterion of structure minimization. |
| kmod | 3 | The definite number of randomly selected low-modes used to drive LMOD moves at each LMOD iteration step. |
| nrotran_dof | 6 | The number of rotational and translational degrees of freedom. This is related to the number of frozen or tethered atoms in the system: 0 atoms dof=6, 1 atom dof=3, 2 atoms dof=1, >=3 atoms dof=0. Default is 6, no frozen or tethered atoms. See section 1.5.7, note (5). |
| nconf | 10 | The maximum number of low-energy conformations stored in conflib[]. Note that the calling program is responsible for allocating memory for conflib[]. |
| energy_window | 50.0 | The energy window for conformation storage; the energy of a stored structure will be in the interval [global_min, global_min + energy_window]. |
| eig_recalc | 5 | The frequency, measured in LMOD iterations, of the recalculation of eigenvectors. |
| ndim_arnoldi | 0 | The dimension of the ARPACK Arnoldi factorization. The default, zero, specifies the whole space, that is, three times the number of atoms. See note below. |

| *keyword* | *default* | *meaning* |
|---|---|---|
| lmod_restart | 10 | The frequency, in LMOD iterations, of updating the conflib storage, that is, discarding structures outside the energy window, and restarting LMOD with a randomly chosen structure from the low-energy pool defined by n_best_struct below. A value >maxiter will prevent LMOD from doing any restarts. |
| n_best_struct | 10 | Number of the lowest-energy structures found so far at a particular LMOD restart point. The structure to be used for the restart will be chosen randomly from this pool. n_best_struct = 1 allows the user to explore the neighborhood of the then current global minimum. |
| mc_option | 1 | The Monte Carlo method.<br>1= Metropolis Monte Carlo (see rtemp below).<br>2= "Total_Quench", which means that the LMOD trajectory always proceeds towards the lowest lying neighbor of a particular energy well found after exhaustive search along all of the randomly selected kmod low-modes.<br>3= "Quick_Quench", which means that the LMOD trajectory proceeds towards the first neighbor found, which is lower in energy than the current point on the path, without exploring the remaining modes. |
| rtemp | 1.5 | The value of RT in NAB energy units. This is utilized in the Metropolis criterion. |
| lmod_step_size_min | 2.0 | The minimum length of a single LMOD ZIG move in Å. See section 1.5.2. |
| lmod_step_size_max | 5.0 | The maximum length of a single LMOD ZIG move in Å. See section 1.5.2. |
| nof_lmod_steps | 0 | The number of LMOD ZIG-ZAG moves. The default, zero, means that the number of ZIG-ZAG moves is not pre-defined, instead LMOD will attempt to cross the barrier in as many ZIG-ZAG moves as it is necessary. The criterion of crossing an energy barrier is stated above in section 1.5.2. nof_lmod_steps $> 0$ means that multiple barriers may be crossed and LMOD can carry the molecule to a large distance on the potential energy surface without severely distorting the geometry. |
| lmod_relax_grms | 1.0 | The gradient RMS convergence criterion of structure relaxation, see ZAG move in section 1.5.2. |
| nlig | 0 | Number of ligands considered for flexible docking. The default, zero, means no docking. |
| apply_rigdock | 2 | The frequency, measured in LMOD iterations, of the application of rigid-body rotational and translational motions to the ligand(s). At each apply_rigdock-th LMOD iteration nof_pose_to-try rotations and translations are applied to the ligand(s). |
| nof_poses_to_try | 10 | The number of rigid-body rotational and translational motions applied to the ligand(s). Such applications occur at each apply_rigdock-th LMOD iteration. In case nof_pose_to_try > 1, it is always the lowest energy pose that is kept, all other poses are discarded. |
| random_seed | 314159 | The seed of the random number generator. A value of zero requests hardware seeding based on the system clock. |

| *keyword* | *default* | *meaning* |
|---|---|---|
| print_level | 0 | Amount of debugging printout. 0= No output. 1= Basic output. 2= Detailed output. 3= Copious debugging output including ARPACK details. |
| lmod_time | N/A | CPU time in seconds used by LMOD itself. |
| aux_time | N/A | CPU time in seconds used by auxiliary routines. |
| error_flag | N/A | A nonzero value indicates an error. In case of an error LMOD will always print a descriptive error message. |

Notes on the *ndim_arnoldi* parameter: Basically, the ARPACK package used for the eigenvector calculations solves multiple "small" eigenvalue problems instead of a single "large" problem, which is the diagonalization of the three times the number of atoms by three times the number of atoms Hessian matrix. This parameter is the user specified dimension of the "small" problem. The allowed range is nmod + 1 <= ndim_arnoldi <= 3*natm. The default means that the "small" problem and the "large" problem are identical. This is the preferred, i.e., fastest, calculation for small to medium size systems, because ARPACK is guaranteed to converge in a single iteration. The ARPACK calculation scales with three times the number of atoms times the Arnoldi dimension squared and, therefore, for larger molecules there is an optimal ndim_arnoldi much less than three times the number of atoms that converges much faster in multiple iterations (possibly thousands or tens of thousands of iterations). The key to good performance is to select ndim_arnoldi such that all the ARPACK storage fits in memory. For proteins, ndim_arnoldi =1000 is generally a good value, but often a very small ∼50-100 Arnoldi dimension provides the fastest net computational cost with very many iterations.

### 1.5.6 Sample LMOD program

The following sample program, which is based on the test program tlmod.nab, reads a molecular structure from a PDB file, runs a short LMOD search, and saves the low-energy conformations in PDB files.

```
1  //   LMOD reverse communication external minimization package.
2  //   Written by Istvan Kolossvary.
3
4  #include "xmin_opt.h"
5  #include "lmod_opt.h"
6
7  // M A I N  P R O G R A M  to carry out LMOD simulation on a molecule/complex:
8
9  struct xmin_opt xo;
10 struct lmod_opt lo;
11
12 molecule mol;
13 int   natm;
14 float energy;
15 int lig_start[ dynamic ], lig_end[ dynamic ], lig_cent[ dynamic ];
16 float xyz[ dynamic ], grad[ dynamic ], conflib[ dynamic ], lmod_trajectory[ dynamic ];
17 float tr_min[ dynamic ], tr_max[ dynamic ], rot_min[ dynamic ], rot_max[ dynamic ];
18 float glob_min_energy;
19 point dummy;
20
21     lmod_opt_init( lo, xo );   //  set up defaults
22
23     lo.niter          = 3;     //  non-default options are here
24     lo.mc_option      = 2;
25     lo.nof_lmod_steps = 5;
26     lo.random_seed    = 99;
27     lo.print_level    = 2;
28
```

```
    xo.ls_maxatmov    = 0.15;

    mol = getpdb( "trpcage.pdb" );
    readparm( mol, "trpcage.top" );
    natm = mol.natoms;

    allocate xyz[ 3*natm ]; allocate grad[ 3*natm ];
    allocate conflib[ lo.nconf * 3*natm ];
    allocate lmod_trajectory[ (lo.niter+1) * 3*natm ];
    setxyz_from_mol( mol, NULL, xyz );

    mm_options( "ntpr=5000, gb=0, cut=999.0, nsnb=9999, diel=R ");
    mme_init( mol, NULL, "::ZZZ", dummy, NULL );

    mme( xyz, grad, 1 );
    glob_min_energy = lmod( natm, xyz, grad, energy,
          conflib, lmod_trajectory, lig_start, lig_end, lig_cent,
          tr_min, tr_max, rot_min, rot_max, xo, lo );

    printf( "\nGlob. min. E         = %12.3lf kcal/mol\n", glob_min_energy );


// E N D  M A I N
```

The corresponding screen output should look similar to this.

```
Reading parm file (trpcage.top)
title:

     mm_options:  ntpr=5000
     mm_options:  gb=0
     mm_options:  cut=999.0
     mm_options:  nsnb=9999
     mm_options:  diel=R
_____________________________________________________________________
                 Low-Mode Simulation
---------------------------------------------------------------------------
    1    E =     -118.117 ( 0.054)  Rg =    5.440
  1  / 6  E =     -89.2057 ( 0.090)  Rg =    2.625  rmsd=  8.240  p= 0.0000
  1  / 8  E =      -51.682 ( 0.097)  Rg =    5.399  rmsd=  8.217  p= 0.0000
  3  /12  E =     -120.978 ( 0.091)  Rg =    3.410  rmsd=  7.248  p= 1.0000
  3  /10  E =     -106.292 ( 0.099)  Rg =    5.916  rmsd=  4.829  p= 0.0004
  4  / 6  E =     -106.788 ( 0.095)  Rg =    4.802  rmsd=  3.391  p= 0.0005
  4  / 3  E =     -111.501 ( 0.097)  Rg =    5.238  rmsd=  2.553  p= 0.0121
---------------------------------------------------------------------------
    2    E =     -120.978 ( 0.091)  Rg =    3.410
  1  / 4  E =     -137.867 ( 0.097)  Rg =    2.842  rmsd=  5.581  p= 1.0000
  1  / 9  E =     -130.025 ( 0.100)  Rg =    4.282  rmsd=  5.342  p= 1.0000
  4  / 3  E =     -123.559 ( 0.089)  Rg =    3.451  rmsd=  1.285  p= 1.0000
  4  / 4  E =     -107.253 ( 0.095)  Rg =    3.437  rmsd=  2.680  p= 0.0001
  5  / 5  E =     -113.119 ( 0.096)  Rg =    3.136  rmsd=  2.074  p= 0.0053
  5  / 4  E =       -134.1 ( 0.091)  Rg =    3.141  rmsd=  2.820  p= 1.0000
---------------------------------------------------------------------------
    3    E =     -130.025 ( 0.100)  Rg =    4.282
  1  / 8  E =     -150.556 ( 0.093)  Rg =    3.347  rmsd=  5.287  p= 1.0000
  1  / 4  E =     -123.738 ( 0.079)  Rg =    4.218  rmsd=  1.487  p= 0.0151
  2  / 8  E =     -118.254 ( 0.095)  Rg =    3.093  rmsd=  5.296  p= 0.0004
  2  / 7  E =     -115.027 ( 0.090)  Rg =    4.871  rmsd=  4.234  p= 0.0000
```

```
  4  / 7  E =     -128.905 ( 0.099)  Rg =    4.171  rmsd=  2.113  p= 0.4739
  4  /11  E =      -133.85 ( 0.099)  Rg =    3.290  rmsd=  4.464  p= 1.0000

-------------------------------------------------------------------
 Full list:
       1  E =     -150.556 / 1  Rg =    3.347
       2  E =     -137.867 / 1  Rg =    2.842
       3  E =       -134.1 / 1  Rg =    3.141
       4  E =      -133.85 / 1  Rg =    3.290
       5  E =     -130.025 / 1  Rg =    4.282
       6  E =     -128.905 / 1  Rg =    4.171
       7  E =     -123.738 / 1  Rg =    4.218
       8  E =     -123.559 / 1  Rg =    3.451
       9  E =     -120.978 / 1  Rg =    3.410
      10  E =     -118.254 / 1  Rg =    3.093

Glob. min. E         =     -150.556 kcal/mol
```

The first few lines come from *mm_init()* and *mme()*. The screen output below the horizontal line originates from LMOD. Each LMOD-iteration is represented by a multi-line block of data numbered in the upper left corner by the iteration count. Within each block, the first line displays the energy and, in parentheses, the gradient RMS as well as the radius of gyration (assigning unit mass to each atom), of the current structure along the LMOD pseudo simulation-path. The successive lines within the block provide information about the LMOD ZIG-ZAG moves (see section 1.5.2). The number of lines is equal to 2 times kmod (2x3 in this example). Each selected mode is explored in both directions, shown in two separate lines. The leftmost number is the serial number of the mode (randomly selected from the set of nmod modes) and the number after the slash character gives the number of ZIG-ZAG moves taken. This is followed by, respectively, the minimized energy and gradient RMS, the radius of gyration, the RMSD distance from the base structure, and the Boltzmann probability with respect to the energy of the base structure and rtemp, of the minimized structure at the end of the ZIG-ZAG path. Note that exploring the same mode along both directions can result in two quite different structures. Also note that the number of ZIG-ZAG moves required to cross the energy barrier (see section 1.5.2) in different directions can vary quite a bit, too. Occasionally, an exclamation mark next to the energy (!E = ...) denotes a structure that could not be fully minimized.

After finishing all the computation within a block, the corresponding LMOD step is completed by selecting one of the ZIG-ZAG endpoint structures as the base structure of the next LMOD iteration. The selection is based on the *mc_option* and the Boltzmann probability. The LMOD pseudo simulation-path is defined by the series of these *mc_option*-selected structures and it is stored in *lmod_traj[]*. Note that the sample program saves these structures in a multi- PDB disk file called *lmod_trajectory.pdb*. The final section of the screen output lists the nconf lowest energy structures found during the LMOD search. Note that some of the lowest energy structures are not necessarily included in the *lmod_traj[]* list, as it depends on the *mc_option* selection. The list displays the energy, the number of times a particular conformation was found (increasing numbers are somewhat indicative of a more complete search), and the radius of gyration. The glob. min. energy is printed from the sample NAB program, not from LMOD. The sample program in *$AMBERHOME/AmberTools/examples/nab/lmod_dock* shows how one could write the top ten low-energy structures in separate, numbered PDB files.

As a final note, it is instructive to be aware of a simple safeguard that LMOD applies . A copy of the *conflib[]* array is saved periodically in a binary disk file called *conflib.dat*. Since LMOD searches might run for a long time, in case of a crash low-energy structures can be recovered from this file. The format of *conflib.dat* is as follows. Each conformation is represented by 3 numbers (double energy, double radius of gyration, and int number of times found), followed by the double (x, y, z) coordinates of the atoms.

### 1.5.7 Tricks of the trade of running LMOD searches

1. The AMBER atom types HO, HW, and ho all have zero van der Waals parameters in all of the AMBER (and some other) force fields. Corresponding Aij and Bij coefficients in the PRMTOP file are set to zero. This means there is no repulsive wall to prevent two oppositely charged atoms, one being of type HO,

HW or ho, to fuse as a result of the ever decreasing electrostatic energy as they come closer and closer to each other. This potential problem is rarely manifest in molecular dynamics simulations, but it presents a nuisance when running LMOD searches. The problem is local minimization, especially "aggressive" TNCG minimization (XMIN xo.method=3) that can easily result in atom fusion. Therefore, before running an LMOD simulation, the PRMTOP file (let's call it prmtop.in) must be processed by running the script "lmodprmtop prmtop.in prmtop.out". This script will replace all the repulsive Aij coefficients set to zero in prmtop.in with a high value of 1e03 in prmtop.out in order to re-create the van der Waals wall. It is understood that this procedure is parameter fudging; however, note that the primary goal of using LMOD is the quick generation of approximate, low-energy structures that can be further refined by high-accuracy MD.

2. LMOD requires that the potential energy surface is continuous everywhere to a great degree. Therefore, always use a distance dependent dielectric constant in mm_options when running searches in vacuo, or use GB solvation (note that GB calculations will be slow), and always apply a large cut-off. It does make sense to run quick and dirty LMOD searches in vacuo to generate low-energy starting structures for MD runs. Note that the most likely symptom of discontinuities causing a problem is when your NAB program utilizing LMOD is grabbing CPU time, but the LMOD search does not seem to progress. This is the result of NaN's that often can be seen when print_level is set to $> 0$.

3. LMOD is NOT INTENDED to be used with explicit water models and periodic boundary conditions. Although explicit-water solvation representation is not recommended, LMOD docking can be readily used with crystallographic water molecules as ligands.

4. Conformations in the conflib and lmod_trajectory files can have very different orientations. One trick to keep them in a common orientation is to restrain the position of, e.g., a single benzene ring. This will ensure that the molecule cannot be translated or rotated as a whole. However, when applying this trick you should set nrotran_dof = 0.

5. A subset of the atoms of a molecular system can be frozen or tethered/restrained in NAB by two different methods. Atoms can either be frozen by using the first atom expression argument in *mme_init()* or restrained by using the second atom expression argument and the reference coordinate array in *mme_init()* along with the *wcons* option in mm_options. LMOD searches, especially docking calculations can be run much faster if parts of the molecular system can be frozen, because the effective degrees of freedom is determined by the size of the flexible part of the system. Application of frozen atoms means that a much smaller number of moving atoms are moving in the fixed, external potential of the frozen atoms. The tethered atom model is expected to give similar results to the frozen atom model, but note that the number of degrees of freedom and, therefore, the computational cost of a tethered calculation is comparable to that of a fully unrestrained system. However, the eigenvector calculations are likely to converge faster with the tethered systems.

## 1.6 The Generalized Born with Hierarchical Charge Partitioning (GB-HCP)

GB-HCP (and its latest version, GB-HCPO[20] ) is a multi-scale, yet fully atomistic, approach to perform MD simulations based on the generalized Born model, mainly intended for large and very large structures. For example, it was used to refine a 1.1M atom structure of 30nm chromatin fiber[20]. Compared to the reference GB model without further approximations, GB-HCP can deliver up to 3 orders of magnitude speedup, depending on structure size. In contrast to cutoff GB that completely ignores the effect of long range electrostatic interactions beyond a certain distance, which can lead to serious artifacts under many circumstances such as for highly charged systems, GB-HCP takes into account the long range electrostatic interactions by using N log N Hierarchical Charge Partitioning (HCP) approximation [21, 22]. Based on this method, structures are partitioned into multiple hierarchical levels of components using the natural organization of the biomolecular structures - atoms, groups, chains, and complexes. The charge distribution for each of these components is approximated by 1 (hcp=1) or 2 (hcp=2 and hcp=4) charges. Setting hcp=4 (strongly recommended) uses GB-HCPO, which takes advantage of the Optimal Point Charge Approximation approach for placing the approximate point charges[23]: two point charges are placed so that the three lowest order multipole moments of the reference charge distribution are optimally reproduced. The

Figure 1.1: *The HCP threshold distance. For the level 1 approximation shown here, groups within the threshold distance are treated exactly using atomic charges, while groups beyond the threshold distance are approximated by a small number of charges, e.g. 1 charge for hcp=1 shown here.*

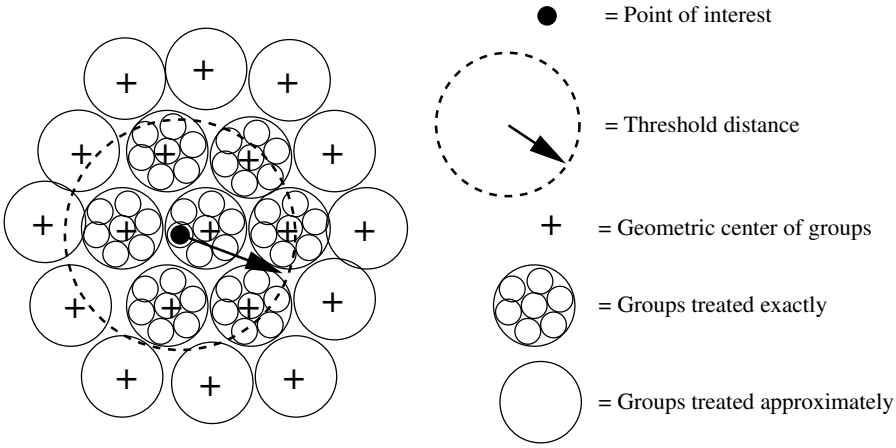


approximate charges are then used for computing electrostatic interactions with distant components while the full set of atomic charges are used for nearby components (Figure 40.1). The HCP can be used for generalized Born (gb=1-8) simulations, for gas phase (dielec=C) and distant dependent dielectric (dielec=R/RL), with or without Langevin dynamics (gamma_ln>0).

The usage of the new feature (hcp=4) requires that the separation between the two charges used to approximate the uncharged components is specified by dhcp. The value of dhcp is empirically adjusted so that the RMS error in force, compared to the GB without further approximation, is minimized. Our testing on a various set of structures suggests that dhcp=0.25 is optimal for many systems. However, if further accuracy is desired for specific systems, the value for dhcp can be further optimized within the range of 0.1 and 0.4 following the steps below. To find the optimal value for hcp, one time step simulation for the starting configuration of the structure can be performed using the GB model without approximation (hcp=0), and with e_debug=1setting, that automatically prints out the forces on each atom into a text file called reference.frc. Rename reference.frc to exact.frc. Then, run one step of the starting configuration of the structure using the GB-HCP (hcp=4) by setting the dhcp parameter within the range of 0.1 and 0.4 in increments of 0.05. The reference.frc file produced for each value of dhcp can be compared to the exact.frc to compute the RMS error in force. The following command line computes the RMS error:

```
paste exact.frc reference.frc | awk '{x+=($9-$20)^2+($10-$21)^2+($11-$22)^2}END{print sqrt(x/NR)}'
```

The optimal value for dhcp is the one that results in minimum RMS error in the force.

### 1.6.1 Level 1 HCP approximation

The HCP option can now be used with one level of approximation (groups) using NAB molecular dynamics scripts. No additional manipulation of the input structure files is required for one level of approximation. For an example see AmberTools/examples/hcp/2trx.nab. The level 1 approximation is recommended for single domain and small (< 10,000 atoms) multi-domain structures. Speedups of 2x-10x can be realized using the level 1 approximation, depending on structure size.

### 1.6.2 Level 2 and 3 HCP approximation

For larger multi-domain structures higher levels of approximations (chains and complexes) can be used to achieve up to 3 orders of magnitude speedups, depending on structure size. The following additional steps are

required to include information about these higher level components in the prmtop file. For an example see AmberTools/examples/hcp/1kx5.nab. A fully working example (including the MD run scripts) of a 3 level partitioning of a giant structure, one million atom chromatin fiber, can be found at http://people.cs.vt.edu/onufriev/software.php.

1. Ensure the pdb file identifies the higher level structures: Chains (level 2) separated by TER, and Complexes (level 3) separated by REMARK END-OF-COMPLEX:
   ...
   ATOM ...
   TER (end of chain)
   ATOM ...
   ...
   ATOM ...
   TER (end of chain)
   REMARK END-OF-COMPLEX
   ATOM ...
2. Execute hcp_getpdb to generate prmtop entries for HCP: hcp_getpdb pdb-filename hcp-prmtop
3. Concatenate the HCP prmtop entries to the end of the standard prmtop file generated by LEaP: cat prmtop-file hcp-prmtop > new-prmtop
4. Use this new prmtop file in the NAB molecular dynamics scripts instead of the prmtop file generated by LEaP

# Bibliography


[1] R. Brown; D. Case. Second derivatives in generalized Born theory. *J. Comput. Chem.*, **2006**, *27*, 1662–1675.

[2] H. J. C. Berendsen; J. P. M. Postma; W. F. van Gunsteren; A. DiNola; J. R. Haak. Molecular dynamics with coupling to an external bath. *J. Chem. Phys.*, **1984**, *81*, 3684–3690.

[3] R. J. Loncharich; B. R. Brooks; R. W. Pastor. Langevin dynamics of peptides: The frictional dependence of isomerization rates of N-actylananyl-N'-methylamide. *Biopolymers*, **1992**, *32*, 523–535.

[4] C. Brooks; A. Brünger; M. Karplus. Active site dynamics in protein molecules: A stochastic boundary molecular-dynamics approach. *Biopolymers*, **1985**, *24*, 843–865.

[5] V. Tsui; D. A. Case. Theory and applications of the generalized Born solvation model in macromolecular simulations. *Biopolymers (Nucl. Acid. Sci.)*, **2001**, *56*, 275–291.

[6] A. Onufriev; D. Bashford; D. A. Case. Modification of the generalized Born model suitable for macromolecules. *J. Phys. Chem. B*, **2000**, *104*, 3712–3720.

[7] A. Onufriev; D. Bashford; D. A. Case. Exploring protein native states and large-scale conformational changes with a modified generalized Born model. *Proteins*, **2004**, *55*, 383–394.

[8] J. Mongan; C. Simmerling; J. A. McCammon; D. A. Case; A. Onufriev. Generalized Born with a simple, robust molecular volume correction. *J. Chem. Theory Comput.*, **2007**, *3*, 156–169.

[9] J. Weiser; P. S. Shenkin; W. C. Still. Approximate Atomic Surfaces from Linear Combinations of Pairwise Overlaps (LCPO). *J. Comput. Chem.*, **1999**, *20*, 217–230.

[10] J. Johnson; D. A. Case; T. Yamazaki; S. Gusarov; A. Kovalenko; T. Luchko. Small molecule solvation energy and entropy from 3D-RISM. *J. Phys. Condens. Mat.*, **2016**.

[11] D. T. Nguyen; D. A. Case. On finding stationary states on large-molecule potential energy surfaces. *J. Phys. Chem.*, **1985**, *89*, 4020–4026.

[12] I. Kolossváry; W. C. Guida. Low mode search. An efficient, automated computational method for conformational analysis: Application to cyclic and acyclic alkanes and cyclic peptides. *J. Am. Chem. Soc.*, **1996**, *118*, 5011–5019.

[13] I. Kolossváry; W. C. Guida. Low-mode conformational search elucidated: Application to $C_{39}H_{80}$ and flexible docking of 9-deazaguanine inhibitors into PNP. *J. Comput. Chem.*, **1999**, *20*, 1671–1684.

[14] I. Kolossváry; G. M. Keserü. Hessian-free low-mode conformational search for large-scale protein loop optimization: Application to c-jun N-terminal kinase JNK3. *J. Comput. Chem.*, **2001**, *22*, 21–30.

[15] G. M. Keserü; I. Kolossváry. Fully flexible low-mode docking: Application to induced fit in HIV integrase. *J. Am. Chem. Soc.*, **2001**, *123*, 12708–12709.

[16] Z. J. Shi; J. Shen. New inexact line search method for unconstrained optimization. *J. Optim. Theory Appl.*, **2005**, *127*, 425–446.

[17] W. H. Press; B. P. Flannery; S. A. Teukolsky; W. T. Vetterling. *Numerical Recipes: The Art of Scientific Computing*. Cambridge University Press, New York, 1989.

[18] D. C. Liu; J. Nocedal. On the limited memory method for large scale optimization. *Math. Programming B*, **1989**, *45*, 503–528.

[19] J. Nocedal; J. L. Morales. Automatic preconditioning by limited memory quasi-Newton updating. *SIAM J. Opt.*, **2000**, *10*, 1079–1096.

[20] S. Izadi; R. Anandakrishnan; A. V. Onufriev. Implicit solvent model for Million-Atom atomistic simulations: Insights into the organization of 30-nm chromatin fiber. *J. Chem. Theory Comput.*, **2016**, *12*, 5946–5959.

[21] R. Anandakrishnan; A. V. Onufriev. An N log N approximation based on the natural organization of biomolecules for speeding up the computation of long range interactions. *J. Comput. Chem.*, **2010**, *31*, 691–706.

[22] R. Anandakrishnan; M. Daga; A. V. Onufriev. An n log n Generalized Born Approximation. *J. Chem. Theory Comput.*, **2011**, *7*, 544–559.

[23] R. Anandakrishnan; C. Baker; S. Izadi; A. V. Onufriev. Point charges optimally placed to represent the multipole expansion of charge distributions. *PloS one*, **2013**, *8*, e67715.

[24] F. Hirata. In *Molecular Theory of Solvation* [537], chapter 1.

[25] A. Kovalenko. In Hirata [537], chapter 4.

[26] J. I. Mendieta-Moreno; R. C. Walker; J. P. Lewis; P. Gómez-Puertas; J. Mendieta; J. Ortega. FIREBALL/AMBER: An efficient local-orbital DFT QM/MM method for biomolecular systems. *J. Chem. Theory Comput.*, **2014**, *10*, 2185–2193.

[27] J. P. Lewis; P. Jelínek; J. Ortega; A. A. Demkov; D. G. Trabada; B. Haycock; H. Wang; G. Adams; J. K. Tomfohr; E. Abad; H. Wang; D. A. Drabold. Advances and applications in the FIREBALL ab initio tight-binding molecular-dynamics formalism. *Phys. Status Solidi B*, **2011**, *248*, 1989–2007.

[28] M. Kállay; Z. Rolik; J. Csontos; I. Ladjánszki; L. Szegedy; B. Ladoćzki; G. Samu; K. Petrov; M. Farkas; P. Nagy; D. Mester; B. Hegely. Mrcc, a quantum chemical program suite. www.mrcc.hu.

[29] S. N. Steinmann; R. Ferreira de Morais; A. W. Götz; P. Fleurat-Lessard; M. Iannuzzi; P. Sautet; C. Michel. *J. Chem. Theory Comput.*, **2018**.

[30] S. N. Steinmann; P. Fleurat-Lessard; A. W. Götz; C. Michel; R. Ferreira de Morais; P. Sautet. Molecular mechanics models for the image charge, a comment on "including image charge effects in the molecular dynamics simulations of molecules on metal surfaces". *J. Comput. Chem.*, **2017**, *38*, 2127–2129.

[31] Z. Rolik; L. Szegedy; I. Ladjánszki; B. Ladóczki; M. Kállay. An efficient linear-scaling CCSD(T) method based on local natural orbitals. *J. Chem. Phys.*, **2013**, *139*, 094105.

[32] B. Hégely; P. R. Nagy; G. G. Ferenczy; M. Kállay. Exact density functional and wave function embedding schemes based on orbital localization. *J. Chem. Phys.*, **2016**, *145*, 064107.

[33] M. Gaus; Q. Cui; M. Elstner. DFTB3: Extension of the self-consistent-charge density-functional tight-binding method (SCC-DFTB). *J. Chem. Theory Comput.*, **2011**, *7*, 931–948.

[34] Å. Skjevik; B. D. Madej; C. J. Dickson; C. Lin; K. Teigen; R. C. Walker; I. R. Gould. Simulations of lipid bilayer self-assembly using all-atom lipid force fields. *Phys. Chem. Chem. Phys.*, **2016**, *18*, 10573–10584.

[35] Å. Skjevik; B. D. Madej; C. J. Dickson; K. Teigen; R. C. Walker; I. R. Gould. All-atom lipid bilayer self-assembly with the amber and charmm lipid force fields. *Chem. Commun.*, **2015**, *51*, 4402–4405.

[36] H. T. Nguyen; S. A. Pabit; S. P. Meisburger; L. Pollack; D. A. Case. Accurate small and wide angle X-ray scattering profiles from atomic models of proteins and nucleic acids. *J. Chem. Phys.*, **2014**, *141*, 22D508.

[37] S. Park; J. P. Bardhan; B. Roux; L. Makowski. Simulated X-ray scattering of protein solutions using explicit-solvent models. *J. Chem. Phys.*, **2009**, *130*, 134114.

[38] Y. Shao; L. Fusti-Molnar; Y. Jung; J. Kussmann; C. Ochsenfeld; S. T. Brown; A. T. B. Gilbert; L. V. Slipchenko; S. V. Levchenko; D. P. O'Neill; R. A. DiStasio, Jr.; R. C. Lochan; T. Wang; G. J. O. Beran; N. A. Besley; J. M. Herbert; C. Y. Lin; T. V. Voorhis; S. H. Chien; A. Sodt; R. P. Steele; V. A. Rassolov; P. E. Maslen; P. P. Korambath; R. D. Adamson; B. Austin; J. Baker; E. F. C. Byrd; H. Daschel; R. J. Doerksen; A. Dreuw; B. D. Dunietz; A. D. Dutoi; T. R. Furlani; S. R. Gwaltney; A. Heyden; S. Hirata; C.-P. Hsu; G. Kedziora; R. Z. Khaliullin; P. Klunzinger; A. M. Lee; M. S. Lee; W. Liang; I. Lotan; N. Nair; B. Peters; E. I. Proynov; P. A. Pieniazek; Y. M. Rhee; J. Ritchie; E. Rosta; C. D. Sherrill; A. C. Simmonett; J. E. Subotnik; H. L. Woodcock, III; W. Zhang; A. T. Bell; A. K. Chakraborty; D. M. Chipman; F. J. Keil; A. Warshel; W. J. Hehre; H. F. Schaefer, III; J. Kong; A. I. Krylov; P. M. W. Gill; M. Head-Gordon. Advances in methods and algorithms in a modern quantum chemistry program package. *Phys. Chem. Chem. Phys.*, **2006**, *8*, 3172–3191.

[39] R. Assaraf; M. Caffarel; A. C. Kollias. Chaotic versus nonchaotic stochastic dynamics in monte carlo simulations: A route for accurate energy differences in n-body systems. *Phys. Rev. Lett.*, **2011**, *106*, 150601.

[40] K. Park; A. W. Götz; R. C. Walker; F. Paesani. Application of adaptive qm/mm methods to molecular dynamics simulations of aqueous systems. *J. Chem. Theory Comput.*, **2012**, *8*, 2868–2877.

[41] R. E. Bulo; C. Michel; P. Fleurat-Lessard; P. Sautet. Multiscale modeling of chemistry in water: Are we there yet? *J. Chem. Theory Comput.*, **2013**, *9*, 5567–5577.

[42] R. E. Bulo; B. Ensing; J. Sikkema; L. Visscher. Toward a practical method for adaptive qm/mm simulations. *J. Chem. Theory Comput.*, **2009**, *9*, 2212–2221.

[43] A. W. Götz; M. A. Clark; R. C. Walker. An extensible interface for QM/MM molecular dynamics simulations with AMBER. *J. Comput. Chem.*, **2014**, *35*, 95–108.

[44] B. E. Hingerty; S. Figueroa; T. L. Hayden; S. Broyde. Prediction of DNA Structure from Sequence: A Build-up Technique. *Biopolymers*, **1989**, *28*, 1195–1222.

[45] P. Jurecka; J. Cerný; P. Hobza; D. R. Salahub. Density functional theory augmented with an empirical dispersion term. Interaction energies and geometries of 80 noncovalent complexes compared with ab initio quantum mechanics calculations. *J. Comp. Chem.*, **2007**, *28*, 555–569.

[46] M. Korth. Third-generation hydrogen-bonding corrections for semiempirical qm methods and force fields. *J. Chem. Theory Comput.*, **2010**, *6*, 3808.

[47] M. Korth; M. Pitonak; J. Rezac; P. Hobza. A transferable h-bonding correction for semiempirical quantum-chemical methods. *J. Chem. Theory Comput.*, **2010**, *6*, 344–352.

[48] W. Thiel; A. A. Voityuk. Extension of the MNDO formalism to d orbitals: Integral approximations and preliminary numerical results. *Theoret. Chim. Acta*, **1992**, *81*, 391–404.

[49] W. Thiel; A. A. Voityuk. Erratum: Extension of MNDO to d orbitals: Parameters and results for the second-row elements and for the zinc group. *J. Phys. Chem.*, **1996**, *100*, 616–626.

[50] W. Thiel; A. A. Voityuk. Extension of the MNDO formalism to d orbitals: Integral approximations and preliminary numerical results. *Theoret. Chim. Acta*, **1996**, *93*, 315.

[51] D. A. Erie; K. J. Breslauer; W. K. Olson. A Monte Carlo Method for Generating Structures of Short Single-Stranded DNA Sequences. *Biopolymers*, **1993**, *33*, 75–105.

[52] D. A. Pearlman; S.-H. Kim. Conformational Studies of Nucleic Acids I. A Rapid and Direct Method for Generating Coordinates from the Pseudorotation Angle. *J. Biomol. Struct. Dyn.*, **1985**, *3*, 85–98.

[53] D. A. Pearlman; S.-H. Kim. Conformational Studies of Nucleic Acids II. The Conformational Energetics of Commonly Occurring Nucleosides. *J. Biomol. Struct. Dyn.*, **1985**, *3*, 99–125.

[54] D. A. Pearlman; S.-H. Kim. Conformational Studies of Nucleic Acids: III. Empirical Multiple Correlation Functions for Nucleic Acid Torsion Angles. *J. Biomol. Struct. Dyn.*, **1986**, *4*, 49–67.

[55] D. A. Pearlman; S.-H. Kim. Conformational Studies of Nucleic Acids: IV. The Conformational Energetics of Oligonucleotides: d(ApApApA) and ApApApA. *J. Biomol. Struct. Dyn.*, **1986**, *4*, 69–98.

[56] D. A. Pearlman; S.-H. Kim. Conformational Studies of Nueleic Acids. V. Sequence Specificities of in the Conformational Energetics of Oligonucleotides: The Homo-Tetramers. *Biopolymers*, **1988**, *27*, 59–77.

[57] T. Schlick. A Modular Strategy for Generating Starting Conformations and Data Structures of Polynucleotide Helices for Potential Energy Calculations. *J. Comput. Chem.*, **1988**, *9*, 861–889.

[58] J. Gabarro-Arpa; J. A. H. Cognet; M. Le Bret. Object Command Language: a formalism to build molecule models and to analyze structural parameters in macromolecules, with applications to nucleic acids. *J. Mol. Graph.*, **1992**, *10*, 166–173.

[59] R. Lavery. in *Unusual DNA Structures*, R. D. Wells; S. C. Harvey, Eds. Springer-Verlag, New York, 1988.

[60] L. Shen; I. Tinoco. The Structure of an RNA Pseudoknot that Causes Efficient Frameshift in Mouse Mammary Tumor Virus. *J. Mol. Biol.*, **1995**, *247*, 963–978.

[61] J. M. Hubbard; J. E. Hearst. Predicting the Three-Dimensional Folding of Transfer RNA with a Computer Modeling Protocol. *Biochemistry*, **1991**, *30*, 5458–5465.

[62] S.-H. Chou; L. Zhu; B. R. Reid. The Unusual Structure of the Human Centromere (GGA)2 Motif. *J. Mol. Biol.*, **1994**, *244*, 259–268.

[63] M. Levitt. Detailed Molecular Model for Transfer Ribonucleic Acid. *Nature*, **1969**, *224*, 759–763.

[64] M. S. Babcock; E. P. D. Pednault; W. K. Olson. Nucleic Acid Structure Analysis. *J. Mol. Biol.*, **1994**, *237*, 125–156.

[65] J. M. Hubbard; J. E. Hearst. Computer Modeling 16S Ribosomal RNA. *J. Mol. Biol.*, **1991**, *221*, 889–907.

[66] F. Major; M. Turcotte; D. Gautheret; G. Lapalme; E. Fillon; R. Cedergren. The Combination of Symbolic and Numerical Computation for Three-Dimensional Modeling of RNA. *Science*, **1991**, *253*, 1255–1260.

[67] T. Schlick; W. K. Olson. Supercoiled DNA Energetics and Dynamics by Computer Simulation. *J. Mol. Biol.*, **1992**, *223*, 1089–1119.

[68] R. E. Dickerson. Definitions and Nomenclature of Nucleic Acid Structure Parameters. *J. Biomol. Struct. Dyn.*, **1989**, *6*, 627–634.

[69] S. R. Holbrook; J. L. Sussman; R. W. Warrant; S.-H. Kim. Crystal Structure of Yeast Phenylalanine Transfer RNA II. Structural Features and and Functional Implications. *J. Mol. Biol.*, **1978**, *123*, 631–660.

[70] B. N. Conner; C. Yoon; J. Dickerson; R. E. Dickerson. Helix Geometry and Hydration in an A-DNA Tetramer: C-C-G-G. *J. Mol. Biol.*, **1984**, *174*, 663–695.

[71] M. Le Bret; J. Gabarro-Arpa; J. C. Gilbert; C. Lemarechal. MORCAD an object-oriented molecular modeling package. *J. Chim. Phys.*, **1991**, *88*, 2489–2496.

[72] V. B. Zhurkin; Y. P. Lysov; V. I. Ivanov. Different Families of Double Stranded Conformations of DNA as Revealed by Computer Calculations. *Biopolymers*, **1978**, *17*, 277–312.

[73] A. T. Brünger. *X-PLOR: A System for Crystallography and NMR, Version 3.1*. Yale University, New Haven, CT, 1992.

[74] J. R. Wyatt; J. D. Puglisi; I. Tinoco Jr. RNA Pseudoknots. Stability and Loop Size Requirements. *J. Mol. Biol.*, **1990**, *214*, 455–470.

[75] J. D. Puglisi; J. R. Wyatt; I. Tinoco Jr. Conformation of an RNA Pseudoknot. *J. Mol. Biol.*, **1990**, *214*, 437–453.

[76] G. Kuila; J. A. Fee; J. R. Schoonover; W. H. Woodruff. Resonance Raman Spectra of the [2Fe-2S] Clusters of the Rieske Protein from Thermus and Phthalate Dioxygenase from Pseudomonas. *J. Am. Chem. Soc.*, **1987**, *109*, 1559–1561.

[77] B. Lewin. in *Genes IV*, pp 409–425. Cell Press, Cambridge, Mass., 1990.

[78] W. H. Press; S. A. Teukolsky; W. T. Vettering; B. P. Flannery. in *Numerical Recipes in C*, pp 113–117. Cambridge, New York, 1992.

[79] V. B. Zhurkin; G. Raghunathan; N. B. Ulynaov; R. D. Camerini-Otero; R. L. Jernigan. A Parallel DNA Triplex as a Model for the Intermediate in Homologous Recombination. *J. Mol. Biol.*, **1994**, *239*, 181–200.

[80] W. Saenger. in *Principles of Nucleic Acid Structure*, p 120. Springer-Verlag, New York, 1984.

[81] M. Turcotte; G. Lapalme; F. Major. Exploring the conformations of nucleic acids. *J. Funct. Program.*, **1995**, *5*, 443–460.

[82] C.-S. Tung; E. S. Carter, II. Nucleic acid modeling tool (NAMOT): an interactive graphic tool for modeling nucleic acid structures. *CABIOS*, **1994**, *10*, 427–433.

[83] E. S. Carter, II; C.-S. Tung. NAMOT2–a redesigned nucleic acid modeling tool: construction of non-canonical DNA structures. *CABIOS*, **1996**, *12*, 25–30.

[84] R. Lavery; K. Zakrzewska; H. Skelnar. JUMNA (junction minimisation of nucleic acids). *Comp. Phys. Commun.*, **1995**, *91*, 135–158.

[85] G. M. Crippen; T. F. Havel. *Distance Geometry and Molecular Conformation*. Research Studies Press, Taunton, England, 1988.

[86] D. C. Spellmeyer; A. K. Wong; M. J. Bower; J. M. Blaney. Conformational analysis using distance geometry methods. *J. Mol. Graph. Model.*, **1997**, *15*, 18–36.

[87] M. E. Hodsdon; J. W. Ponder; D. P. Cistola. The NMR solution structure of intestinal fatty acid-binding protein complexed with palmitate: Application of a novel distance geometry algorithm. *J. Mol. Biol.*, **1996**, *264*, 585–602.

[88] T. Macke; S.-M. Chen; W. J. Chazin. in *Structure and Function, Volume 1: Nucleic Acids*, R. H. Sarma; M. H. Sarma, Eds., pp 213–227. Adenine Press, Albany, 1992.

[89] B. C. M. Potts; J. Smith; M. Akke; T. J. Macke; K. Okazaki; H. Hidaka; D. A. Case; W. J. Chazin. The structure of calcyclin reveals a novel homodimeric fold S100 $Ca^{2+}$-binding proteins. *Nature Struct. Biol.*, **1995**, *2*, 790–796.

[90] J. J. Love; X. Li; D. A. Case; K. Giese; R. Grosschedl; P. E. Wright. DNA recognition and bending by the architectural transcription factor LEF-1: NMR structure of the HMG domain complexed with DNA. *Nature*, **1995**, *376*, 791–795.

[91] T. J. Giese; D. M. York. Charge-dependent model for many-body polarization, exchange, and dispersion interactions in hybrid quantum mechanical/molecular mechanical calculations. *J. Chem. Phys.*, **2007**, *127*, 194101–194111.

[92] R. J. Gurbiel; P. E. Doan; G. T. Gassner; T. J. Macke; D. A. Case; T. Ohnishi; J. A. Fee; D. P. Ballou; B. M. Hoffman. Active site structure of Rieske-type proteins: Electron nuclear double resonance studies of isotopically labeled phthalate dioxygenase from *Pseudomonas cepacia and Rieske protein from Rhodobacter capsulatus* and molecular modeling studies of a Rieske center. *Biochemistry*, **1996**, *35*, 7834–7845.

[93] T. J. Macke. *NAB, a Language for Molecular Manipulation*. Ph.D. thesis, The Scripps Research Institute, 1996.

[94] D. Gautheret; F. Major; R. Cedergren. Modeling the three-dimensional structure of RNA using discrete nucleotide conformational sets. *J. Mol. Biol.*, **1993**, *229*, 1049–1064.

[95] R. Tan; S. Harvey. Molecular Mechanics Model of Supercoiled DNA. *J. Mol. Biol.*, **1989**, *205*, 573–591.

[96] T. F. Havel. An evaluation of computational strategies for use in the determination of protein structure from distance constraints obtained by nuclear magnetic resonance. *Prog. Biophys. Mol. Biol.*, **1991**, *56*, 43–78.

[97] J. Kuszewski; M. Nilges; A. T. Brünger. Sampling and efficiency of metric matrix distance geometry: A novel partial metrization algorithm. *J. Biomolec. NMR*, **1992**, *2*, 33–56.

[98] B. L. deGroot; D. M. F. van Aalten; R. M. Scheek; A. Amadei; G. Vriend; H. J. C. Berendsen. Prediction of protein conformational freedom from distance constraints. *Proteins*, **1997**, *29*, 240–251.

[99] T. F. Havel; I. D. Kuntz; G. M. Crippen. The theory and practice of distance geometry. *Bull. Math. Biol.*, **1983**, *45*, 665–720.

[100] D. K. Agrafiotis. Stochastic Proximity Embedding. *J. Comput. Chem.*, **2003**, *24*, 1215–1221.

[101] D. A. Pearlman; D. A. Case; J. W. Caldwell; W. S. Ross; T. E. Cheatham, III; S. DeBolt; D. Ferguson; G. Seibel; P. Kollman. AMBER, a package of computer programs for applying molecular mechanics, normal mode analysis, molecular dynamics and free energy calculations to simulate the structural and energetic properties of molecules. *Comp. Phys. Commun.*, **1995**, *91*, 1–41.

[102] S. Harvey; J. A. McCammon. *Dynamics of Proteins and Nucleic Acids*. Cambridge University Press, Cambridge, 1987.

[103] M. P. Allen; D. J. Tildesley. *Computer Simulation of Liquids*. Clarendon Press, Oxford, 1987.

[104] D. Frenkel; B. Smit. *Understanding Molecular Simulation: From Algorithms to Applications. Second edition*. Academic Press, San Diego, 2002.

[105] W. F. van Gunsteren; P. K. Weiner; A. J. Wilkinson, eds. *Computer Simulations of Biomolecular Systems, Vol. 3.* ESCOM Science Publishers, Leiden, 1997.

[106] W. F. van Gunsteren; P. K. Weiner; A. J. Wilkinson, eds. *Computer Simulations of Biomolecular Systems, Vol. 2.* ESCOM Science Publishers, Leiden, 1993.

[107] L. R. Pratt; G. Hummer, eds. *Simulation and Theory of Electrostatic Interactions in Solution*. American Institute of Physics, Melville, NY, 1999.

[108] J. Wang; P. Cieplak; P. A. Kollman. How well does a restrained electrostatic potential (RESP) model perform in calculating conformational energies of organic and biological molecules? *J. Comput. Chem.*, **2000**, *21*, 1049–1074.

[109] R. W. Dixon; P. A. Kollman. Advancing beyond the atom-centered model in additive and nonadditive molecular mechanics. *J. Comput. Chem.*, **1997**, *18*, 1632–1646.

[110] W. D. Cornell; P. Cieplak; C. I. Bayly; I. R. Gould; K. M. Merz, Jr.; D. M. Ferguson; D. C. Spellmeyer; T. Fox; J. W. Caldwell; P. A. Kollman. A second generation force field for the simulation of proteins, nucleic acids, and organic molecules. *J. Am. Chem. Soc.*, **1995**, *117*, 5179–5197.

[111] M. D. Beachy; R. A. Friesner. Accurate ab intio quantum chemical determination of the relative energies of peptide conformations and assessment of empirical force fields. *J. Am. Chem. Soc.*, **1997**, *119*, 5908–5920.

[112] P. A. Kollman; R. Dixon; W. Cornell; T. Fox; C. Chipot; A. Pohorille. in *Computer Simulation of Biomolecular Systems, Vol. 3*, A. Wilkinson; P. Weiner; W. F. van Gunsteren, Eds., pp 83–96. Elsevier, 1997.

[113] J. Higo; N. Ito; M. Kuroda; S. Ono; N. Nakajima; H. Nakamura. Energy landscape of a peptide consisting of $\alpha$-helix, $3_{10}$ helix, $\beta$-turn, $\beta$-hairpin and other disordered conformations. *Prot. Sci.*, **2001**, *10*, 1160–1171.

[114] L. Wang; Y. Duan; R. Shortle; B. Imperiali; P. A. Kollman. Study of the stability and unfolding mechanism of BBA1 by molecular dynamics simulations at different temperatures. *Prot. Sci.*, **1999**, *8*, 1292–1304.

[115] T. E. Cheatham, III; P. Cieplak; P. A. Kollman. A modified version of the Cornell et al. force field with improved sugar pucker phases and helical repeat. *J. Biomol. Struct. Dyn.*, **1999**, *16*, 845–862.

[116] S. J. Weiner; P. A. Kollman; D. A. Case; U. C. Singh; C. Ghio; G. Alagona; S. Profeta, Jr.; P. Weiner. A new force field for molecular mechanical simulation of nucleic acids and proteins. *J. Am. Chem. Soc.*, **1984**, *106*, 765–784.

[117] S. J. Weiner; P. A. Kollman; D. T. Nguyen; D. A. Case. An all-atom force field for simulations of proteins and nucleic acids. *J. Comput. Chem.*, **1986**, *7*, 230–252.

[118] J. Åqvist. Ion-water interaction potentials derived from free energy perturbation simulations. *J. Phys. Chem.*, **1990**, *94*, 8021–8024.

[119] J. Åqvist; A. Warshel. Computer simulation of the initial proton-transfer step in human carbonic anhydrase-I. *J. Mol. Biol.*, **1992**, *224*, 7–14.

[120] W. L. Jorgensen; J. Chandrasekhar; J. Madura; M. L. Klein. Comparison of simple potential functions for simulating liquid water. *J. Chem. Phys.*, **1983**, *79*, 926–935.

[121] W. L. Jorgensen; J. D. Madura. Temperature and size dependence for Monte Carlo simulations of TIP4P water. *Mol. Phys.*, **1985**, *56*, 1381–1392.

[122] M. W. Mahoney; W. L. Jorgensen. A five-site model for liquid water and the reproduction of the density anomaly by rigid, nonpolarizable potential functions. *J. Chem. Phys.*, **2000**, *112*, 8910–8922.

[123] H. J. C. Berendsen; J. R. Grigera; T. P. Straatsma. The missing term in effective pair potentials. *J. Phys. Chem.*, **1987**, *91*, 6269–6271.

[124] T. Darden; D. York; L. Pedersen. Particle mesh Ewald–an Nlog(N) method for Ewald sums in large systems. *J. Chem. Phys.*, **1993**, *98*, 10089–10092.

[125] U. Essmann; L. Perera; M. L. Berkowitz; T. Darden; H. Lee; L. G. Pedersen. A smooth particle mesh Ewald method. *J. Chem. Phys.*, **1995**, *103*, 8577–8593.

[126] C. Sagui; T. A. Darden. in *Simulation and Theory of Electrostatic Interactions in Solution*, L. R. Pratt; G. Hummer, Eds., pp 104–113. American Institute of Physics, Melville, NY, 1999.

[127] A. Toukmaji; C. Sagui; J. Board; T. Darden. Efficient particle-mesh Ewald based approach to fixed and induced dipolar interactions. *J. Chem. Phys.*, **2000**, *113*, 10913–10927.

[128] G. D. Hawkins; C. J. Cramer; D. G. Truhlar. Pairwise solute descreening of solute charges from a dielectric medium. *Chem. Phys. Lett.*, **1995**, *246*, 122–129.

[129] G. D. Hawkins; C. J. Cramer; D. G. Truhlar. Parametrized models of aqueous free energies of solvation based on pairwise descreening of solute atomic charges from a dielectric medium. *J. Phys. Chem.*, **1996**, *100*, 19824–19839.

[130] J. Srinivasan; M. W. Trevathan; P. Beroza; D. A. Case. Application of a pairwise generalized Born model to proteins and nucleic acids: inclusion of salt effects. *Theor. Chem. Acc.*, **1999**, *101*, 426–434.

[131] W. C. Still; A. Tempczyk; R. C. Hawley; T. Hendrickson. Semianalytical treatment of solvation for molecular mechanics and dynamics. *J. Am. Chem. Soc.*, **1990**, *112*, 6127–6129.

[132] D. Bashford; D. A. Case. Generalized Born models of macromolecular solvation effects. *Annu. Rev. Phys. Chem.*, **2000**, *51*, 129–152.

[133] A. Bondi. van der Waals volumes and radii. *J. Phys. Chem.*, **1964**, *68*, 441–451.

[134] H. J. C. Berendsen; J. P. M. Postma; W. F. van Gunsteren; A. DiNola; J. R. Haak. Molecular dynamics with coupling to an external bath. *J. Chem. Phys.*, **1984**, *81*, 3684–3690.

[135] T. Morishita. Fluctuation formulas in molecular-dynamics simulations with the weak coupling heat bath. *J. Chem. Phys.*, **2000**, *113*, 2976.

[136] J.-P. Ryckaert; G. Ciccotti; H. J. C. Berendsen. Numerical integration of the cartesian equations of motion of a system with constraints: Molecular dynamics of n-alkanes. *J. Comput. Phys.*, **1977**, *23*, 327–341.

[137] S. Miyamoto; P. A. Kollman. SETTLE: An analytical version of the SHAKE and RATTLE algorithm for rigid water models. *J. Comput. Chem.*, **1992**, *13*, 952–962.

[138] C. R. Sanders, II; B. J. Hare; K. P. Howard; J. H. Prestegard. Magnetically-oriented phospholipid micelles as a tool for the study of membrane-associated molecules. *Prog. NMR Spectr.*, **1994**, *26*, 421–444.

[139] D. A. Case. Calculations of NMR dipolar coupling strengths in model peptides. *J. Biomol. NMR*, **1999**, *15*, 95–102.

[140] B. M. Duggan; G. B. Legge; H. J. Dyson; P. E. Wright. SANE (Structure Assisted NOE Evaluation): An automated model-based approach for NOE assignment. *J. Biomol. NMR*, **2001**, *19*, 321–329.

[141] G. P. Gippert; P. F. Yip; P. E. Wright; D. A. Case. Computational methods for determining protein structures from NMR data. *Biochem. Pharm.*, **1990**, *40*, 15–22.

[142] D. A. Case; P. E. Wright. in *NMR in Proteins*, G. M. Clore; A. Gronenborn, Eds., pp 53–91. MacMillan, New York, 1993.

[143] D. A. Case; H. J. Dyson; P. E. Wright. Use of chemical shifts and coupling constants in nuclear magnetic resonance structural studies on peptides and proteins. *Meth. Enzymol.*, **1994**, *239*, 392–416.

[144] R. Brüschweiler; D. A. Case. Characterization of biomolecular structure and dynamics by NMR cross-relaxation. *Prog. NMR Spectr.*, **1994**, *26*, 27–58.

[145] D. A. Case. The use of chemical shifts and their anisotropies in biomolecular structure determination. *Curr. Opin. Struct. Biol.*, **1998**, *8*, 624–630.

[146] D. S. Wishart; D. A. Case. Use of chemical shifts in macromolecular structure determination. *Meth. Enzymol.*, **2001**, *338*, 3–34.

[147] A. E. Torda; R. M. Scheek; W. F. VanGunsteren. Time-dependent distance restraints in molecular dynamics simulations. *Chem. Phys. Lett.*, **1989**, *157*, 289–294.

[148] D. A. Pearlman; P. A. Kollman. Are time-averaged restraints necessary for nuclear magnetic resonance refinement? A model study for DNA. *J. Mol. Biol.*, **1991**, *220*, 457–479.

[149] A. E. Torda; R. M. Brunne; T. Huber; H. Kessler; W. F. van Gunsteren. Structure refinement using time-averaged J-coupling constant restraints. *J. Biomol. NMR*, **1993**, *3*, 55–66.

[150] D. A. Pearlman. How well to time-averaged J-coupling restraints work? *J. Biomol. NMR*, **1994**, *4*, 279–299.

[151] D. A. Pearlman. How is an NMR structure best defined? An analysis of molecular dynamics distance-based approaches. *J. Biomol. NMR*, **1994**, *4*, 1–16.

[152] A. Kalk; H. J. C. Berendsen. Proton magnetic relaxation and spin diffusion in proteins. *J. Magn. Reson.*, **1976**, *24*, 343–366.

[153] E. T. Olejniczak; M. A. Weiss. Are methyl groups relaxation sinks in small proteins? *J. Magn. Reson.*, **1990**, *86*, 148–155.

[154] J. W. Caldwell; P. A. Kollman. Structure and properties of neat liquids using nonadditive molecular dynamics: Water, methanol and N-methylacetamide. *J. Phys. Chem.*, **1995**, *99*, 6208–6219.

[155] B. Honig; A. Nicholls. Classical electrostatics in biology and chemistry. *Science*, **1995**, *268*, 1144–1149.

[156] D. Sitkoff; K. A. Sharp; B. Honig. Accurate calculation of hydration free energies using macroscopic solvent models. *J. Phys. Chem.*, **1994**, *98*, 1978–1988.

[157] J. Srinivasan; T. E. Cheatham, III; P. Cieplak; P. Kollman; D. A. Case. Continuum solvent studies of the stability of DNA, RNA, and phosphoramidate–DNA helices. *J. Am. Chem. Soc.*, **1998**, *120*, 9401–9409.

[158] L. T. Chong; Y. Duan; L. Wang; I. Massova; P. A. Kollman. Molecular dynamics and free-energy calculations applied to affinity maturation in antibody 48G7. *Proc. Natl. Acad. Sci. USA*, **1999**, *96*, 14330–14335.

[159] P. A. Kollman; I. Massova; C. Reyes; B. Kuhn; S. Huo; L. Chong; M. Lee; T. Lee; Y. Duan; W. Wang; O. Donini; P. Cieplak; J. Srinivasan; D. A. Case; T. E. Cheatham, III. Calculating structures and free energies of complex molecules: Combining molecular mechanics and continuum models. *Accts. Chem. Res.*, **2000**, *33*, 889–897.

[160] M. L. Connolly. Analytical molecular surface calculation. *J. Appl. Cryst.*, **1983**, *16*, 548–558.

[161] R. Elber; M. Karplus. Enhanced sampling in molecular dynamics. Use of the time-dependent Hartree approximation for a simulation of carbon monoxide diffusion through myoglobin. *J. Am. Chem. Soc.*, **1990**, *112*, 9161–9175.

[162] A. Roitberg; R. Elber. Modeling side chains in peptides and proteins: Application of the locally enhanced sampling and the simulated annealing methods to find minimum energy conformations. *J. Chem. Phys.*, **1991**, *95*, 9277.

[163] C. Simmerling; T. Fox; P. A. Kollman. Use of Locally Enhanced Sampling in Free Energy Calculations: Testing and Application of the alpha to beta Anomerization of Glucose. *J. Am. Chem. Soc.*, **1998**, *120*, 5771–5782.

[164] C. Simmerling; J. L. Miller; P. A. Kollman. Combined locally enhanced sampling and particle mesh Ewald as a strategy to locate the experimental structure of a nonhelical nucleic acid. *J. Am. Chem. Soc.*, **1998**, *120*, 7149–7155.

[165] C. Simmerling; M. R. Lee; A. R. Ortiz; A. Kolinski; J. Skolnick; P. A. Kollman. Combining MONSSTER and LES/PME to Predict Protein Structure from Amino Acid Sequence: Application to the Small Protein CMTI-1. *J. Am. Chem. Soc.*, **2000**, *122*, 8392–8402.

[166] C. Simmerling; R. Elber. Hydrophobic "collapse" in a cyclic hexapeptide: Computer simulations of CHDLFC and CAAAAC in water. *J. Am. Chem. Soc.*, **1994**, *116*, 2534–2547.

[167] A. Miranker; M. Karplus. Functionality maps of binding sites: A multiple copy simultaneous search method. *Proteins: Str. Funct. Gen.*, **1991**, *11*, 29–34.

[168] J. E. Straub; M. Karplus. Enery partitioning in the classical time-dependent Hartree approximation. *J. Chem. Phys.*, **1991**, *94*, 6737.

[169] A. Ulitsky; R. Elber. The thermal equilibrium aspects of the time-dependent Hartree and the locally enhanced sampling approximations: Formal properties, a correction, and computational examples for rare gas clusters. *J. Chem. Phys.*, **1993**, *98*, 3380.

[170] W. S. Ross; C. C. Hardin. Ion-induced stabilization of the G-DNA quadruplex: Free energy perturbation studies. *J. Am. Chem. Soc.*, **1994**, *116*, 6070–6080.

[171] A. Vedani; D. W. Huhta. A new force field for modeling metalloproteins. *J. Am. Chem. Soc.*, **1990**, *112*, 4759–4767.

[172] D. L. Veenstra; D. M. Ferguson; P. A. Kollman. How transferable are hydrogen parameters in molecular mechanics calculations? *J. Comput. Chem.*, **1992**, *13*, 971–978.

[173] F. H. Allen; O. Kennard; D. G. Watson; L. Brammer; A. G. Orpen; R. Taylor. *J. Chem. Soc. Perkin Trans. II*, **1987**, pp S1–S19.

[174] M. D. Harmony; R. W. Laurie; R. L. Kuczkowski; R. H. Schwendemann; D. A. Ramsay; F. J. Lovas; W. J. Lafferty; A. G. Maki. *J. Phys. Chem. Ref. Data*, **1979**, *8*, 619.

[175] A. J. Hopfinger; R. A. Pearlstein. Molecular mechanics force-field parameterization procedures. *J. Comput. Chem.*, **1985**, *5*, 486–499.

[176] J. F. Cannon. AMBER force-field parameters for guanosine triphosphate and its imido and methylene analogs. *J. Comput. Chem.*, **1993**, *14*, 995–1005.

[177] P. Cieplak; W. D. Cornell; C. Bayly; P. A. Kollman. Application of the multimolecule and multiconformational RESP methodology to biopolymers: Charge derivation for DNA, RNA and proteins. *J. Comput. Chem.*, **1995**, *16*, 1357–1377.

[178] W. D. Cornell; P. Cieplak; C. I. Bayly; P. A. Kollman. Application of RESP charges to calculate conformational energies, hydrogen bond energies and free energies of solvation. *J. Am. Chem. Soc.*, **1993**, *115*, 9620–9631.

[179] C. I. Bayly; P. Cieplak; W. D. Cornell; P. A. Kollman. A well-Behaved electrostatic potential based method using charge restraints for determining atom-centered charges: The RESP model. *J. Phys. Chem.*, **1993**, *97*, 10269–10280.

[180] A. E. Howard; P. Cieplak; P. A. Kollman. A molecular mechanical model that reproduces the relative energies for chair and twist-boat conformations of 1,3-dioxanes. *J. Comp. Chem.*, **1995**, *16*, 243–261.

[181] A. St.-Amant; W. D. Cornell; P. A. Kollman; T. A. Halgren. Calculation of molecular geometries, relative conformational energies, dipole moments, and molecular electrostatic potential fitted charges of small organic molecules of biochemical interest by density functional theory. *J. Comput. Chem.*, **1995**, *16*, 1483–1506.

[182] B. Jayaram; D. Sprous; D. L. Beveridge. Solvation free energy of biomacromolecules: Parameters for a modified generalized Born model consistent with the AMBER force field. *J. Phys. Chem. B*, **1998**, *102*, 9571–9576.

[183] V. Tsui; D. A. Case. Molecular dynamics simulations of nucleic acids using a generalized Born solvation model. *J. Am. Chem. Soc.*, **2000**, *122*, 2489–2498.

[184] T. A. Halgren. Merck Molecular Force Field (MMFF94). Part I-V. *J. Comput. Chem.*, **1996**, *17*, 490–641.

[185] J. Wang; P. Morin; W. Wang; P. A. Kollman. Use of MM-PBSA in reproducing the binding free energies to HIV-1 RT of TIBO derivatives and predicting the binding mode to HIV-1 RT of efavirenz by docking and MM-PBSA. *J. Am. Chem. Soc.*, **2001**, *123*, 5221–5230.

[186] W. Wang; P. Kollman. Free energy calculations on dimer stability of the HIV protease using molecular dynamics and a continuum solvent model. *J. Mol. Biol.*, **2000**, *303*, 567.

[187] C. Reyes; P. Kollman. Structure and thermodynamics of RNA-protein binding: Using molecular dynamics and free energy analyses to calculate the free energies of binding and conformational change. *J. Mol. Biol.*, **2000**, *297*, 1145–1158.

[188] M. R. Lee; Y. Duan; P. A. Kollman. Use of MM-PB/SA in estimating the free energies of proteins: Application to native, intermediates, and unfolded vilin headpiece. *Proteins*, **2000**, *39*, 309–316.

[189] P. Cieplak; J. Caldwell; P. Kollman. Molecular mechanical models for organic and biological systems going beyond the atom centered two body additive approximation: Aqueous solution free energies of methanol and N-methyl acetamide, nucleic acid base, and amide hydrogen bonding and chloroform/water partition coefficients of the nucleic acid bases. *J. Comput. Chem.*, **2001**, *22*, 1048–1057.

[190] E. Meng; P. Cieplak; J. W. Caldwell; P. A. Kollman. Accurate solvation free energies of acetate and methylammonium ions calculated with a polarizable water model. *J. Am. Chem. Soc.*, **1994**, *116*, 12061–12062.

[191] G. Hummer; A. Szabo. Calculation of free-energy differences from computer simulations of initial and final states. *J. Chem. Phys.*, **1996**, *105*, 2004–2010.

[192] T. Simonson. in *Computational Biochemistry and Biophysics*, O. Becker; A. D. MacKerell; B. Roux; M. Watanabe, Eds. Marcel Dekker, New York, 2001.

[193] J. Wang; P. A. Kollman. Automatic parameterization of force field by systematic search and genetic algorithms. *J. Comput. Chem.*, **2001**, *22*, 1219–1228.

[194] P. Kollman. Free energy calculations: Applications to chemical and biochemical phenomena. *Chem. Rev.*, **1993**, *93*, 2395–2417.

[195] D. L. Beveridge; F. M. DiCapua. Free energy simulation via molecular simulations: Applications to chemical and biomolecular systems. *Annu. Rev. Biophys. Biophys. Chem.*, **1989**, *18*, 431–492.

[196] C. Chipot; P. A. Kollman; D. A. Pearlman. Alternative approaches to potential of mean force calculations: free energy perturbation versus thermodynamics integration. Case study of some representative nonpolar interactions. *J. Comput. Chem*, **1996**, *17*, 1112–1131.

[197] D. A. Pearlman; P. A. Kollman. The overlooked bond-stretching contribution in free energy perturbation calculations. *J. Chem. Phys.*, **1991**, *94*, 4532–4545.

[198] D. A. Pearlman. Determining the contributions of constraints in free energy calculations: Development, characterization, and recommendations. *J. Chem. Phys.*, **1993**, *98*, 8946–8957.

[199] D. A. Pearlman. Free energy derivatives: A new method for probing the convergence problem in free energy calculations. *J. Comput. Chem.*, **1994**, *15*, 105–123.

[200] D. A. Pearlman. A comparison of alternative approaches to free energy calculations. *J. Phys. Chem.*, **1994**, *98*, 1487–1493.

[201] D. A. Pearlman; B. G. Rao. in *Encyclopedia of Computational Chemistry*, P. von R. Schleyer; N. L. Allinger; T. Clark; J. Gasteiger; P. A. Kollman; I. H. F. Schaefer, Eds., pp 1036–1061. John Wiley, Chichester, 1998.

[202] R. J. Radmer; P. A. Kollman. Free energy calculation methods: A theoretical and empirical comparison of numerical errors and a new method for qualitative estimates of free energy changes. *J. Comput. Chem.*, **1997**, *18*, 902–919.

[203] D. A. Pearlman; P. A. Kollman. A new method for carrying out free energy perturbation calculations: dynamically modified windows. *J. Chem. PHys.*, **1989**, *90*, 2460–2470.

[204] H.-A. Yu; M. Karplus. A thermodynamic analysis of solvation. *J. Chem. Phys.*, **1988**, *89*, 2366–2379.

[205] G. Hummer. Fast-growth thermodynamic integration: Error and efficiency analysis. *J. Chem. Phys.*, **2001**, *114*, 7330–7337.

[206] S. H. Fleischman; C. L. Brooks, III. Thermodynamic calculations on biological systems: Solution properties of alcohols and alkanes. *J. Chem. Phys.*, **1988**, *87*, 221–234.

[207] A. Jakalian; B. L. Bush; D. B. Jack; C. I. Bayly. Fast, efficient generation of high-quality atomic charges. AM1-BCC model: I. Method. *J. Comput. Chem.*, **2000**, *21*, 132–146.

[208] A. Jakalian; D. B. Jack; C. I. Bayly. Fast, efficient generation of high-quality atomic charges. AM1-BCC model: II. Parameterization and Validation. *J. Comput. Chem.*, **2002**, *23*, 1623–1641.

[209] J. J. Vincent; K. M. Merz, Jr. A highly portable parallel implementation of AMBER4 using the message passing interface standard. *J. Comput. Chem.*, **1995**, *16*, 1420–1427.

[210] K. J. Cross; P. E. Wright. Calibration of ring-current models for the heme ring. *J. Magn. Reson.*, **1985**, *64*, 220–231.

[211] K. Ösapay; D. A. Case. A new analysis of proton chemical shifts in proteins. *J. Am. Chem. Soc.*, **1991**, *113*, 9436–9444.

[212] D. A. Case. Calibration of ring-current effects in proteins and nucleic acids. *J. Biomol. NMR*, **1995**, *6*, 341–346.

[213] R. Radmer; P. Kollman. The application of three approximate free energy calculations methods to structure based ligand design: Trypsin and its complex with inhibitors. *J. Comput.-Aided Mol. Design*, **1998**, *12*, 215–228.

[214] S. R. Niketic; K. Rasmussen. *The Consistent Force Field: A Documentation*. Springer-Verlag, New York, 1977.

[215] C. Cerjan; W. H. Miller. On finding transition states. *J. Chem. Phys.*, **1981**, *75*, 2800.

[216] D. T. Nguyen; D. A. Case. On finding stationary states on large-molecule potential energy surfaces. *J. Phys. Chem.*, **1985**, *89*, 4020–4026.

[217] G. Lamm; A. Szabo. Langevin modes of macromolecules. *J. Chem. Phys.*, **1986**, *85*, 7334–7348.

[218] J. Kottalam; D. A. Case. Langevin modes of macromolecules: application to crambin and DNA hexamers. *Biopolymers*, **1990**, *29*, 1409–1421.

[219] S. Huo; I. Massova; P. A. Kollman. Computational Alanine Scanning of the 1:1 Human Growth Hormone-Receptor Complex. *J. Comput. Chem.*, **2002**, *23*, 15–27.

[220] M. Schaefer; C. Froemmel. A precise analytical method for calculating the electrostatic energy of macromolecules in aqueous solution. *J. Mol. Biol.*, **1990**, *216*, 1045–1066.

[221] M. Schaefer; H. W. T. Van Vlijmen; M. Karplus. Electrostatic contributions to molecular free energies in solution. *Adv. Protein Chem.*, **1998**, *51*, 1–57.

[222] T. Darden; D. Pearlman; L. G. Pedersen. Ionic charging free energies: Spherical versus periodic boundary conditions. *J. Chem. Phys.*, **1998**, *109*, 10921–10935.

[223] R. M. Levy; M. Karplus; J. Kushick; D. Perahia. Evaluation of the configurational entropy for proteins: Application to molecular dynamics simulations of an $\alpha$-helix. *Macromolecules*, **1984**, *17*, 1370–1374.

[224] E. Gallicchio; M. M. Kubo; R. M. Levy. Enthalpy-entropy and cavity decomposition of alkane hydration free energies: Numerical results and implications for theories of hydrophobic solvation. *J. Phys. Chem.*, **2000**, *104*, 6271–6285.

[225] S. Arnott; P. J. Campbell-Smith; R. Chandrasekaran. in *Handbook of Biochemistry and Molecular Biology, 3rd ed. Nucleic*, G. P. Fasman, Ed., pp 411–422. CRC Press, Cleveland, 1976.

[226] V. Tsui; L. Zhu; T. H. Huang; P. E. Wright; D. A. Case. Assessment of zinc finger orientations by residual dipolar coupling constants. *J. Biomol. NMR*, **2000**, *16*, 9–21.

[227] O. Becker; A. D. MacKerell; B. Roux; M. Watanabe, eds. *Computational Biochemistry and Biophysics*. Marcel Dekker, New York, 2001.

[228] A. R. Leach. *Molecular Modelling. Principles and Applications, Second Edition*. Prentice-Hall, Harlow, England, 2001.

[229] T. E. Cheatham, III; B. R. Brooks; P. A. Kollman. in *Current Protocols in Nucleic Acid Chemistry*, pp Sections 7.5, 7.8, 7.9, 7.10. Wiley, New York, 1999.

[230] M. F. Crowley; T. A. Darden; T. E. Cheatham, III; D. W. Deerfield, II. Adventures in improving the scaling and accuracy of a parallel molecular dynamics program. *J. Supercomput.*, **1997**, *11*, 255–278.

[231] G. Sigalov; P. Scheffel; A. Onufriev. Incorporating variable environments into the generalized Born model. *J. Chem. Phys.*, **2005**, *122*, 094511.

[232] G. Sigalov; A. Fenley; A. Onufriev. Analytical electrostatics for biomolecules: Beyond the generalized Born approximation . *J. Chem. Phys.*, **2006**, *124*, 124902.

[233] M. Feig; A. Onufriev; M. Lee; W. Im; D. A. Case; C. L. Brooks, III. Performance comparison of the generalized Born and Poisson methods in the calculation of the electrostatic solvation energies for protein structures. *J. Comput. Chem.*, **2004**, *25*, 265–284.

[234] A. Mitsutake; Y. Sugita; Y. Okamoto. Generalized-ensemble algorithms for molecular simulations of biopolymers. *Biopolymers*, **2001**, *60*, 96–123.

[235] J. J. Prompers; R. Brüschweiler. Dynamic and structural analysis of isotropically distributed molecular ensembles. *Proteins*, **2002**, *46*, 177–189.

[236] J. J. Prompers; R. Brüschweiler. General framework for studying the dynamics of folded and nonfolded proteins by NMR relaxation spectroscopy and MD simulation. *J. Am. Chem. Soc.*, **2002**, *124*, 4522–4534.

[237] T. A. Andrea; W. C. Swope; H. C. Andersen. The role of long ranged forces in determining the structure and properties of liquid water. *J. Chem. Phys.*, **1983**, *79*, 4576–4584.

[238] H. C. Andersen. Molecular dynamics simulations at constant pressure and/or temperature. *J. Chem. Phys.*, **1980**, *72*, 2384–2393.

[239] R. W. Pastor; B. R. Brooks; A. Szabo. An analysis of the accuracy of Langevin and molecular dynamics algorithms. *Mol. Phys.*, **1988**, *65*, 1409–1419.

[240] J. P. Valleau; G. M. Torrie. in *Modern Theoretical Chemistry, Vol. 5: Statistical Mechanics, Part A,*, B. J. Berne, Ed. Plenum Press, New York, 1977.

[241] S. Kumar; D. Bouzida; R. H. Swendsen; P. A. Kollman; J. M. Rosenberg. The weighted histogram analysis method for free-energy calculations on biomolecules. I. The method. *J. Comput. Chem.*, **1992**, *13*, 1011–1021.

[242] S. Kumar; J. M. Rosenberg; D. Bouzida; R. H. Swendsen; P. A. Kollman. Multidimensional free-energy calculations using the weighted histogram analysis method. *J. Comput. Chem.*, **1995**, *16*, 1339–1350.

[243] J. Kottalam; D. A. Case. Dynamics of ligand escape from the heme pocket of myoglobin. *J. Am. Chem. Soc.*, **1988**, *110*, 7690–7697.

[244] B. Roux. The calculation of the potential of mean force using computer simulations. *Comput. Phys. Comm.*, **1995**, *91*, 275–282.

[245] J. A. Izaguirre; D. P. Catarello; J. M. Wozniak; R. D. Skeel. Langevin stabilization of molecular dynamics. *J. Chem. Phys.*, **2001**, *114*, 2090–2098.

[246] J. W. Ponder; D. A. Case. Force fields for protein simulations. *Adv. Prot. Chem.*, **2003**, *66*, 27–85.

[247] W. H. Press; B. P. Flannery; S. A. Teukolsky; W. T. Vetterling. in *Numerical Recipes: The Art of Scientific Computing*. Cambridge University Press, New York, 1989.

[248] C. J. Cramer; D. G. Truhlar. Implicit solvation models: Equilibria, structure, spectra, and dynamics. *Chem. Rev.*, **1999**, *99*, 2161–2200.

[249] P. Beroza; D. A. Case. Calculations of proton-binding thermodynamics in proteins. *Meth. Enzymol.*, **1998**, *295*, 170–189.

[250] J. D. Madura; M. E. Davis; M. K. Gilson; R. C. Wade; B. A. Luty; J. A. McCammon. Biological applications of electrostatic calculations and brownian dynamics simulations. *Rev. Computat. Chem.*, **1994**, *5*, 229–267.

[251] M. K. Gilson. Theory of electrostatic interactions in macromolecules. *Curr. Opin. Struct. Biol.*, **1995**, *5*, 216–23.

[252] M. Scarsi; J. Apostolakis; A. Caflisch. Continuum electrostatic energies of macromolecules in aqueous solutions. *J. Phys. Chem. A*, **1997**, *101*, 8098–8106.

[253] R. Luo; L. David; M. K. Gilson. Accelerated Poisson-Boltzmann calculations for static and dynamic systems. *J. Comput. Chem.*, **2002**, *23*, 1244–1253.

[254] H. Wei; R. Qi; J. Wang; P. Cieplak; Y. Duan; R. Luo. Efficient Formulation of polarizable Gaussian Multipole Electrostatics for Biomolecular Simulations. *J. Chem. Phys.*, **2020**, *153*, 114116.

[255] H. Wei; P. Cieplak; Y. Duan; R. Luo. Stress tensor and constant pressure simulation for polarizable gaussian multipole model. *The Journal of Chemical Physics*, **2022**.

[256] H. Wei; A. Luo; T. Qiu; R. Luo; R. Qi. Improved Poisson-Boltzmann Methods for High-Performance Computing. *J. Chem. Theory Comput.*, **2019**, *15*, 6190.

[257] H. Wei; R. Luo; R. Qi. An Efficient Second-Order Poisson-Boltzmann Method. *J. Comput. Chem.*, **2019**, *40*, 1257.

[258] D. Greene; R. Qi; R. Nguyen; T. Qiu; R. Luo. Heterogeneous dielectric implicit membrane model for the calculation of mmpbsa binding free energies. *J. Chem. Infom. Model.*, **2019**, *59*, 3041.

[259] L. Xiao; J. Diao; D. Greene; J. Wang; R. Luo. A Continuum Poisson-Boltzmann Model for Membrane Channel Proteins. *J. Chem. Theory Comput.*, **2017**, *13*, 3398.

[260] C. Wang; P. Ren; R. Luo. Ionic solution: What goes right and wrong with continuum solvation modeling. *J. Phys. Chem. B*, **2017**, *121*, 11169.

[261] E. King; R. Qi; H. Li; R. Luo; E. Aitchison. Estimating the roles of protonation and electronic polarization in absolute binding affinity simulations. *J. Chem. Theory Comput.*, **2021**, *17*, 0000.

[262] Z. Li; I. K. *The Immersed Interface Method: Numerical Solutions of PDEs Involving Interfaces and Irregular Domains*. SIAM Frontiers in Applied Mathematics, Philadelphia, 2006.

[263] J. Wang; Q. Cai; Z. Li; H. Zhao; R. Luo. Achieving Energy Conservation in Poisson-Boltzmann Molecular Dynamics: Accuracy and Precision with Finite-difference Algorithms. *Chem. Phys. Lett.*, **2009**, *468*, 112.

[264] J. Wang; R. Luo. Assessment of Linear Finite-Difference Poisson-Boltzmann solvers. *J. Comput. Chem.*, **2010**, *31*, 1689–1698.

[265] Q. Cai; J. Wang; H. Zhao; R. Luo. On removal of charge singularity in Poisson-Boltzmann equation. *J. Chem. Phys.*, **2009**, *130*, 145101.

[266] Q. Cai; M.-J. Hsieh; J. Wang; R. Luo. Performance of Nonlinear Finite-Difference Poisson-Boltzmann Solvers. *J. Chem. Theory Comput.*, **2010**, *6*, 203.

[267] Q. Cai; X. Ye; J. Wang; R. Luo. Dielectric boundary force in numerical Poisson-Boltzmann methods: Theory and numerical strategies. *Chem. Phys. Lett.*, **2011**, *514*, 368.

[268] Q. Cai; X. Ye; J. Wang; R. Luo. On-the-Fly Numerical Surface Integration for Finite-Difference Poisson-Boltzmann Methods. *J. Chem. Theory Comput.*, **2011**, *7*, 3608–3619.

[269] Q. Cai; X. Ye; R. Luo. Dielectric Pressure in Continuum Electrostatic Solvation of Biomolecules. *Phys. Chem. Chem. Phys.*, **2012**, *14*, 15917–15925.

[270] W. M. Botello-Smith; X. Liu; Q. Cai; Z. Li; H. Zhao; R. Luo. Numerical Poisson-Boltzmann Model for Continuum Membrane Systems. *Chem. Phys. Lett.*, **2013**, *555*, 274.

[271] J. S. Smith; B. T. Nebgen; R. Zubatyuk; N. Lubbers; C. Devereux; K. Barros; S. Tretiak; O. Isayev; A. E. Roitberg. Approaching coupled cluster accuracy with a general-purpose neural network potential through transfer learning. *Nat. Commun.*, **2019**, *10*.

[272] X. Ye; J. Wang; R. Luo. A Revised Density Function for Molecular Surface Calculation in Continuum Solvent Models. *J. Chem. Theory Comput.*, **2010**, *6*, 1157–1169.

[273] C. Wang; P. Nguyen; K. Pham; D. Huynh; T. Le; H. Wang; P. Ren; R. Luo. Calculating protein-ligand binding affinities with MMPBSA: Method and error analysis. *J. Comput. Chem.*, **2016**, *37*, 2436–2446.

[274] R. Qi; W. Botello-Smith; R. Luo. Acceleration of Linear Finite-Difference Poisson-Boltzmann Methods on Graphics Processing Units. *J. Chem. Theory Comput.*, **2017**, *13*, 3378–3387.

[275] R. Qi; R. Luo. Robustness and Efficiency of Poisson-Boltzmann Modeling on Graphics Processing Units. *J. Chem. Inf. Model.*, **2019**, *59*, 409–420.

[276] T. Simonson. Electrostatics and dynamics of proteins. *Rep. Prog. Phys.*, **2003**, *66*, 737–787.

[277] D. Bashford; M. Karplus. p‘K sub a‘’s of ionizable groups in proteins: Atomic detail from a continuum electrostatic model. *Biochemistry*, **1990**, *29*, 10219–10225.

[278] M. Schaefer; M. Karplus. A comprehensive analytical treatment of continuum electrostatics. *J. Phys. Chem.*, **1996**, *100*, 1578–1599.

[279] S. R. Edinger; C. Cortis; P. S. Shenkin; R. A. Friesner. Solvation free energies of peptides: Comparison of approximate continuum solvation models with accurate solution of the Poisson-Boltzmann equation. *J. Phys. Chem. B*, **1997**, *101*, 1190–1197.

[280] A. Ghosh; C. S. Rapp; R. A. Friesner. Generalized Born model based on a surface integral formulation. *J. Phys. Chem. B*, **1998**, *102*, 10983–10990.

[281] B. N. Dominy; C. L. Brooks, III. Development of a generalized Born model parameterization for proteins and nucleic acids. *J. Phys. Chem. B*, **1999**, *103*, 3765–3773.

[282] N. Calimet; M. Schaefer; T. Simonson. Protein molecular dynamics with the generalized Born/ACE solvent model. *Proteins*, **2001**, *45*, 144–158.

[283] A. Onufriev; D. A. Case; D. Bashford. Effective Born radii in the generalized Born approximation: The importance of being perfect. *J. Comput. Chem.*, **2002**, *23*, 1297–1304.

[284] F. M. Richards. Areas, volumes, packing, and protein structure. *Ann. Rev. Biophys. Bioeng.*, **1977**, *6*, 151–176.

[285] Y. Duan; C. Wu; S. Chowdhury; M. C. Lee; G. Xiong; W. Zhang; R. Yang; P. Cieplak; R. Luo; T. Lee. A point-charge force field for molecular mechanics simulations of proteins based on condensed-phase quantum mechanical calculations. *J. Comput. Chem.*, **2003**, *24*, 1999–2012.

[286] J. D. Jackson. *Classical Electrodynamics*. Wiley and Sons, New York, 1975.

[287] M. S. Lee; F. R. Salsbury, Jr.; C. L. Brooks, III. Novel generalized Born methods. *J. Chem. Phys.*, **2002**, *116*, 10606–10614.

[288] Q. Lu; R. Luo. A Poisson-Boltzmann dynamics method with nonperiodic boundary condition. *J. Chem. Phys.*, **2003**, *119*, 11035–11047.

[289] C. H. Tan; L. J. Yang; R. Luo. How well does Poisson-Boltzmann implicit solvent agree with explicit solvent? A quantitative analysis. *J. Phys. Chem. B*, **2006**, *110*, 18680–18687.

[290] C. H. Tan; Y. H. Tan; R. Luo. Implicit nonpolar solvent models. *J. Phys. Chem. B*, **2007**, *111*, 12263–12274.

[291] M. Feig; J. Karanicolas; C. L. Brooks, III. MMTSB Tool Set: Enhanced sampling and multiscale modeling methods for application in structural biology. *J. Mol. Graphics Mod.*, **2004**, *22*, 377–395.

[292] C. Simmerling; B. Strockbine; A. E. Roitberg. All-atom structure prediction and folding simulations of a stable protein. *J. Am. Chem. Soc.*, **2002**, *124*, 11258–11259.

[293] A. E. García; K. Y. Sanbonmatsu. $\alpha$-helical stabilization by side chain shielding of backbone hydrogen bonds. *Proc. Natl. Acad. Sci. USA*, **2002**, *99*, 2782–2787.

[294] J. Wang; R. M. Wolf; J. W. Caldwell; P. A. Kollamn; D. A. Case. Development and testing of a general Amber force field. *J. Comput. Chem.*, **2004**, *25*, 1157–1174.

[295] K. N. Kirschner; R. J. Woods. Solvent interactions determine carbohydrate conformation. *Proc. Natl. Acad. Sci. USA*, **2001**, *98*, 10541–10545.

[296] M. Basma; S. Sundara; D. Calgan; T. Venali; R. J. Woods. Solvated ensemble averaging in the calculation of partial atomic charges. *J. Comput. Chem.*, **2001**, *22*, 1125–1137.

[297] K. N. Kirschner; R. J. Woods. Quantum mechanical study of the nonbonded forces in water-methanol complexes. *J. Phys. Chem. A*, **2001**, *105*, 4150–4155.

[298] K. A. Sharp; B. Honig. Electrostatic interactions in macromolecules: Theory and experiment. *Annu. Rev. Biophys. Biophys. Chem.*, **1990**, *19*, 301–332.

[299] M. K. Gilson; K. A. Sharp; B. H. Honig. Calculating the electrostatic potential of molecules in solution: method. *J. Comput. Chem.*, **1988**, *9*, 327–35.

[300] J. Warwicker; H. C. Watson. Calculation of the electric potential in the active site cleft due to. *J. Mol. Biol.*, **1982**, *157*, 671–679.

[301] I. Klapper; R. Hagstrom; R. Fine; K. Sharp; B. Honig. Focussing of electric fields in the active stie of Cu, Zn superoxide dismutase. *Proteins*, **1986**, *1*, 47–59.

[302] A. Nicholls; B. Honig. A rapid finite difference algorithm, utilizing successive over-relaxation to solve the Poisson-Boltzmann equation. *J. Comput. Chem.*, **1991**, *12*, 435–445.

[303] M. E. Davis; J. A. McCammon. Dielectric boundary smoothing in finite difference solutions of the Poisson equation: An approach to improve accuracy and convergence. *J. Comput. Chem.*, **1991**, *12*, 909–912.

[304] M. E. Davis; J. A. McCammon. Electrostatics in biomolecular structure and dynamics. *Chem. Rev.*, **1990**, *90*, 509–521.

[305] M. E. Davis; J. A. McCammon. Solving the finite-difference linearized Poisson-Boltzmann equation – a comparison of relaxation and conjugate gradient methods. *J. Comput. Chem.*, **1989**, *10*, 386–391.

[306] D. Bashford. An object-oriented programming suite for electrostatic effects in biological molecules. *Lect. Notes Comput. Sci.*, **1997**, *1343*, 233–240.

[307] B. A. Luty; M. E. Davis; J. A. McCammon. Electrostatic energy calculations by a finite-difference method: Rapid calculation of charge-solvent interaction energies. *J. Comput. Chem.*, **1992**, *13*, 768–771.

[308] U. C. Singh; S. J. Weiner; P. A. Kollman. Molecular dynamics simulations of d(C-G-C-G-A).d(T-C-G-C-G) with and without "hydrated" counterions. *Proc. Nat. Acad. Sci.*, **1985**, *82*, 755–759.

[309] J. Gao. Absolute free energy of solvation from Monte Carlo simulations using combined quantum and molecular mechanical potentials. *J. Phys. Chem.*, **1992**, *96*, 537–540.

[310] A. Warshel; M. Levitt. Theoretical studies of enzymic reactions: Dielectric, electrostatic and steric stabilization of the carbonium ion in the reaction of lysozyme. *J. Mol. Biol.*, **1976**, *103*, 227–249.

[311] M. J. Field; P. A. Bash; M. Karplus. A combined quantum mechanical and molecular mechanical potential for molecular dynamics simulations. *J. Comput. Chem.*, **1990**, *11*, 700–733.

[312] R. V. Stanton; D. S. Hartsough; K. M. Merz, Jr. An examination of a density functional/molecular mechanical coupled potential. *J. Comput. Chem.*, **1994**, *16*, 113–128.

[313] R. V. Stanton; L. R. Little; K. M. Merz, Jr. An examination of a Hartree-Fock/molecular mechanical coupled potential. *J. Phys. Chem.*, **1995**, *99*, 17344–17348.

[314] R. V. Stanton; D. S. Hartsough; K. M. Merz, Jr. Calculations of solvation free energies using a density functional/molecular dynamics coupled potential. *J. Phys. Chem.*, **1993**, *97*, 11868–11870.

[315] W. Yang; T.-S. Lee. A density-matrix divide-and-conquer approach for electronic structure calculations of large molecules. *J. Chem. Phys.*, **1995**, *103*, 5674–5678.

[316] S. L. Dixon; K. M. Merz, Jr. Semiempirical molecular orbital calculations with linear system size scaling. *J. Chem. Phys.*, **1996**, *104*, 6643–6649.

[317] S. L. Dixon; K. M. Merz, Jr. Fast, accurate semiempirical molecular orbital calculations for macromolecules. *J. Chem. Phys.*, **1997**, *107*, 879–893.

[318] J. Nocedal; S. J. Wright. *Numerical Optimization*. Springer-Verlag, New York, 1999.

[319] S. G. Nash. A survey of truncated-Newton methods. *J. of Computational and Applied Mathematics*, **2000**, *124*, 45–59.

[320] X. Cheng; V. Hornak; C. Simmerling. Improved conformational sampling through an efficient combination of mean-field simulation approaches. *J. Phys. Chem. B*, **2004**, *108*.

[321] M. C. Lee; Y. Duan. Distinguish protein decoys by using a scoring function based on a new Amber force field, short molecular dynamics simulations, and the generalized Born solvent model. *Proteins*, **2004**, *55*, 620–634.

[322] J. Chu; B. L. Trout; B. R. Brooks. A super-linear minimization scheme for the nudged elastic band method. *J. Chem. Phys.*, **2003**, *119*, 12708–12717.

[323] R. Elber; M. Karplus M. A method for determining reaction paths in large molecules: Application to myoglobin. *Chem. Phys. Lett.*, **1987**, *139*, 375–380.

[324] G. Henkelman; H. Jönsson. Improved tangent estimate in the nudged elastic band method for finding minimum energy paths and saddle points. *J. Chem. Phys.*, **2000**, *113*, 9978–9985.

[325] G. Henkelman; B. P. Uberuaga; H. Jönsson. A climbing image nudged elastic band method for finding saddle points and minimum energy paths. *J. Chem. Phys.*, **2000**, *113*, 9901–9904.

[326] H. Jönsson; G. Mills; K. W. Jacobsen. in *Classical and Quantum Dynamics in Condensed Phase Simulations*, B. J. Berne; G. Ciccoti; D. F. Coker, Eds., pp 385–404. World Scientific, Singapore, 1998.

[327] G. Mills; H. Jönsson. Quantum and thermal effects in $H_2$ dissociative adsorption: Evaluation of free energy barriers in multidimensional quantum systems. *Phys. Rev. Lett.*, **1994**, *72*, 1124–1127.

[328] J. Mongan; D. A. Case; J. A. McCammon. Constant pH molecular dynamics in generalized Born implicit solvent. *J. Comput. Chem.*, **2004**, *25*, 2038–2048.

[329] J. Moody; C. J. Darken. Fast Learning in Networks of Locally-Tuned Processing Units. *Neural Comput.*, **1989**, *1*, 281–294.

[330] R. C. Walker; M. F. Crowley; D. A. Case. The implementation of a fast and accurate QM/MM potential method in Amber. *J. Comput. Chem.*, **2008**, *29*, 1019–1031.

[331] G. M. Seabra; R. C. Walker; M. Elstner; D. A. Case; A. E. Roitberg. Implementation of the SCC-DFTB Method for Hybrid QM/MM Simulations within the Amber Molecular Dynamics Package. *J. Phys. Chem. A.*, **2007**, *20*, 5655–5664.

[332] D. A. Case; T. Cheatham; T. Darden; H. Gohlke; R. Luo; K. M. Merz, Jr.; A. Onufriev; C. Simmerling; B. Wang; R. Woods. The Amber biomolecular simulation programs. *J. Computat. Chem.*, **2005**, *26*, 1668–1688.

[333] X. Wu; B. R. Brooks. Isotropic periodic sum: A method for the calculation of long-range interactions. *J. Chem. Phys.*, **2005**, *122*, 044107.

[334] X. Wu; B. R. Brooks. Using the Isotropic Periodic Sum Method to Calculate Long-Range Interactions of Heterogeneous Systems. *J. Chem. Phys.*, **2008**, *129*, 154115.

[335] X. Wu; B. R. Brooks. Isotropic periodic sum of electrostatic interactions for polar systems. *J. Chem. Phys.*, **2009**, *131*, 024107.

[336] R. M. Venable; L. E. Chen; R. W. Pastor. Comparison of the Extended Isotropic Periodic Sum and Particle Mesh Ewald Methods for Simulations of Lipid Bilayers and Monolayers. *J. Phys. Chem. B*, **2009**, *113*, 5855–5862.

[337] E. J. Sorin; V. S. Pande. Exploring the helix-coil transition via all-atom equilibrium ensemble simulations. *Biophys. J.*, **2005**, *88*, 2472–2493.

[338] T. Kruger; M. Elstner; P. Schiffels; T. Frauenheim. Validation of the density-functional based tight-binding approximation. *J. Chem. Phys.*, **2005**, *122*, 114110.

[339] P. Ren; J. W. Ponder. Temperature and pressure dependence of the AMOEBA water model. *J. Phys. Chem. B*, **2004**, *108*, 13427–13437.

[340] P. Ren; J. W. Ponder. Consistent treatment of inter- and intramolecular polarization in molecular mechanics calculations. *J. Comput. Chem.*, **2002**, *23*, 1497–1506.

[341] L. Yang; C. Tan; M.-J. Hsieh; J. Wang; Y. Duan; P. Cieplak; J. Caldwell; P. A. Kollman; R. Luo. New-generation Amber united-atom force field. *J. Phys. Chem. B*, **2006**, *110*, 13166–13176.

[342] B. Wang; K. M. Merz, Jr. A fast QM/MM (quantum mechanical/molecular mechanical) approach to calculate nuclear magnetic resonance chemical shifts for macromolecules. *J. Chem. Theory Comput.*, **2006**, *2*, 209–215.

[343] R. C. Rizzo; T. Aynechi; D. A. Case; I. D. Kuntz. Estimation of absolute free energies of hydration using continuum methods: Accuracy of partial charge models and optimization of nonpolar contributions. *J. Chem. Theory Comput.*, **2006**, *2*, 128–139.

[344] Z.-X. Wang; W. Zhang; C. Wu; H. Lei; P. Cieplak; Y. Duan. Strike a Balance: Optimization of backbone torsion parameters of AMBER polarizable force field for simulations of proteins and peptides. *J. Comput. Chem.*, **2006**, *27*, 781–790.

[345] S. C. Harvey; R. K. Tan; T. E. Cheatham, III. The flying ice cube: Velocity rescaling in molecular dynamics leads to violation of energy equipartition. *J. Comput. Chem.*, **1998**, *19*, 726–740.

[346] X. Wu; B. R. Brooks. Self-guided Langevin dynamics simulation method. *Chem. Phys. Lett.*, **2003**, *381*, 512–518.

[347] K. Nam; J. Gao; D. York. An efficient linear-scaling Ewald method for long-range electrostatic interactions in combined QM/MM calculations. *J. Chem. Theory Comput.*, **2005**, *1*, 2–13.

[348] K. Nam; Q. Cui; J. Gao; D. M. York. Specific Reaction Parametrization of the AM1/d Hamiltonian for Phosphoryl Transfer Reactions: H, O, and P Atoms. *J. Chem. Theory Comput.*, **2007**, *3*, 486–504.

[349] E. Pellegrini; M. J. Field. A generalized-Born solvation model for macromolecular hybrid-potential calculations. *J. Phys. Chem. A.*, **2002**, *106*, 1316–1326.

[350] D. Porezag; T. Frauenheim; T. Kohler; G. Seifert; R. Kaschner. Construction of tight-binding-like potentials on the basis of density-functional-theory: Applications to carbon. *Phys. Rev. B*, **1995**, *51*, 12947.

[351] G. Seifert; D. Porezag; T. Frauenheim. Calculations of molecules, clusters and solids with a simplified LCAO-DFT-LDA scheme. *Int. J. Quantum Chem.*, **1996**, *58*, 185.

[352] M. Elstner; D. Porezag; G. Jungnickel; J. Elsner; M. Haugk; T. Frauenheim; S. Suhai; G. Seifert. Self-consistent charge density functional tight-binding method for simulation of complex material properties. *Phys. Rev. B*, **1998**, *58*, 7260.

[353] M. Elstner; P. Hobza; T. Frauenheim; S. Suhai; E. Kaxiras. Hydrogen bonding and stacking interactions of nucleic acid base pairs: a density-functional-theory based treatment. *J. Chem. Phys.*, **2001**, *114*, 5149.

[354] R. P. Feynman; A. R. Hibbs. *Quantum Mechanics and Path Integrals*. McGraw-Hill, New York, 1965.

[355] R. P. Feynman. *Statistcal Mechanics*. Benjamin, Reading, MA, 1972.

[356] H. Kleinert. *Path Integrals in Quantum Mechanics, Statistics, and Polymer Physics*. World Scientific, Singapore, 1995.

[357] L. S. Schulman. *Techniques and Applications of Path Integration*. Wiley & Sons, New York, 1996.

[358] A. Messiah. *Quantum Mechanics*. Wiley & Sons, New York, 1958.

[359] D. Chandler; P. G. Wolynes. Exploiting the isomorphism between quantum theory and classical statistical mechanics of polyatomic fluids. *J. Chem. Phys.*, **1981**, *74*, 4078–4095.

[360] D. M. Ceperley. Path integrals in the theory of condensed helium. *Rev. Mod. Phys.*, **1995**, *67*, 279–355.

[361] J. Cao; B. J. Berne. On energy estimators in path integral Monte Carlo simulations: Dependence of accuracy on algorithm. *J. Chem. Phys.*, **1989**, *91*, 6359–6366.

[362] A. Mudi; C. Chakravarty. Effect of the Berendsen thermostat on the dynamical properties of water. *Mol. Phys.*, **2004**, *102*, 681–685.

[363] M. J. S. Dewar; W. Thiel. Ground states of molecules. 38. The MNDO method, approximations and parameters. *J. Am. Chem. Soc.*, **1977**, *99*, 4899–4907.

[364] M. J. S. Dewar; E. G. Zoebisch; E. F. Healy; J. J. P. Stewart. AM1: A new general purpose quantum mechanical molecular model. *J. Am. Chem. Soc.*, **1985**, *107*, 3902–3909.

[365] J. J. P. Stewart. Optimization of parameters for semiempirical methods I. Method. *J. Comput. Chem.*, **1989**, *10*, 209–220.

[366] J. W. Storer; D. J. Giesen; C. J. Cramer; D. G. Truhlar. Class IV charge models: A new semiempirical approach in quantum chemistry. *J. Comput.-Aided Mol. Design*, **1995**, *9*, 87–110.

[367] J. Li; C. J. Cramer; D. G. Truhlar. New class IV charge model for extracting accurate partial charges from Wave Functions. *J. Phys. Chem. A.*, **1998**, *102*, 1820–1831.

[368] P. Imhof; F. Noé; S. Fischer; J. C. Smith. AM1/d Parameters for Magnesium in Metalloenzymes. *J. Chem. Theory Comput.*, **2006**, *2*, 1050–1056.

[369] A. van der Vaart; K. M. Merz, Jr. Divide and conquer interaction energy decomposition. *J. Phys. Chem. A*, **1999**, *103*, 3321–3329.

[370] A. V. Mitin. The dynamic level shift method for improving the convergence of the SCF procedure. *J. Comput. Chem.*, **1988**, *9*, 107–110.

[371] M. D. Ermolaeva; A. van der Vaart; K. M. Merz, Jr. Implementation and testing of a frozen density matrix - divide and conquer algorithm. *J. Phys. Chem.*, **1999**, *103*, 1868–1875.

[372] B. Wang; E. N. Brothers; A. van der Vaart; K. M. Merz Jr. Fast semiempirical calculations for nuclear magnetic resonance chemical shifts: A divide-and-conquer approach. *J. Chem. Phys.*, **2004**, *120*, 11392–11400.

[373] B. Wang; K. Raha; K. M. Merz Jr. Pose scoring by NMR. *J. Am. Chem. Soc.*, **2004**, *126*, 11430–11431.

[374] K. Raha; A. van der Vaart; K. E. Riley; M. B. Peters; L. M. Westerhoff; H. Kim; K. M. Merz Jr. Pairwise decomposition of residue interaction energies using semiempirical quantum mechanical methods in studies of protein-ligand interaction. *J. Am. Chem. Soc.*, **2005**, *127*, 6583–6594.

[375] M. P. Repasky; J. Chandrasekhar; W. L. Jorgensen. PDDG/PM3 and PDDG/MNDO: Improved semiempirical methods. *J. Comput. Chem.*, **2002**, *23*, 1601–1622.

[376] J. P. McNamara; A. M. Muslim; H. Abdel-Aal; H. Wang; M. Mohr; I. H. Hillier; R. A. Bryce. Towards a quantum mechanical force field for carbohydrates: A reparameterized semiempirical MO approach. *Chem. Phys. Lett.*, **2004**, *394*, 429–436.

[377] J. J. P. Stewart. Optimization of parameters for semiempirical methods V: Modification of NDDO approximations and application to 70 elements. *J. Mol. Mod.*, **2007**, *13*, 1173–1213.

[378] A. Luzhkov; A. Warshel. Microscopic models for quantum-mechanical calculations of chemical processes in solutions - Ld/Ampac and Scaas/Ampac calculations of solvation energies. *J. Comp. Chem.*, **1992**, *13*, 199–213.

[379] U. C. Singh; P. A. Kollman. A combined Ab initio quantum-mechanical and molecular mechanical method for carrying out simulations on complex molecular systems - Applications to the Ch3Cl + Cl- exchange-reaction and gas-phase protonation of polyethers. *J. Comp. Chem.*, **1986**, *7*, 718–730.

[380] I. B. Bersuker; M. K. Leong; J. E. Boggs; R. S. Pearlman. A method of combined quantum mechanical (QM) molecular mechanics (MM) treatment of large polyatomic systems with charge transfer between the QM and MM fragments. *Int. J. Quant. Chem.*, **1997**, *63*, 1051–1063.

[381] F. Maseras; K. Morokuma. Imomm - a new integrated ab-initio plus molecular geometry optimization scheme of equilibrium structures and transition-states. *J. Comp. Chem.*, **1995**, *16*, 1170–1179.

[382] Y. K. Zhang; T. S. Lee; W. T. Yang. A pseudobond approach to combining quantum mechanical and molecular mechanical methods. *J. Chem. Phys.*, **1999**, *110*, 46–54.

[383] J. L. Gao; P. Amara; C. Alhambra; M. J. Field. A generalized hybrid orbital (GHO) method for the treatment of boundary atoms in combined QM/MM calculations. *J Phys Chem A*, **1998**, *102*, 4714–4721.

[384] D. M. Philipp; R. A. Friesner. Mixed ab initio QM/MM modeling using frozen orbitals and tests with alanine dipeptide and tetrapeptide. *J. Comp. Chem.*, **1999**, *20*, 1468–1494.

[385] M. J. Field; M. Albe; C. Bret; F. Proust-De Martin; A. Thomas. The Dynamo library for molecular simulations using hybrid quantum mechanical and molecular mechanical potentials. *J. Comp. Chem.*, **2000**, *21*, 1088–1100.

[386] V. Hornak; R. Abel; A. Okur; B. Strockbine; A. Roitberg; C. Simmerling. Comparison of multiple Amber force fields and development of improved protein backbone parameters. *Proteins*, **2006**, *65*, 712–725.

[387] A. Okur; L. Wickstrom; M. Layten; R. Geney; K. Song; V. Hornak; C. Simmerling. Improved efficiency of replica exchange simulations through use of a hybrid explicit/implicit solvation model. *J. Chem. Theory Comput.*, **2006**, *2*, 420–433.

[388] R. Geney; M. Layten; R. Gomperts; C. Simmerling. Investigation of salt bridge stability in a generalized Born solvent model. *J. Chem. Theory Comput.*, **2006**, *2*, 115–127.

[389] F. Floris; J. Tomasi. Evaluation of the dispersion contribution to the solvation energy. A simple computational model in the continuum approximation. *J. Comput. Chem.*, **1989**, *10*, 616–627.

[390] R. M. Levy; E. Gallicchio. Computer simulations with explicit solvent: recent progress in the thermodynamic decomposition of free energies and in modeling electrostatic effects. *Annu. Rev. Phys. Chem.*, **1999**, *49*, 531–567.

[391] H. Nymeyer; S. Gnanakaran; A. García. Atomic simulations of protein folding using the replica exchange algorithm. *Meth. Enzymol.*, **2004**, *383*, 119–149.

[392] D. H. Mathews; D. A. Case. Nudged Elastic Band calculation of minimal energy pathways for the conformational change of a GG mismatch. *J. Mol. Biol.*, **2006**, *357*, 1683–1693.

[393] X. Cheng; G. Cui; V. Hornak; C. Simmerling. Modified replica exchange simulation methods for local structure refinement. *J. Phys. Chem. B*, **2005**, *109*, 8220–8230.

[394] J. Wang; W. Wang; P. A. Kollman; D. A. Case. Automatic atom type and bond type perception in molecular mechanical. *J. Mol. Graphics Model.*, **2006**, *25*, 247–260.

[395] V. Hornak; A. Okur; R. Rizzo; C. Simmerling. HIV-1 protease flaps spontaneously open and reclose in molecular dynamics simulations. *Proc. Nat. Acad. Sci. USA*, **2006**, *103*, 915–920.

[396] V. Hornak; A. Okur; R. Rizzo; C. Simmerling. HIV-1 protease flaps spontaneously close when an inhibitor binds to the open state. *J. Am. Chem. Soc.*, **2006**, *128*, 2812–2813.

[397] C. Jarzynski. Nonequilibrium equality for free energy differences. *Phys. Rev. Lett.*, **1997**, *78*, 2690–2693.

[398] G. Hummer; A. Szabo. Free energy reconstruction from nonequilibrium single-molecule pulling experiments. *Proc. Natl. Acad. Sci. USA*, **2001**, *98*, 3658.

[399] G. Hummer; A. Szabo. Kinetics from nonequilibrium single-molecule pulling experiments. *Biophys. J.*, **2003**, *85*, 5–15.

[400] M. O. Jensen; S. Park; E. d; K. Schulten. Energetics of glycerol conduction through aquaglyceroporin GlpF. *Proc. Natl. Acad. Sci. USA*, **2002**, *99*, 6731–6736.

[401] A. Crespo; M. A. Marti; D. A. Estrin; A. E. Roitberg. Multiple-steering QM-MM calculation of the free energy profile in chorismate mutase. *J. Am. Chem. Soc.*, **2005**, *127*, 6940–6941.

[402] L. Banci; I. Bertini; G. Gori-Savellini; A. Romagnoli; P. Turano; M. A. Cremonini; C. Luchinat; H. B. Gray. Pseudocontact shifts as constraints for energy minimization and molecular dynamics calculations on solution structures of paramagnetic metalloproteins. *Proteins*, **1997**, *29*, 68.

[403] P. Y. Ren; J. W. Ponder. Polarizable atomic multipole water model for molecular mechanics simulation. *J. Phys. Chem. B*, **2003**, *107*, 5933–5947.

[404] P. Y. Ren; J. W. Ponder. Tinker polarizable atomic multipole force field for proteins. *to be published.*, **2006**.

[405] C. Sagui; L. G. Pedersen; T. A. Darden. Towards an accurate representation of electrostatics in classical force fields: Efficient implementation of multipolar interactions in biomolecular simulations. *J. Chem. Phys.*, **2004**, *120*, 73–87.

[406] J. Kästner; W. Thiel. Bridging the gap between thermodynamic integration and umbrella sampling provides a novel analysis method: "Umbrella integration". *J. Chem. Phys.*, **2005**, *123*, 144104.

[407] A. M. Wollacott; K. M. Merz, Jr. Development of a parameterized force field to reproduce semiempirical geometries. *J. Chem. Theory Comput.*, **2006**, *2*, 1070–1077.

[408] C. P. Sosa; T. Hewitt; M. S. Lee; D. A. Case. Vectorization of the generalized Born model for molecular dynamics on shared-memory computers. *J. Mol. Struct. (Theochem)*, **2001**, *549*, 193–201.

[409] A. Warshel. *Computer Modeling of Chemical Reactions in Enzymes and Solutions*. John Wiley and Sons, New York, 1991.

[410] S. R. Billeter; S. P. Webb; T. Iordanov; P. K. Agarwal; S. Hammes-Schiffer. Hybrid approach for including electronic and nuclear quantum effects in molecular dynamics simulations of hydrogen transfer reactions in enzymes. *J. Chem. Phys.*, **2001**, *114*, 6925.

[411] C. Simmerling; R. Elber. Hydrophobic "collapse" in a cyclic hexapeptide: Computer simulations of CHDLFC and CAAAAC in water. *J. Am. Chem. Soc.*, **1994**, *116*, 2534–2547.

[412] B. P. Uberuaga; M. Anghel; A. F. Voter. Synchronization of trajectories in canonical molecular-dynamics simulations: Observation, explanation, and exploitation. *J. Chem. Phys.*, **2004**, *120*, 6363–6374.

[413] W. Kabsch; C. Sander. Dictionary of protein secondary structure: pattern recognition of hydrogen-bonded and geometrical features. *Biopolymers*, **1983**, *22*, 2577–2637.

[414] G. B. Rocha; R. O. Freire; A. M. Simas; J. J. P. Stewart. RM1: A Reparameterization of AM1 for H, C, N, O, P, S, F, Cl, Br and I. *J. Comp. Chem.*, **2006**, *27*, 1101–1111.

[415] T. E. Cheatham, III; M. A. Young. Molecular dynamics simulation of nucleic acids: Successes, limitations and promise. *Biopolymers*, **2001**, *56*, 232–256.

[416] Y. Deng; B. Roux. Calculation of standard binding free energies: Aromatic molecules in the T4 lysozyme L99A mutant. *J. Chem. Theor. Comput.*, **2006**, *2*, 1255–1273.

[417] T. Steinbrecher; D. A. Case; A. Labahn. A multistep approach to structure-based drug design: Studying ligand binding at the human neutrophil elastase. *J. Med.. Chem.*, **2006**, *49*, 1837–1844.

[418] T. Steinbrecher; D. L. Mobley; D. A. Case. Non-linear scaling schemes for Lennard-Jones interactions in free energy calculations. *J. Chem. Phys.*, **2007**, *127*, 214108.

[419] T. Steinbrecher; A. Hrenn; K. Dormann; I. Merfort; A. Labahn. Bornyl (3,4,5-trihydroxy)-cinnamate - An optimized human neutrophil elastase inhibitor designed by free energy calculations. *Bioorg. Med. Chem.*, **2008**, *16*, 2385–2390.

[420] T. Steinbrecher; I. Joung; D. A. Case. Soft-core potentials in thermodynamic integration: Comparing one- and two-step transformations. *J. Comp. Chem.*, **2011**, *32*, 3253–3263.

[421] J. Kaus; L. C. T. Pierce; R. C. Walker; J. A. McCammon. Improving the Efficiency of Free Energy Calculations in the Amber Molecular Dynamics Package. *J. Chem. Theory Comput.*, **2013**, *9*, 4131–4139.

[422] L. Marinelli; S. Cosconati; T. Steinbrecher; V. Limongelli; A. Bertamino; E. Novellino; D. A. Case. Homology Modeling of NR2B Modulatory Domain of NMDA Receptor and Analysis of Ifenprodil Binding. *ChemMedChem*, **2007**, *2,*, 1498–1510.

[423] K. N. Kirschner; A. B. Yongye; S. M. Tschampel; J. González-Outeiriño; C. R. Daniels; B. L. Foley; R. J. Woods. GLYCAM06: A generalizable biomolecular force field. Carbohydrates. *J. Comput. Chem.*, **2008**, *29*, 622–655.

[424] S. M. Tschampel; M. R. Kennerty; R. J. Woods. TIP5P-consistent treatment of electrostatics for biomolecular simulations. *J. Chem. Theory Comput.*, **2007**, *3*, 1721–1733.

[425] M. B. Tessier; M. L. DeMarco; A. B. Yongye; R. J. Woods. Extension of the GLYCAM06 biomolecular force field to lipids, lipid bilayers and glycolipids. *Mol. Simul.*, **2008**, *34*, 349–363.

[426] J. B. Klauda; X. Wu; R. W. Pastor; B. R. Brooks. Long-Range Lennard-Jones and Electrostatic Interactions in Interfaces. *J. Phys. Chem. B*, **2007**, *111*, 4393–4400.

[427] K. Takahashi; K. Yasuoka; T. Narumi. Cutoff radius effect of isotropic periodic sum method for transport. *J. Chem. Phys.*, **2007**, *127*, 114511.

[428] F. Paesani; W. Zhang; D. A. Case; T. E. Cheatham; G. A. Voth. An accurate and simple quantum model for liquid water. *J. Chem. Phys.*, **2006**, *125*, 184507.

[429] A. Okur; D. R. Roe; G. Cui; V. Hornak; C. Simmerling. Improving convergence of replica-exchange simulations through coupling to a high-temperature structure reservoir. *J. Chem. Theory comput.*, **2007**, *3*, 557–568.

[430] A. E. Roitberg; A. Okur; C. Simmerling. Coupling of replica exchange simulations to a non-Boltzmann structure reservoir. *J. Phys. Chem. B*, **2007**, *111*, 2415–2418.

[431] J. A. Kalinowski; B. Lesyng; J. D. Thompson; C. J. Cramer; D. G. Truhlar. Class IV charge model for the self-consistent charge density-functional tight-binding method. *J. Phys. Chem. A*, **2004**, *108*, 2545–2549.

[432] H. B. Schlegel; J. L. Sonnenberg. Empirical valence-bond models for reactive potential energy surfaces using distributed Gaussians. *J. Chem. Theory Comput.*, **2006**, *2*, 905.

[433] J. L. Sonnenberg; H. B. Schlegel. Empirical valence bond models for reactive potential energy surfaces. II. Intramolecular proton transfer in pyridone and the Claisen reaction of allyl vinyl ether. *Mol. Phys.*, **2007**, *105*, 2719.

[434] Y. Saad; M. H. Schultz. GMRES: A generalized minimal residual algorithm for solving nonsymmetric linear systems. *SIAM J. Sci. Stat. Comput.*, **1986**, *7*, 856.

[435] P. Pulay. Convergence acceleration of iterative sequencies. The case of SCF iteration. *Chem. Phys. Lett.*, **1980**, *73*, 393.

[436] P. Pulay. Improved SCF convergence acceleration. *J. Comput. Chem.*, **1982**, *3*, 556.

[437] M. J. Frisch; G. W. Trucks; H. B. Schlegel; G. E. Scuseria; M. A. Robb; J. R. Cheeseman; G. Scalmani; V. Barone; B. Mennucci; G. A. Petersson; H. Nakatsuji; M. Caricato; X. Li; H. P. Hratchian; A. F. Izmaylov; J. Bloino; G. Zheng; J. L. Sonnenberg; M. Hada; M. Ehara; K. Toyota; R. Fukuda; J. Hasegawa; M. Ishida; T. Nakajima; Y. Honda; O. Kitao; H. Nakai; T. Vreven; J. A. Montgomery, Jr.; J. E. Peralta; F. Ogliaro; M. Bearpark; J. J. Heyd; E. Brothers; K. N. Kudin; V. N. Staroverov; R. Kobayashi; J. Normand; K. Raghavachari; A. Rendell; J. C. Burant; S. S. Iyengar; J. Tomasi; M. Cossi; N. Rega; J. M. Millam; M. Klene; J. E. Knox; J. B. Cross; V. Bakken; C. Adamo; J. Jaramillo; R. Gomperts; R. E. Stratmann; O. Yazyev; A. J. Austin; R. Cammi; C. Pomelli; J. W. Ochterski; R. L. Martin; K. Morokuma; V. G. Zakrzewski; G. A. Voth; P. Salvador; J. J. Dannenberg; S. Dapprich; A. D. Daniels; O. Farkas; J. B. Foresman; J. V. Ortiz; J. Cioslowski; D. J. Fox. Gaussian 09 Revision A.1. Gaussian Inc. Wallingford CT 2009.

[438] A. K. Rappe; C. J. Casewit; K. S. Colwell; W. A. Goddard III; W. M. Skiff. UFF, a Full Periodic Table Force Field for Molecular Mechanics and Molecular Dynamics Simulations. *J. Am. Chem. Soc.*, **1992**, *114*, 10024–10035.

[439] G. A. Voth; D. Chandler; W. H. Miller. Rigorous Formulation of Quantum Transition State Theory and Its Dynamical Corrections. *J. Chem. Phys.*, **1989**, *91*, 7749–7760.

[440] G. J. Martyna; M. L. Klein; M. Tuckerman. Nosé-Hoover chains: The canonical ensemble via continuous dynamics. *J. Chem. Phys.*, **1992**, *97*, 2635.

[441] G. J. Martyna; A. Hughes; M. E. Tuckerman. Molecular dynamics algorithms for path integrals at constant pressure. *J. Chem. Phys.*, **1999**, *110*, 3275.

[442] B. J. Berne; D. Thirumalai. On the simulation of quantum systems: path integral methods. *Annu. Rev. Phys. Chem.*, **1986**, *37*, 401.

[443] G. A. Voth. Path-integral centroid methods in quantum statistcal mechanics and dynamics. *Adv. Chem. Phys.*, **1996**, *93*, 135.

[444] I. R. Craig; D. E. Manolopoulos. Quantum statistics and classical mechnanics: Real time correlation functions from ring polymer molecular dynamics. *J. Chem. Phys.*, **2004**, *121*, 3368.

[445] T. F. Miller; D. E. Manolopoulos. Quantum diffusion in liquid water from ring polymer molecular dynamics. *J. Chem. Phys.*, **2005**, *123*, 154504.

[446] J. Cao; G. A. Voth. The formulation of quantum statistical mechanics based on the Feynman path centroid density. IV. Algorithms for centroid molecular dynamics. *J. Chem. Phys.*, **1994**, *101*, 6168.

[447] J. Vaníček; W. H. Miller; J. F. Castillo; F. J. Aoiz. Quantum-instanton evalution of the kinetic isotope effects. *J. Chem. Phys.*, **2005**, *123*, 054108.

[448] J. Vaníček; W. H. Miller. Efficient estimators for quantum instanton evaluation of the kinetic isotope effects: application to the intramolecular hydrogen transfer in pentadiene. *J. Chem. Phys.*, **2007**, *127*, 114309.

[449] W. H. Miller; Y. Zhao; M. Ceotto; S. Yang. Quantum instanton approximation for thermal rate constants of chemical. *J. Chem. Phys.*, **2003**, *119*, 1329–1342.

[450] W. H. Miller. Semiclassical limit of quantum mechanical transition state theory for nonseparable systems. *J. Chem. Phys.*, **1975**, *62*, 1899.

[451] T. Yamamoto; W. H. Miller. On the efficient path integral evaluation of thermal rate constants with the quantum instanton approximation. *J. Chem. Phys.*, **2004**, *120*, 3086–3099.

[452] T. Yamamoto; W. H. Miller. Path integral evaluation of the quantum instanton rate constant for proton transfer in a polar solvent. *J. Chem. Phys.*, **2005**, *122*, 044106.

[453] W. H. Miller; S. D. Schwartz; J. W. Tromp. Quantum mechanical rate constants for bimolecular reactions. *J. Chem. Phys.*, **1983**, *79*, 4889–4898.

[454] A. T. Brünger; P. D. Adams; G. M. Clore; W. L. Delano; P. Gros; R. W. Grosse-Kunstleve; J.-S. Jiang; J. Kuszewski; M. Nilges; N. S. Pannu; R. J. Read; L. M. Rice; T. Simonson; G. L. Warren. Crystallography and NMR system (CNS): A new software system for macromolecular structure determination. *Acta Cryst. D*, **1998**, *54*, 905–921.

[455] N. Yu; H. P. Yennawar; K. M. Merz, Jr. Refinement of protein crystal structures using energy restraints derived from linear-scaling quantum mechanics . *Acta Cryst. D*, **2005**, *61*, 322–332.

[456] N. Yu; X. Li; G. Cui; S. Hayik; K. M. Merz, Jr. Critical assessment of quantum mechanics based energy restraints in protein crystal structure refinement. *Prot. Sci.*, **2006**, *15*, 2773–2784.

[457] H. Kopitz; A. Zivkovic; J. W. Engels; H. Gohlke. Determinants of the unexpected stability of RNA fluorobenzene self pairs. *ChemBioChem*, **2008**, *9*, 2619–2622.

[458] S. Fulle; H. Gohlke. Analyzing the flexibility of RNA structures by constraint counting. *Biophys. J.*, **2008**, *DOI:10.1529/biophysj.107.113415*.

[459] H. Gohlke; L. A. Kuhn; D. A. Case. Change in protein flexibility upon complex formation: Analysis of Ras-Raf using molecular dynamics and a molecular framework approach. *Proteins*, **2004**, *56*, 322–327.

[460] A. Ahmed; H. Gohlke. Multiscale modeling of macromolecular conformational changes combining concepts from rigidity and elastic network theory. *Proteins*, **2006**, *63*, 1038–1051.

[461] Y. Wu; H. L. Tepper; G. A. Voth. Flexible simple point-charge water model with improved liquid-state properties. *J. Chem. Phys.*, **2006**, *124*, 024503.

[462] D. J. Price; C. L. Brooks. A modified TIP3P water potential for simulation with Ewald summation. *J. Chem. Phys.*, **2004**, *121*, 10096–10103.

[463] H. W. Horn; W. C. Swope; J. W. Pitera; J. D. Madura; T. J. Dick; G. L. Hura; T. Head-Gordon. Development of an improved four-site water model for biomolecular simulations: TIP4P-Ew. *J. Chem. Phys.*, **2004**, *120*, 9665–9678.

[464] H. W. Horn; W. C. Swope; J. W. Pitera. Characterization of the TIP4P-Ew water model: Vapor pressure and boiling point. *J. Chem. Phys.*, **2005**, *123*, 194504.

[465] R. J. Woods. Derivation of net atomic charges from molecular electrostatic potentials. *J. Comput. Chem.*, **1990**, *11*, 29–310.

[466] M. L. DeMarco; R. J. Woods. Bridging computational biology and glycobiology: A game of snakes and ladders. *Glycobiology*, **2008**, *18*, 426–440.

[467] R. J. Woods. Restrained electrostatic potential charges for condensed phase simulations of carbohydrates. *J. Mol. Struct (Theochem)*, **2000**, *527*, 149–156.

[468] E. F. Pettersen; T. D. Goddard; C. C. Huang; G. S. Couch; D. M. Greenblatt; E. C. Meng; T. E. Ferrin. UCSF Chimera - A visualization system for exploratory research and analysis. *J. Comput. Chem.*, **2004**, *25*, 1605–1612.

[469] H. Sasaki; N. Ochi; A. Del; M. Fukuda. Site-specific glycosylation of human recombinant erythropoietin: Analysis of glycopeptides or peptides at each glycosylation site by fast atom bombardment mass spectrometry. *Biochemistry*, **1988**, *27*, 8618–8626.

[470] S. Dube; J. W. Fisher; J. S. Powell. Glycosylation at specific sites of erythropoietin is essential for biosynthesis, secretion, and biological function. *J. Biol. Chem.*, **1988**, *263*, 17516–17521.

[471] R. J. Darling; U. Kuchibhotla; W. Glaesner; R. Micanovic; D. R. Witcher; J. M. Beals. Glycosylation of erythropoietin effects receptor binding kinetics: Role of electrostatic interactions. *Biochemistry*, **2002**, *41*, 14524–14531.

[472] J. C. Cheetham; D. M. Smith; K. H. Aoki; J. L. Stevenson; T. J. Hoeffel; R. S. Syed; J. Egrie; T. S. Harvey. NMR structure of human erythropoietin and a comparison with its receptor bound conformation. *Nat. Struct. Biol.*, **1998**, *5*, 861–866.

[473] K. L. Dormann; R. Brueckner. Variable Synthesis of the Optically Active Thiotetronic Acid Antibiotics Thiolactomycin, Thiotetromycin, and 834-B1. *Angew. Chem. Int. Ed.*, **2007**, *46*, 1160–1163.

[474] B. Jojart; T. A. Martinek. Performance of the general amber force field in modeling aqueous POPC membrane bilayers. *J. Comput. Chem.*, **2007**, *28*, 2051–2058.

[475] L. Rosso; I. R. Gould. Structure and dynamics of phospholipid bilayers using recently developed general all-atom force fields. *J. Comput. Chem.*, **2008**, *29*, 24–37.

[476] A. P. Graves; D. M. Shivakumar; S. E. Boyce; M. P. Jacobson; D. A. Case; B. K. Shoichet. Rescoring docking hit lists for model cavity sites: Predictions and experimental testing. *J. Mol. Biol.*, **2008**, *377*, 914–934.

[477] T. Huber; A. E. Torda; W. F. van Gunsteren. Local elevation: a method for improving the searching properties of molecular dynamics simulation. *J. Comput. Aided. Mol. Des.*, **1994**, *8*, 695–708.

[478] V. Babin; C. Roland; C. Sagui. Adaptively biased molecular dynamics for free energy calculations. *J. Chem. Phys.*, **2008**, *128*, 134101.

[479] A. Laio; M. Parrinello. Escaping free-energy minima. *Proc. Natl. Acad. Sci.*, **2002**, *99*, 12562–12566.

[480] S. Piana; A. Laio. A bias-exchange approach to protein folding. *J. Phys. Chem. B*, **2007**, *111*, 4553–4559.

[481] P. Raiteri; A. Laio; F. L. Gervasio; C. Micheletti; M. Parrinello. Efficient reconstruction of complex free energy landscapes by multiple walkers metadynamics. *J. Phys. Chem.*, **2006**, *110*, 3533–3539.

[482] M. Matsumoto; T. Nishimura. Mersenne twister: a 623-dimensionally equidistributed uniform pseudo-random number generator. *ACM Trans. Model. Comput. Simul.*, **1998**, *8*, 3–30.

[483] S. Park; F. Khalili-Araghi; E. Tajkhorshid; K. Schulten. Free energy calculation from steered molecular dynamics simulations using Jarzynski's equality. *J. Chem. Phys.*, **2003**, *119*, 3559–3566.

[484] Y. Sugita; A. Kitao; Y. Okamoto. Multidimensional replica-exchange method for free-energy calculations. *J. Chem. Phys.*, **2000**, *113*, 6042–6051.

[485] G. Bussi; F. L. Gervasio; A. Laio; M. Parrinello. Free-energy landscape for $\beta$ hairpin folding from combined parallel tempering and metadynamics. *J. Am. Chem. Soc.*, **2006**, *128*, 13435–13441.

[486] E. Darve; A. Pohorille. Calculating free energies using average force. *J. Chem. Phys.*, **2001**, *115*, 9169–9183.

[487] F. Wang; D. P. Landau. Efficient, multiple-range random walk algorithm to calculate the density of states. *Phys. Rev. Lett.*, **2001**, *86*, 2050–2053.

[488] T. Lelièvre; M. Rousset; G. Stoltz. Computation of free energy profiles with parallel adaptive dynamics. *J. Chem. Phys.*, **2007**, *126*, 134111.

[489] E. A. Coutsias; C. Seok; K. A. Dill. Using quaternions to calculate RMSD. *J. Comput. Chem.*, **2004**, *25*, 1849–1857.

[490] M. Iannuzzi; A. Laio; M. Parrinello. Efficient exploration of reactive potential energy surfaces using car-parrinello molecular dynamics. *Phys. Rev. Lett.*, **2003**, *90*, 238302–1.

[491] A. Okur; L. Wickstrom; C. Simmerling. Evaluation of salt bridge structure and energetics in peptides using explicit, implicit and hybrid solvation models. *J. Chem. Theory Comput.*, **2008**, *4*, 488–498.

[492] A. Perez; I. Marchan; D. Svozil; J. Sponer; T. E. Cheatham; C. A. Laughton; M. Orozco. Refinement of the AMBER Force Field for Nucleic Acids: Improving the Description of alpha/gamma Conformers. *Biophys. J.*, **2007**, *92*, 3817–3829.

[493] L. Dang. Mechanism and thermodynamics of ion selectivity in aqueous solutions of 18-crown-6 ether: A molecular dynamics study. *J. Am. Chem. Soc.*, **1995**, *117*, 6954–6960.

[494] S. Joung; T. E. Cheatham, III. Determination of alkali and halide monovalent ion parameters for use in explicitly solvated biomolecular simulations. *J. Phys. Chem. B*, **2008**, *112*, 9020–9041.

[495] R. Aduri; B. T. Psciuk; P. Saro; H. Taniga; H. B. Schlegel; J. SantaLucia, Jr. AMBER force field parameters for the naturally occurring modified nucleosides in RNA. *J. Chem. Theory Comput.*, **2007**, *3*, 1465–1475.

[496] J. Shao; S. W. Tanner; N. Thompson; T. E. Cheatham, III. Clustering molecular dynamics trajectories: 1. Characterizing the performance of different clustering algorithms. *J. Chem. Theory Comput.*, **2007**, *3*, 2312–2334.

[497] P. Auffinger; T. E. Cheatham, III; A. C. Vaiana. Spontaneous formation of KCl aggregates in biomolecular simulations: a force field issue? *J. Chem. Theory Comput.*, **2007**, *3*, 1851–1859.

[498] D. R. Roe; A. Okur; L. Wickstrom; V. Hornak; C. Simmerling. Secondary Structure Bias in Generalized Born Solvent Models: Comparison of Conformational Ensembles and Free Energy of Solvent Polarization from Explicit and Implicit Solvation. *J. Phys. Chem. B*, **2007**, *111*, 1846–1857.

[499] J. Torras; G. Seabra; E. Deumens; S. B. Trickey; A. E. Roitberg. A versatile AMBER-Gaussian QM/MM interface through PUPIL. *J. Comput. Chem.*, **2008**, *29*, 1564–1573.

[500] J. Torras; Y. He; C. Cao; K. Muralidharan; E. Deumens; H. Cheng; S. Trickey. PUPIL: A systematic approach to software integration in multi-scale simulations. *Comput. Phys. Comm.*, **2007**, *177*, 265–279.

[501] P. Cieplak; F.-Y. Dupradeau; Y. Duan; J. Wang. Polarization effects in molecular mechanical force fields. *J. Phys.: Condens. Matter*, **2009**, *21*, 333102.

[502] Y. Yang; H. Yu; D. M. York; Q. Cui; M. Elstner. Extension of the self-consistent charge density-functional tight-binding method: Third-order expansion of the density functional theory total energy and introduction of a modified effective Coulomb interaction. *J. Phys. Chem. A*, **2007**, *111*, 10861–10873.

[503] A. D. MacKerell Jr.; D. Bashford; M. Bellott; R. L. Dunbrack; J. D. Evanseck; M. J. Field; S. Fischer; J. Gao; H. Guo; S. Ha; D. Joseph-McCarthy; L. Kuchnir; K. Kuczera; F. T. K. Lau; C. Mattos; S. Michnick; T. Ngo; D. T. Nguyen; B. Prodhom; W. E. Reiher; B. Roux; M. Schlenkrich; J. C. Smith; R. Stote; J. Straub; M. Watanabe; J. Wiorkiewicz-Kuczera; D. Yin; M. Karplus. All-Atom Empirical Potential for Molecular Modeling and Dynamics Studies of Proteins. *J. Phys. Chem. B*, **1998**, *102*, 3586–3616.

[504] A. D. MacKerell Jr.; N. Banavali; N. Foloppe. Development and current status of the CHARMM force field for nucleic acids. *Biopolymers*, **2000**, *56*, 257–265.

[505] B. R. Brooks; R. E. Bruccoleri; D. J. Olafson; D. J. States; S. Swaminathan; M. Karplus. CHARMM: A Program for Macromolecular Energy, Minimization, and Dynamics Calculations. *J. Computat. Chem.*, **1983**, *4*, 187–217.

[506] B. R. Brooks; C. L. Brooks; A. D. Mackerell; L. Nilsson; R. J. Petrella; B. Roux; Y. Won; G. Archontis; C. Bartels; S. Boresch; A. Caflisch; L. Caves; Q. Cui; A. R. Dinner; M. Feig; S. Fischer; J. Gao; M. Hodoscek; W. Im; K. Kuczera; T. Lazaridis; J. Ma; V. Ovchinnikov; E. Paci; R. W. Pastor; C. B. Post; J. Z. Pu; M. Schaefer; B. Tidor; R. M. Venable; H. L. Woodcock; X. Wu; W. Yang; D. M. York; M. Karplus. CHARMM: the biomolecular simulation program. *J. Comput. Chem.*, **2009**, *30*, 1545–1614.

[507] A. D. MacKerell, Jr.; M. Feig; C. L. Brooks III. Improved Treatment of the Protein Backbone in Empirical Force Fields. *J. Am. Chem. Soc.*, **2004**, *126*, 698–699.

[508] A. D. MacKerell, Jr.; M. Feig; C. L. Brooks III. Extending the treatment of backbone energetics in protein force fields: Limitations of gas-phase quantum mechanics in reproducing protein conformational distributions in molecular dynamics simulations. *J. Computat. Chem.*, **2004**, *25*, 1400–1415.

[509] M. F. Crowley; M. J. Williamson; R. C. Walker. CHAMBER: Comprehensive support for CHARMM force fields within the AMBER software. *Int. J. Quant. Chem.*, **2009**, *109*, 3767–3772.

[510] B. J. Berne; G. D. Harp. *Adv. Chem. Phys.*, **1970**, *17*, 63.

[511] R. Kubo; M. Toda; N. Hashitsume. *Statistical Physics II: Nonequilibrium Statistical Mechanics, 2nd ed.* Springer-Verlag, Heidelberg, 1991.

[512] W. H. Miller. *Adv. Chem. Phys.*, **1974**, *25*, 69.

[513] W. H. Miller. Including quantum effects in the dynamics of complex (i.e., large) molecular systems. *J. Chem. Phys.*, **2006**, *125*, 132305.

[514] H. Wang; X. Sun; W. H. Miller. Semiclassical approximations for the calculation of thermal rate constants for chemical reactions in complex molecular systems. *J. Chem. Phys.*, **1998**, *108*, 9726.

[515] X. Sun; H. Wang; W. H. Miller. Semiclassical theory of electronically nonadiabatic dynamics: Results of a linearized approximation to the initial value representation. *J. Chem. Phys.*, **1998**, *109*, 7064.

[516] J. Liu; W. H. Miller. A simple model for the treatment of imaginary frequencies in chemical reaction rates and molecular liquids. *J. Chem. Phys.*, **2009**, *131*, 074113.

[517] J. Liu; W. H. Miller; F. Paesani; W. Zhang; D. A. Case. Quantum dynamical effects in liquid water: A semiclassical study on the diffusion and the infrared absorption spectrum. *J. Chem. Phys.*, **2009**, *131*, 164509.

[518] J. Liu. Recent advances in the linearized semiclassical initial value representation/classical wigner model for the thermal correlation function. *International Journal of Quantum Chemistry*, **2015**, *115*, 657–670.

[519] J. Liu; W. H. Miller. Real time correlation function in a single phase space integral beyond the linearized semiclassical initial value representation. *J. Chem. Phys.*, **2007**, *126*, 234110.

[520] J. Liu; W. H. Miller. Test of the consistency of various linearized semiclassical initial value time correlation functions in application to inelastic neutron scattering from liquid para-hydrogen. *J. Chem. Phys.*, **2008**, *128*, 144511.

[521] J. W. Ponder; C. Wu; P. Ren; V. S. Pande; J. D. Chodera; M. J. Schieders; I. Haque; D. L. Mobley; D. S. Lambrecht; R. A. DiStasio, Jr.; M. Head-Gordon; G. N. I. Clark; M. E. Johnson; T. Head-Gordon. Current status of the AMOEBA polarizable force field. *J. Phys. Chem. B*, **2010**, *114*, 2549–2564.

[522] L. Wickstrom; A. Okur; C. Simmerling. Evaluating the performance of the ff99SB force field based on NMR scalar coupling data. *Biophys. J.*, **2009**, *97*, 853–856.

[523] Q. Shi; E. Giva. *J. Chem. Phys. A*, **2003**, *107*, 9059.

[524] M.-J. Hsieh; R. Luo. Balancing simulation accuracy and efficiency with the Amber united atom force field. *J. Phys. Chem. B*, **2010**, *114*, 2886–2893.

[525] C. Bergonzo; A. J. Campbell; R. C. Walker; C. Simmerling. A Partial Nudged Elastic Band Implementation for Use with Large or Explicitly Solvated Systems. *Int J Quantum Chem*, **2009**, *109*, 3781–3790.

[526] V. Babin; C. Sagui. Conformational free energies of methyl-alpha-l-iduronic and methyl-beta-d-glucuronic acids in water. *J. Chem. Phys.*, **2010**, *132*, 104108.

[527] Q. T. Wang; R. A. Bryce. Improved hydrogen bonding at the NDDO-type semiempirical quantum mechanical/molecular mechanical interface. *J. Chem. Theory Comput.*, **2009**, *5*, 2206–2211.

[528] D. J. Sindhikara; S. Kim; A. F. Voter; A. E. Roitberg. Bad seeds sprout perilous dynamics: Stochastic thermostat induced trajectory synchronization in biomolecules. *J. Chem. Theory Comput.*, **2009**, *5*, 1624–1631.

[529] T. Luchko; S. Gusarov; D. R. Roe; C. Simmerling; D. A. Case; J. Tuszynski; A. Kovalenko. Three-dimensional molecular theory of solvation coupled with molecular dynamics in Amber. *J. Chem. Theory Comput.*, **2010**, *6*, 607–624.

[530] I. Omelyan; A. Kovalenko. MTS-MD of biomolecules steered with 3D-RISM-KH mean solvation forces accelerated with generalized solvation force extrapolation. *J. Chem. Theory Comput.*, **2015**, *11*, 1875–1895.

[531] J.-F. Truchon; B. M. Pettitt; P. Labute. A cavity corrected 3D-RISM functional for accurate solvation free energies. *J. Chem. Theory Comput.*, **2014**, *10*, 934–941.

[532] V. Sergiievskyi; G. Jeanmairet; M. Levesque; D. Borgis. Solvation free-energy pressure corrections in the three dimensional reference interaction site model. *J. Chem. Phys.*, **2015**, *143*, 184116.

[533] D. Chandler; H. C. Andersen. Optimized cluster expansions for classical fluids. ii. theory of molecular liquids. *J. Chem. Phys.*, **1972**, *57*, 1930–1937.

[534] F. Hirata; P. J. Rossky. An extended RISM equation for molecular polar fluids. *Chem. Phys. Lett.*, **1981**, pp 329–334.

[535] F. Hirata; B. M. Pettitt; P. J. Rossky. Application of an extended rism equation to dipolar and quadrupolar fluids. *J. Chem. Phys.*, **1982**, *77*, 509–520.

[536] F. Hirata; P. J. Rossky; B. M. Pettitt. The interionic potential of mean force in a molecular polar solvent from an extended rism equation. *J. Chem. Phys.*, **1983**, *78*, 4133–4144.

[537] F. Hirata, Ed. *Molecular Theory of Solvation*. Kluwer Academic Publishers, 2003.

[538] D. Beglov; B. Roux. Numerical solution of the hypernetted chain equation for a solute of arbitrary geometry in three dimensions. *J. Chem. Phys.*, **1995**, *103*, 360–364.

[539] D. Beglov; B. Roux. An integral equation to describe the solvation of polar molecules in liquid water. *J. Phys. Chem. B*, **1997**, *101*, 7821–7826.

[540] A. Kovalenko; F. Hirata. Three-dimensional density profiles of water in contact with a solute of arbitrary shape: a RISM approach. *Chem. Phys. Lett.*, **1998**, *290*, 237–244.

[541] A. Kovalenko; F. Hirata. Self-consistent description of a metal–water interface by the Kohn–Sham density functional theory and the three-dimensional reference interaction site model. *J. Chem. Phys.*, **1999**, *110*, 10095–10112.

[542] A. Kovalenko; S. Ten-No; F. Hirata. Solution of three-dimensional reference interaction site model and hypernetted chain equations for simple point charge water by modified method of direct inversion in iterative subspace. *J. Comput. Chem*, **1999**, *20*, 928–936.

[543] A. Kovalenko; F. Hirata. Potentials of mean force of simple ions in ambient aqueous solution. i: Three-dimensional reference interaction site model approach. *J. Chem. Phys.*, **2000**, *112*, 10391–10402.

[544] A. Kovalenko; F. Hirata. Potentials of mean force of simple ions in ambient aqueous solution. ii: Solvation structure from the three-dimensional reference interaction site model approach, and comparison with simulations. *J. Chem. Phys.*, **2000**, *112*, 10403–10417.

[545] J.-P. Hansen; I. R. McDonald. *Theory of simple liquids*. Academic Press, London, 1990.

[546] M. Frigo. A fast Fourier transform compiler. in *Proc. 1999 ACM SIGPLAN Conf. on Programming Language Design and Implementation*, volume 34, pp 169–180. ACM, 1999.

[547] M. Frigo; S. G. Johnson. FFTW: An adaptive software architecture for the FFT. in *Proc. 1998 IEEE Intl. Conf. Acoustics Speech and Signal Processing*, volume 3, pp 1381–1384. IEEE, 1998.

[548] S. Gusarov; T. Ziegler; A. Kovalenko. Self-consistent combination of the three-dimensional RISM theory of molecular solvation with analytical gradients and the amsterdam density functional package. *J. Phys. Chem. A*, **2006**, *110*, 6083–6090.

[549] T. Miyata; F. Hirata. Combination of molecular dynamics method and 3D-RISM theory for conformational sampling of large flexible molecules in solution. *J. Comput. Chem.*, **2007**, *29*, 871–882.

[550] S. Genheden; T. Luchko; S. Gusarov; A. Kovalenko; U. Ryde. An MM/3D-RISM approach for ligand-binding affinities. *J. Phys. Chem.*, **2010**. Accepted.

[551] M. E. Tuckerman; B. J. Berne; G. J. Martyna. Molecular dynamics algorithm for multiple time scales: Systems with long range forces. *J. Chem. Phys.*, **1991**, *94*, 6811–6815.

[552] M. Tuckerman; B. J. Berne; G. J. Martyna. Reversible multiple time scale molecular dynamics. *J. Chem. Phys.*, **1992**, *97*, 1990–2001.

[553] H. Grubmuumlller; H. Heller; A. Windemuth; K. Schulten. Generalized Verlet algorithm for efficient molecular dynamics simulations with long-range interactions. *Mol. Simulat.*, **1991**, *6*, 121–142.

[554] J. W. Kaminski; S. Gusarov; T. A. Wesolowski; A. Kovalenko. Modeling solvatochromic shifts using the orbital-free embedding potential at statistically mechanically averaged solvent density. *J. Phys. Chem. A*, **2010**, *114*, 6082–6096.

[555] J. S. Perkyns; B. M. Pettitt. A site-site theory for finite concentration saline solutions. *J. Chem. Phys.*, **1992**, *97*, 7656–7666.

[556] D. Chandler; J. McCoy; S. Singer. Density functional theory of nonuniform polyatomic systems. i. general formulation. *J. Chem. Phys.*, **1986**, *85*, 5971–5976.

[557] D. Chandler; J. McCoy; S. Singer. Density functional theory of nonuniform polyatomic systems. ii. rational closures for integral equations. *J. Chem. Phys.*, **1986**, *85*, 5977–5982.

[558] A. W. Goetz; M. J. Williamson; D. Xu; D. Poole; S. L. Grand; R. C. Walker. Routine microsecond molecular dynamics simulations with AMBER - Part I: Generalized Born. *J. Chem. Theory Comput.*, **2012**, *8*, 1542–1555.

[559] R. Salomon-Ferrer; A. W. Goetz; D. Poole; S. L. Grand; R. C. Walker. Routine microsecond molecular dynamics simulations with AMBER - Part 2: Explicit Solvent Particle Mesh Ewald . *J. Chem. Theory Comput.*, **2012**, *in review*.

[560] T. Schlick. *Molecular modeling and simulation: an interdisciplinary guide*. Springer-Verlag New York, Inc., Secaucus, NJ, USA, 2002.

[561] M. K. Gilson; M. Davis; B. A. Luty; J. A. McCammon. Computation of electrostatic forces on solvated molecules using the Poisson-Boltzmann equation. *J Phys Chem*, **1993**, *97*, 3591–3600.

[562] D. W. Li; R. Brüschweiler. NMR-based protein potentials. *Angew. Chem. Int. Ed.*, **2010**, *49*, 6778–6780.

[563] K. Lindorff-Larsen; S. Piana; K. Palmo; P. Maragakis; J. Klepeis; R. O. Dror; D. E. Shaw. Improved side-chain torsion potentials for the Amber ff99SB protein force field. *Proteins*, **2010**, *78*, 1950–1958.

[564] P. Banáš; D. Hollas; M. Zgarbová; P. Jurecka; M. Orozco; T. E. Cheatham, III; J. Šponer; M. Otyepka. Performance of molecular mechanics force fields for RNA simulations: Stability of UUCG and GNRA hairpins. *J. Chem. Theory. Comput.*, **2010**, *6*, 3836–3849.

[565] S. M. Kast; T. Kloss. Closed-form expressions of the chemical potential for integral equation closures with certain bridge functions. *J. Chem. Phys.*, **2008**, *129*, 236101.

[566] W. K. Olson; M. Bansal; S. K. Burley; R. E. Dickerson; M. Gerstein; S. C. Harvey; U. Heinemann; X.-J. Lu; S. Neidle; Z. Shakked; H. Sklenar; M. Suzuki; C.-S. Tung; E. Westhof; C. Wolberger; H. M. Berman. A standard reference frame for the description of nucleic acid base-pair geometry. *J. Mol. Biol.*, **2001**, *313*, 229–237.

[567] D. S. Cerutti; R. E. Duke; T. A. Darden; T. P. Lybrand. Staggered Mesh Ewald: An Extension of the Smooth Particle-Mesh Ewald Method Adding Great Versatility. *J. Chem. Theory Computat.*, **2009**, *5*, 2322–2338.

[568] D. S. Cerutti; D. A. Case. Multi-Level Ewald: A Hybrid Multigrid/Fast Fourier Transform Approach to the Electrostatic Particle-Mesh Problem. *J. Chem. Theory Comput.*, **2010**, *6*, 443–458.

[569] D. S. Cerutti; P. L. Freddolino; R. E. Duke, Jr.; D. A. Case. Simulations of a Protein Crystal with a High Resolution X-ray Structure: Evaluation of Force Fields and Water Models . *J. Phys. Chem. B*, **2010**, pp 12811–12824.

[570] M. B. Peters; Y. Yang; B. Wang; L. Fusti-Molnar; M. N. Weaver; K. M. Merz, Jr. Structural Survey of Zinc-Containing Proteins and Development of the Zinc AMBER Force Field (ZAFF). *J. Chem. Theor. Comput.*, **2010**, *6*, 2935–2947.

[571] M.-J. Hsieh; R. Luo. Exploring a coarse-grained distributive strategy for finite-difference poisson-boltzmann calculations. *J. Molec. Model.*, **2011**.

[572] I. Yildirim; H. A. Stern; S. D. Kennedy; J. D. Tubbs; D. H. Turner. Reparameterization of RNA chi Torsion Parameters for the AMBER Force Field and Comparison to NMR Spectra for Cytidine and Uridine . *J. Chem. Theory Comput.*, **2010**, *6*, 1520–1531.

[573] I. S. Joung; T. E. Cheatham, III. Molecular dynamics simulations of the dynamic and energetic properties of alkali and halide ions using water-model-specific ion parameters. *J. Phys. Chem. B*, **2009**, *113*, 13279–13290.

[574] I. Yildirim; H. A. Stern; J. D. Tubbs; S. D. Kennedy; D. H. Turner. Benchmarking AMBER Force Fields for RNA: Comparisons to NMR Spectra for Single-Stranded r(GACC) Are Improved by Revised chi Torsions. *J. Phys. Chem. B*, **2011**, *115*, 9261–9270.

[575] J. Wang; T. Hou. Application of Molecular Dynamics Simulations in Molecular Property Prediction. 1. Density and Heat of Vaporization. *J. Chem. Theory Comput.*, **2011**, *7*, 2151–2165.

[576] D. S. Palmer; A. I. Frolov; E. L. Ratkova; M. V. Fedorov. Towards a universal method for calculating hydration free energies: a 3D reference interaction site model with partial molar volume correction. *J. Phys.: Condens. Matter*, **2010**, *22*, 492101.

[577] D. Chandler; Y. Singh; D. M. Richardson. Excess electrons in simple fluids. I. General equilibrium theory for classical hard sphere solvents. *J. Chem. Phys.*, **1984**, *81*, 1975–1982.

[578] T. Ichiye; D. Chandler. Hypernetted chain closure reference interaction site method theory of structure and thermodynamics for alkanes in water. *J. Phys. Chem.*, **1988**, *92*, 5257–5261.

[579] P. H. Lee; G. M. Maggiora. Solvation thermodynamics of polar molecules in aqueous solution by the XRISM method. *J. Phys. Chem.*, **1993**, *97*, 10175–10185.

[580] M. Zgarbova; M. Otyepka; J. Sponer; A. Mladek; P. Banas; T. E. Cheatham; P. Jurecka. Refinement of the Cornell et al. Nucleic Acids Force Field Based on Reference Quantum Chemical Calculations of Glycosidic Torsion Profiles. *J. Chem. Theory Comput.*, **2011**, *7*, 2886–2902.

[581] C. Perez; F. Lohr; H. Ruterjans; J. M. Schmidt. Self-Consistent Karplus Parameterization of (3)J couplings depending on the polypeptide side-chain torsion chi(1). *J. Am. Chem. Soc.*, **2001**, *123*, 7081–7093.

[582] J. J. Chou; D. A. Case; A. Bax. Insights into the mobility of methyl-bearing side chains in proteins. *J. Am. Chem. Soc.*, **2003**, *125*, 8959–8966.

[583] X. Wu; B. R. Brooks. Toward canonical ensemble distribution from self-guided Langevin dynamics simulation. *J. Chem. Phys.*, **2011**, *134*, 134108.

[584] X. Wu; B. R. Brooks. Force-momentum-based self-guided Langevin dynamics: a rapid sampling method that approaches the canonical ensemble . *J. Chem. Phys.*, **2011**, *135*, 204101.

[585] Y. Zhang; S. E. Feller; B. R. Brooks; R. W. Pastor. Computer simulation of liquid/liquid interfaces. I. Theory and application to octane/water. *J. Chem. Phys.*, **1995**, *103*, 10252–10266.

[586] H.-A. Yu; B. Roux; M. Karplus. Solvation thermodynamics: An approach from analytic temperature derivatives. *J. Chem. Phys.*, **1990**, *92*, 5020–5033.

[587] T. Yamazaki; N. Blinov; D. Wishart; A. Kovalenko. Hydration effects on the HET-s prion and amyloid-$\beta$2 fibrillous aggregates, studied with three-dimensional molecular theory of solvation. *Biophys. J.*, **2008**, *95*, 4540–4548.

[588] T. Yamazaki; A. Kovalenko; V. V. Murashov; G. N. Patey. Ion solvation in a water-urea mixture. *J. Phys. Chem. B*, **2010**, *114*, 613–619.

[589] N. Homeyer; H. Gohlke. Free energy calculations by the molecular mechanics poisson-boltzmann surface area method. *Mol. Informatics*, **2012**, *DOI: 10.1002/minf.201100135*.

[590] V. Wong; D. A. Case. Evaluating rotational diffusion from protein md simulations. *J. Phys. Chem. B*, **2008**, *112*, 6013–6024.

[591] J. Elegheert; A. Desfosses; A. V. Shkumatov; X. Wu; N. Bracke; K. Verstraete; K. Van Craenenbroeck; B. R. Brooks; D. I. Svergun; B. Vergauwen; I. Gutsche; S. N. Savvides. Extracellular complexes of the hematopoietic human and mouse CSF-1 receptor are driven by common assembly principles . *Structure*, **2011**, *19*, 1762–72.

[592] C. M. Khursigara; G. Lan; S. Neumann; X. Wu; S. Ravindran; M. J. Borgnia; V. Sourjik; J. Milne; Y. Tu; S. Subramaniam. Lateral density of receptor arrays in the membrane plane influences sensitivity of the E. coli chemotaxis response. *Embo J*, **2011**, *30*, 1719–29.

[593] C. M. Khursigara; X. Wu; P. Zhang; J. Lefman; S. Subramaniam. Role of HAMP domains in chemotaxis signaling by bacterial chemoreceptors. *PNAS*, **2008**, *105*, 16555–60.

[594] J. S. Lengyel; K. M. Stott; X. Wu; A. Brooks, B. R.and Balbo; P. Schuck; R. N. Perham; S. Subramaniam; J. L. Milne. Extended polypeptide linkers establish the spatial architecture of a pyruvate dehydrogenase multienzyme complex. *Structure*, **2008**, *16*, 93–103.

[595] C. M. Khursigara; X. Wu; ; S. Subramaniam. Chemoreceptors in Caulobacter crescentus: trimers of receptor dimers in a partially ordered hexagonally packed array. *J Bacteriol*, **2008**, *190*, 6805–10.

[596] X. Wu; B. R. Brooks. Modeling of Macromolecular assemblies with map objects. *Proc. 2007 Int. Conf. Bioinform. Comput. Biol.*, **2007**, *II*, 411–417.

[597] J. L. Milne; X. Wu; M. J. Borgnia; J. S. Lengyel; B. R. Brooks; D. Shi; R. N. Perham; S. Subramaniam. Molecular structure of a 9-MDa icosahedral pyruvate dehydrogenase subcomplex containing the E2 and E3 enzymes using cryoelectron microscopy. *J Biol Chem*, **2006**, *281*, 4364–70.

[598] X. Wu; J. L. Milne; M. J. Borgnia; A. V. Rostapshov; S. Subramaniam; B. R. Brooks. A core-weighted fitting method for docking atomic structures into low-resolution maps: application to cryo-electron microscopy. *J Struct Biol*, **2003**, *141*, 63–76.

[599] D. Hamelberg; C. A. F. de Oliveira; J. McCammon. Sampling of slow diffusive conformational transitions with accelerated molecular dynamics. *J. Chem. Phys.*, **2007**, *127*, 155102–155109.

[600] B. J. Grant; A. A. Gorfe; J. A. McCammon. Ras conformational switching: Simulating nucleotide-dependent conformational transitions with accelerated molecular dynamics. *PLoS Computat. Biol.*, **2009**, *5*, e1000325.

[601] C. A. F. de Oliveira; B. J. Grant; M. Zhou; J. A. McCammon. Large-scale conformational changes of trypanosoma cruzi proline racemase predicted by accelerated molecular dynamics simulation. *PLoS Computat. Biol.*, **2011**, *7*, e1002178.

[602] L. C. T. Pierce; R. Salomon-Ferrer; C. A. F. de Oliveira; J. A. McCammon; R. C. Walker. Routine access to milli-second time scales with accelerated molecular dynamics. *J. Chem. Theory Comput.*, **2012**, *8*, 2997–3002.

[603] D. Hamelberg; J. Mongan; J. A. McCammon. Accelerated molecular dynamics: A promising and efficient simulation method for biomolecules. *J. Chem. Phys.*, **2004**, *120*, 11919–11929.

[604] U. Doshi; D. Hamelberg. Reoptimization of the amber forcefield for peptide bond (omega) torsions using accelerated molecular dynamics. *J. Chem. Phys. B*, **2009**, *113*, 16590–16595.

[605] X. Lu; W. Olson. 3dna: a software package for the analysis, rebuilding and visualization of three-dimensional nucleic acid structures. *NUCLEIC ACIDS RESEARCH*, **2003**, *31*, 5108–5121.

[606] C. Altona; M. Sundaralingam. Conformational analysis of the sugar ring in nucleosides and nucleotides. a new description using the concept of pseudorotation. *J Am Chem Soc*, **1972**, *94*, 8205–8212.

[607] S. Harvey; M. Prabhakaran. Ribose puckering - structure, dynamics, energetics, and the pseudorotation cycle. *J Am Chem Soc*, **1986**, *108*, 6128–6136.

[608] D. Cremer; J. Pople. A general definition of ring puckering coordinates. *J Am Chem Soc*, **1975**, *97*, 1354–1358.

[609] G. te Velde; F. M. Bickelhaupt; E. J. Baerends; C. F. Guerra; S. J. A. van Gisbergen; J. G. Snijders; T. Ziegler. Chemistry with ADF. *J. Comp. Chem.*, **2001**, *22*, 931–967.

[610] ADF2011, SCM, Theoretical Chemistry, Vrije Universiteit, Amsterdam, The Netherlands, http://www.scm.com, 2012.

[611] M. W. Schmidt; K. K. Baldridge; J. A. Boatz; S. T. Elbert; M. S. Gordon; J. H. Jensen; S. Koseki; N. Matsunaga; K. A. Nguyen; S. Su; T. L. Windus; M. Dupuis; J. A. Montgomery, Jr. General atomic and molecular electronic structure system. *J. Comp. Chem.*, **1993**, *14*, 1347–1363.

[612] M. Valiev; E. J. Bylaska; N. Govind; K. Kowalski; T. P. Straatsma; H. J. J. van Dam; D. Wang; J. Niepolcha; E. Apra; T. L. Windus; W. A. de Jong. Nwchem: a comprehensive and scalable open-source solution for large scale molecular simulations. *Comput. Phys. Commun.*, **2010**, *181*, 1477.

[613] M. S. Gordon; M. W. Schmidt. in *Theory and Applications of Computational Chemistry, the first forty years*, C. E. Dykstra; G. Frenking; K. S. Kim; G. E. Scuseria, Eds., chapter 41, pp 1167–1189. Elsevier, Asterdam, 2005.

[614] F. Neese. ORCA - an ab initio, Density Functional and Semiempirical program package, Version 2.8.0, University of Bonn, 2010.

[615] I. S. Ufimtsev; T. J. Martinez. Quantum chemistry on graphical processing units. 3. Analytical energy gradients, geometry optimization, and first principles molecular dynamics. *J. Chem. Theory Comput.*, **2009**, *5*, 2619–2628.

[616] T. Gaillard; D. A. Case. Evaluation of DNA Force Fields in Implicit Solvation. *J. Chem. Theory Comput.*, **2011**, *7*, 3181–3198.

[617] Y. Meng; A. E. Roitberg. Constant pH replica exchange molecular dynamics in biomolecules using a discrete protonation model. *J. Chem. Theory Comput.*, **2010**, *6*, 1401–1412.

[618] Y. Meng; D. Sabri Dashti; A. E. Roitberg. Computing Alchemical Free Energy Differences with Hamiltonian Replica Exchange Molecular Dynamics (H-REMD) Simulations. *J. Chem. Theory Comput.*, **2011**, *7*, 2721–2727.

[619] D. Sabri Dashti; A. E. Roitberg. Optimization of Umbrella Sampling Replica Exchange Molecular Dynamics by Replica Positioning. *J. Chem. Theory Comput.*, **2013**, *9*, 4692–4699.

[620] D. Sabri Dashti; A. E. Roitberg. Calculating the pKa Shift of Titratable Group at Position 66 of Staphylococcal Nuclease Mutant with the Replica Exchange Free Energy Perturbation method (REFEP). *In preparation*, **2012**.

[621] D. Sabri Dashti; Y. Meng; A. E. Roitberg. pH-Replica Exchange Molecular Dynamics in Proteins Using a Discrete Protonation Method. *J. Phys. Chem. B*, **2012**, *116*, 8805–8811.

[622] A. Pohorille; C. Jarzynski; C. Chipot. Good practices in Free-Energy calculations. *J. Phys. Chem. B*, **2010**, *114*, 10235–10253.

[623] M. R. Shirts; J. D. Chodera. Statistically optimal analysis of samples from multiple equilibrium states. *J. Chem. Phys.*, **2008**, *129*, 124105–124105–10.

[624] Å. Skjevik; B. D. Madej; R. C. Walker; K. Teigen. Lipid11: A modular framework for lipid simulations using amber. *J. Phys. Chem. B*, **2012**, *116*, 11124–11136.

[625] D. L. Mobley; C. I. Bayly; M. D. Cooper; M. R. Shirts; K. A. Dill. Small Molecule Hydration Free Energies in Explicit Solvent: An Extensive Test of Fixed-Charge Atomistic Simulations. *J. Chem. Theory Comput.*, **2009**, *5*, 350–358.

[626] M. I. Bernal-Uruchurtu; M. F. Ruiz-López. Basic ideas for the correction of semiempirical methods describing H-bonded systems. *Chem. Phys. Lett.*, **2000**, *330*, 118–124.

[627] O. I. Arillo-Flores; M. F. Ruiz-López; M. I. Bernal-Uruchurtu. Can semi-empirical models describe HCl dissociation in water? *Theoret. Chem. Acc.*, **2007**, *118*, 425–435.

[628] X. Wu; A. Damjanovic; B. R. Brooks. Efficient and unbiased sampling of biomolecular systems in the canonical ensemble: a review of self-guided langevin dynamics. *Adv. Chem. Phys.*, **2012**, *150*, 255–326.

[629] X. Wu; B. R. Brooks. in *Microscopy: advances in scientific research and education*, A. Mendez-Vilas, Ed., pp 39–47. Formatex Research Center, Spain, 2014.

[630] X. Wu; B. R. Brooks. in *Modern electron microscopy in physical and life science*, M. Janecek, Ed., chapter 12, pp 243–262. InTech, 2016.

[631] X. Wu; B. R. Brooks. A virtual mixture approach to the study of multistate equilibrium: application to constant ph simulation in explicit water. *PLOS Computational Biology*, **2015**, *11*, e1004480.

[632] X. Wu; B. R. Brooks. Self-guided langevin dynamics via generalized langevin equation. *J. Comput. Chem.*, **2016**, *37*, 595–601.

[633] A. Bartesaghi; A. Merk; S. Banerjee; D. Matthies; X. Wu; J. L. S. Milne; S. Subramaniam. 2.2 a resolution cryo-em structure of beta-galactosidase in complex with a cell-permeant inhibitor. *Science*, **2015**, *348*, 1147–1151.

[634] X. Yu; X. Wu; G. A. Bermejo; B. R. Brooks; J. W. Taraska. Accurate high-throughput structure mapping and prediction with transition metal ion fret. *Structure*, **2013**, *21*, 9–19.

[635] B. M. Pettitt; P. J. Rossky. Alkali halides in water: Ion-solvent correlations and ion-ion potentials of mean force at infinite dilution. *J. Chem. Phys.*, **1986**, *15*, 5836–5844.

[636] S. J. Singer; D. Chandler. Free energy functions in the extended RISM approximation. *Mol. Phys.*, **1985**, *55*, 621–625.

[637] G. Schmeer; A. Maurer. Development of thermodynamic properties of electrolyte solutions with the help of RISM-calculations at the Born-Oppenheimer level. *Phys. Chem. Chem. Phys.*, **2010**, *12*, 2407–2417.

[638] S. M. Kast. Free energies from integral equation theories: Enforcing path independence. *Phys. Rev. E*, **2003**, *67*, 041203.

[639] P. G. Karamertzanis; P. Raiteri; A. Galindo. The use of anisotropic potentials in modeling water and free energies of hydration. *J. Chem. Theory Comput.*, **2010**, *6*, 3153–3161.

[640] J. Wang; P. Cieplak; J. Li; T. Hou; R. Luo; Y. Duan. Development of Polarizable Models for Molecular Mechanical Calculations I: Parameterization of Atomic Polarizability. *J. Phys. Chem. B*, **2011**, *115*, 3091–3099.

[641] J. Wang; P. Cieplak; J. Li; J. Wang; Q. Cai; M. Hsieh; H. Lei; R. Luo; Y. Duan. Development of Polarizable Models for Molecular Mechanical Calculations II: Induced Dipole Models Significantly Improve Accuracy of Intermolecular Interaction Energies. *J. Phys. Chem. B*, **2011**, *115*, 3100–3111.

[642] J. Wang; P. Cieplak; J. Li; Q. Cai; M. Hsieh; R. Luo; Y. Duan. Development of Polarizable Models for Molecular Mechanical Calculations. 4. van der Waals Parametrization. *J. Phys. Chem. B*, **2012**, *116*, 7088–7101.

[643] J. Wang; P. Cieplak; Q. Cai; M. Hsieh; J. Wang; Y. Duan; R. Luo. Development of Polarizable Models for Molecular Mechanical Calculations. 3. Polarizable Water Models Conforming to Thole Polarization Screening Schemes. *J. Phys. Chem. B*, **2012**, *116*, 7999–8008.

[644] J. Wang; Q. Cai; Y. Xiang; R. Luo. Reducing Grid Dependence in Finite-Difference Poisson-Boltzmann Calculations. *J. Chem. Theory Comput.*, **2012**, *8*, 2741–2751.

[645] B. T. Thole. Molecular polarizabilities calculated with a modified dipole interaction. *Chem. Phys.*, **1981**, *59*, 341–350.

[646] R. Bosque; J. Sales. Polarizabilities of solvents from the chemical composition. *J. Chem. Inf. Comput. Sci.*, **2002**, *42*, 1154–1163.

[647] Z. X. Wang; C. Wu; H. X. Lei; Y. Duan. Accurate ab initio study on the hydrogen-bond pairs in protein secondary structures. *J. Chem. Theory Comput.*, **2007**, *3*, 1527–1537.

[648] J. Graf; P. H. Nguyen; G. Stock; H. Schwalbe. Structure and Dynamics of the Homologous Series of Alanine Peptides: A Joint Molecular Dynamics/NMR Study. *J. Am. Chem. Soc.*, **2007**, *129*, 1179–1189.

[649] T. E. Cheatham, III. Simulation and modeling of nucleic acid structure, dynamics and interactions. *Curr. Opin. Struct. Biol.*, **2004**, *14*, 360–367.

[650] I. Yildirim; S. D. Kennedy; H. A. Stern; J. M. Hart; R. Kierzek; D. H. Turner. Revision of AMBER Torsional Parameters for RNA Improves Free Energy Predictions for Tetramer Duplexes with GC and iGiC Base Pairs. *J. Chem. Theory Comput.*, **2012**, *8*, 172–181.

[651] M. Krepl; M. Zgarbova; P. Stadlbauer; M. Otyepka; P. Banas; J. Koca; T. E. Cheatham, III; J. Sponer. Reference simulations of noncanonical nucleic acids with different chi variants of the AMBER force field: Quadruplex DNA, quadruplex RNA, and Z-DNA. *J. Chem. Theory Comp.*, **2012**, *8*, 2506–2520.

[652] J. Wang; T. Hou. Application of Molecular Dynamics Simulations in Molecular Property Prediction. II. Diffusion coefficient. *J. Comput. Chem.*, **2011**, *32*, 3509–3519.

[653] C. F. Fu; S. X. Tian. A Comparative Study for Molecular Dynamics Simulations of Liquid Benzene. *J. Chem. Theory Comput.*, **2011**, *7*, 2240–2252.

[654] S. Tsuzuki; T. Uchimaru; K. Tanabe; S. Kuwajima. Refinement of Nonbonding Interaction Potential Parameters for Methane on the Basis of the Pair Potential Obtained by Mp3/6-311g(3d,3p)-Level Ab-Initio Molecular-Orbital Calculations - the Anisotropy of H/H Interaction. *J. Phys. Chem.*, **1994**, *98*, 1830–1833.

[655] G. A. Kaminski; R. A. Friesner; J. Tirado-Rives; W. L. Jorgensen. Evaluation and Reparametrization of the OPLS-AA Force Field for Proteins via Comparison with Accurate Quantum Chemical Calculations on Peptides. *J. Phys. Chem. B*, **2001**, *105*, 6474–6487.

[656] I. J. Chen; D. Yin; A. D. MacKerell. Combined Ab initio/Empirical Approach for Optimization of Lennard-Jones Parameters for Polar-Neutral Compounds. *J. Comput. Chem.*, **2002**, *23*, 199–213.

[657] M. L. DeMarco; R. J. Woods. Atomic-resolution conformational analysis of the G(M3) ganglioside in a lipid bilayer and its implications for ganglioside-protein recognition at membrane surfaces. *Glycobiology*, **2009**, *19*, 344–355.

[658] M. L. DeMarco; R. J. Woods; J. H. Prestegard; F. Tian. Presentation of Membrane-Anchored Glycosphingolipids Determined from Molecular Dynamics Simulations and NMR Paramagnetic Relaxation Rate Enhancement. *J. Am. Chem. Soc.*, **2010**, *132*, 1334–1338.

[659] R. Kadirvelraj; O. C. Grant; I. J. Goldstein; H. C. Winter; H. Tateno; E. Fadda; R. J. Woods. Structure and binding analysis of Polyporus squamosus lectin in complex with the Neu5Ac$\alpha$2-6Gal$\beta$1-4GlcNAc human-type influenza receptor. *Glycobiology*, **2011**, *21*, 973–984.

[660] B. L. Foley; M. B. Tessier; R. J. Woods. Carbohydrate force fields. *WIREs Comput. Mol. Sci.*, **2012**, *2*, 652–697.

[661] E. Ficko-Blean; C. P. Stuart; M. D. Suits; M. Cid; M. Tessier; R. J. Woods; A. B. Boraston. Carbohydrate Recognition by an Architecturally Complex $\alpha$-N-Acetylglucosaminidase from Clostridium perfringens. *PLoS ONE*, **2012**, *7*, e33524.

[662] M. L. DeMarco; R. J. Woods. From agonist to antagonist: Structure and dynamics of innate immune glycoprotein MD-2 upon recognition of variably acylated bacterial endotoxins. *Mol. Immunol.*, **2011**, *49*, 124–133.

[663] N. Spackova; T. E. Cheatham; F. Ryjacek; F. Lankas; L. vanMeervelt; P. Hobza; J. Sponer. Molecular Dynamics Simulations and Thermodynamics Analysis of DNA-Drug Complexes. Minor Groove Binding between 4',6-Diamidino-2-phenylindole and DNA Duplexes in Solution. *J. Am. Chem. Soc.*, **2003**, *125*, 1759–1769.

[664] P. Varnai; D. Djuranovic; R. Lavery; B. Hartmann. alpha/gamma Transitions in the B-DNA backbone. *Nucl. Acids Res.*, **2002**, *30*, 5398–5406.

[665] D. Svozil; J. E. Sponer; I. Marchan; A. Perez; T. E. Cheatham; F. Forti; F. J. Luque; M. Orozco; J. Sponer. Geometrical and electronic structure variability of the sugar-phosphate backbone in nucleic acids. *J. Phys. Chem. B*, **2008**, *112*, 8188–8197.

[666] D. S. Cerutti; J. E. Rice; W. C. Swope; D. A. Case. Derivation of fixed partial charges for amino acids accommodating a specific water model and implicit polarization. *J. Phys. Chem. B*, **2013**, *117*, 2328–2338.

[667] T. Steinbrecher; J. Latzer; D. A. Case. Revised AMBER Parameters for Bioorganic Phosphates. *J. Chem. Theory Comput.*, **2012**, *8*, 4405–4412.

[668] F.-Y. Dupradeau; A. Pigache; T. Zaffran; C. Savineau; R. Lelong; N. Grivel; D. Lelong; W. Rosanskia; P. Cieplak. The R. E. D. tools: advances in RESP and ESP charge derivation and force field library building. *PhysChemChemPhys*, **2010**, *12*, 7821–7839.

[669] S. E. Feller. Molecular dynamics simulations of lipid bilayers. *Curr. Opin. Colloid Interface Sci.*, **2000**, *5*, 217–223.

[670] A. Lomize; I. Pogozheva; M. Lomize; H. Mosberg. The role of hydrophobic interactions in positioning of peripheral proteins in membranes. *BMC Struct. Biol.*, **2007**, *7*, 44.

[671] C. J. Dickson; L. Rosso; R. M. Betz; R. C. Walker; I. R. Gould. GAFFlipid: a General Amber Force Field for the accurate molecular dynamics simulation of phospholipid. *Soft Matter*, **2012**, *8*, 9617.

[672] R. M. Betz; N. A. DeBardeleben; R. C. Walker. An Investigation of the effects of hard and soft errors on graphics processing unit-accelerated molecular dynamics simulations. *Concurrency and Computation: Practice and Experience*, **2014**, *26*, 2134.

[673] D. E. Warschawski; P. F. Devaux. Order parameters of unsaturated phospholipids in membranes and the effect of cholesterol: a 1H-13C solid-state NMR study at natural abundance. *Eur. Biophys. J.*, **2005**, *34*, 987–996.

[674] L. Saiz; M. L. Klein. Computer Simulation Studies of Model Biological Membranes. *Acc. Chem. Res.*, **2002**, *35*, 482–489.

[675] J. T. Berryman; T. Schilling. Free Energies by Thermodynamic Integration Relative to an Exact Solution, Used to Find the Handedness-Switching Salt Concentration for DNA. *J. Chem. Theory Comput.*, **2013**, *9*, 679–686.

[676] J. T. Berryman; T. Schilling. Absolute Free Energies for Biomolecules in Implicit or Explicit Solvent. *Physics Procedia*, **2014**, *57*, 7–15.

[677] J. T. Berryman; A. Taghavi; F. Mazur; A. Tkatchenko. Quantum Machine Learning Corrects Classical Force Fields: Stretching DNA Base Pairs in Explicit Solvent. *J. Chem. Phys.*, **2022**. Draft with JCP at time of writing, preprint ArXiv id is: 2203.15525.

[678] T. Schilling; F. Schmid. Computing absolute free energies of disordered structures by molecular simulation. *J. Chem. Phys.*, **2009**, *131*, 231102.

[679] F. Schmid; T. Schilling. A method to compute absolute free energies or enthalpies of fluids. *Physics Procedia*, **2010**, *4*, 131–143.

[680] D. Frenkel; A. J. C. Ladd. New Monte Carlo method to compute the free energy of arbitrary solids. Application to the fcc and hcp phases of hard spheres. *J. Chem. Phys.*, **1984**, *81*, 3188–3193.

[681] C. Vega; E. G. Noya. Revisiting the Frenkel-Ladd method to compute the free energy of solids: the Einstein molecule approach. *J. Chem. Phys.*, **2007**, *127*, 154113.

[682] J. M. Swails; A. E. Roitberg. Enhancing Conformation and Protonation State Sampling of Hen Egg White Lysozyme Using pH Replica Exchange Molecular Dynamics. *J. Chem. Theory Comput.*, **2012**, *8*, 4393–4404.

[683] S. G. Itoh; A. Damjanovic; B. R. Brooks. pH replica-exchange method based on discrete protonation states. *Proteins*, **2011**, *79*, 3420–3436.

[684] S. A. Showalter; R. Brüschweiler. Validation of molecular dynamics simulations of biomolecules using NMR spin relaxation as benchmarks: Application to the Amber99SB force field. *J. Chem. Theory Comput.*, **2007**, *3*, 961–975.

[685] R. B. Best; N.-V. Buchete; G. Hummer. Are Current Molecular Dynamics Force Fields too Helical? *Biophys. J.*, **2008**, *95*, L07–L09; 4494.

[686] R. B. Best; G. Hummer. Optimized Molecular Dynamics Force Fields Applied to the Helix-Coil Transition of Polypeptides. *J. Phys. Chem. B*, **2009**, *113*, 9904–9015.

[687] R. B. Best; J. Mittal. Free-energy landscape of the GB1 hairpin in all-atom explicit solvent simulations with different force fields: Similarities and differences. *Proteins*, **2011**, *79*, 1318–1328.

[688] K. K. Patapati; N. M. Glykos. Three force fields views of the 3-10 helix. *Biophys. J.*, **2011**, *101*, 1766–1771.

[689] S. Le Grand; A. W. Goetz; R. C. Walker. SPFP: Speed without compromise–A mixed precision model for GPU accelerated molecular dynamics simulations. *Comput. Phys. Commun.*, **2013**, *184*, 374–380.

[690] R. Salomon-Ferrer; D. A. Case; R. C. Walker. An overview of the Amber biomolecular simulation package. *WIREs Comput. Mol. Sci.*, **2013**, *3*, 198–210.

[691] PDB Current Holdings Breakdown. **2013**.

[692] M. L. Lundstrom, K. H.; Chiu. *G Protein-Coupled Receptors in Drug Discovery*. Taylor & Francis, London, 2005.

[693] C. Chipot; A. Pohorille, eds. *Free energy calculations. Theory and Applications in Chemistry and Biology*. Springer, Berlin, 2007.

[694] M. Griebel; S. Knapek; G. Zumbusch. *Numerical Simulation in Molecular Dynamics. Numerical Algorithms, Parallelization, Applications*. Springer-Verlag, Berlin, 2010.

[695] M. E. Tuckerman. *Statistical Mechanics: Theory and Molecular Simulation*. Oxford University Press, Oxford, 2010.

[696] M. Ester; H. Kriegel; J. Sander; X. Xu. A Density-Based Algorithm for Discovering Clusters in Large Spatial Databases with Noise. *Proc. Second Int. Conf. Knowledge Disc. Data Mining (KDD-96)*, **1996**, pp 226–231.

[697] B. R. Miller; T. D. McGee; J. M. Swails; N. Homeyer; H. Gohlke; A. E. Roitberg. MMPBSA.py: An Efficient Program for End-State Free Energy Calculations. *J. Chem. Theory Comput.*, **2012**, *8*, 3314–3321.

[698] D. R. Roe; T. E. Cheatham, III. PTRAJ and CPPTRAJ: Software for Processing and Analysis of Molecular Dynamics Trajectory Data. *J. Chem. Theory Comput.*, **2013**, *9*, 3084–3095.

[699] J. M. Swails; D. M. York; A. E. Roitberg. Constant pH replica exchange molecular dynamics in explicit solvent using discrete protonation states: implementation, testing, and validation. *J. Chem. Theory Comput.*, **2014**, *10*, 1341–1352.

[700] M. Arrar; C. A. F. de Oliveira; M. Fajer; W. Sinko; J. A. McCammon. w-REXAMD: A Hamiltonian Replica Exchange Approach to Improve Free Energy Calculations for Systems with Kinetically Trapped Conformations. *J. Chem. Theory Comput.*, **2013**, *9*, 18–23.

[701] M. Fajer; D. Hamelberg; J. A. McCammon. Replica-Exchange Accelerated Molecular Dynamics (REXAMD) Applied to Thermodynamic Integration. *J. Chem. Theory Comput.*, **2008**, *4*, 1565–1569.

[702] P. Li; B. P. Roberts; D. K. Chakravorty; K. M. Merz, Jr. Rational Design of Particle Mesh Ewald Compatible Lennard-Jones Parameters for +2 Metal Cations in Explicit Solvent. *J. Chem. Theory Comput.*, **2013**, *9*, 2733–2748.

[703] P. Li; K. M. Merz, Jr. Taking into Account the Ion-Induced Dipole Interaction in the Nonbonded Model of Ions. *J. Chem. Theory Comput.*, **2014**, *10*, 289–297.

[704] P. Li; L. F. Song; K. M. Merz, Jr. Parameterization of Highly Charged Metal Ions Using the 12-6-4 LJ-Type Nonbonded Model in Explicit Water. *J. Phys. Chem. B*, **2015**, *119*, 883–895.

[705] P. Li; L. F. Song; K. M. Merz, Jr. Systematic Parameterization of Monovalent Ions Employing the Nonbonded Model. *J. Chem. Theory Comput.*, **2015**, *11*, 1645–1657.

[706] M. T. Panteva; G. M. Giambasu; D. M. York. Comparison of Structural, Thermodynamic, Kinetic and Mass Transport Properties of Mg2+ Models Commonly Used in Biomolecular Simulations. *J. Comput. Chem.*, **2015**, *36*, 970–982.

[707] M. T. Panteva; G. M. Giambasu; D. M. York. Force Field for Mg2+, Mn2+, Zn2+ and Cd2+ Ions That Have Balanced Interactions with Nucleic Acids. *J. Phys. Chem. B*, **2015**, *119*, 15460–15470.

[708] A. Ganguly; B. P. Weissman; T. J. Giese; N.-A. Li; S. Hoshika; S. Rao; A. A. Benner; J. A. Piccirilli; D. M. York. Confluence of theory and experiment reveals the catalytic mechanism of the Varkud satellite ribozyme. *Nat. Chem.*, **2020**, *12*, 192–201.

[709] P. Li; K. M. Merz, Jr. MCPB.py: A Python Based Metal Center Parameter Builder. *J. Chem. Inf. Model.*, **2016**, *56*, 599–604.

[710] P. Li; K. M. Merz, Jr. Metal Ion Modeling Using Classical Mechanics. *Chem. Rev.*, **2017**, *117*, 1564–1686.

[711] Z. Yu; P. Li; K. M. Merz, Jr. Extended Zinc AMBER Force Field (EZAFF). *J. Chem. Theory Comput.*, **2018**, *14*, 242–254.

[712] A. Sengupta; A. Seitz; K. M. Merz, Jr. Simulating the Chelate Effect. *J. Am. Chem. Soc.*, **2018**, *140*, 15166–15169.

[713] Z. Li; S. F. Lin; P. Li; K. M. Merz, Jr. Systematic Parametrization of Divalent Metal Ions for the OPC3, OPC, TIP3P-FB, and TIP4P-FB Water Models. *J. Chem. Theory Comput.*, **2020**, *16*, 4429–4442.

[714] S. F. Lin; A. Sengupta; K. M. Merz, Jr. Thermodynamics of Transition Metal Ion Binding to Proteins. *J. Am. Chem. Soc.*, **2020**, *142*, 6365–6374.

[715] P. Li; K. M. Merz, Jr. in *Methods Mol. Biol.*, (Humana Press, New York, NY). volume 2199. pp 257–275. 2021.

[716] A. Sengupta; Z. Li; S. F. Lin; P. Li; K. M. Merz, Jr. Parameterization of Monovalent Ions for the OPC3, OPC, TIP3P-FB, and TIP4P-FB Water Models. *J. Chem. Inf. Model.*, **2021**, *61*, 869–880.

[717] Z. Li; S. F. Lin; P. Li; K. M. Merz, Jr. Parametrization of Trivalent and Tetravalent Metal Ions for the OPC3, OPC, TIP3P-FB, and TIP4P-FB Water Models. *J. Chem. Theory Comput.*, **2021**, *17*, 2342–2354.

[718] E. S. Kolesnikov; I. Y. Gushchin; P. A. Zhilyaev; A. V. Onufriev. Similarities and Differences between Na+ and K+ Distributions around DNA Obtained with Three Popular Water Models. *J. Chem. Theory Comput.*, **2021**, *17*, 7246–7259.

[719] P. Li. Bridging the 12-6-4 Model and the Fluctuating Charge Model. *Front. Chem.*, **2021**, *9*, 721960.

[720] J. M. Seminario. Calculation of Intramolecular Force Fields from Second-Derivative Tensors. *Int. J. Quantum Chem.*, **1996**, *30*, 1271–1277.

[721] P. Eastman; V. S. Pande. OpenMM: A Hardware-Independent Framework for Molecular Simulations. *Computing in Science and Engineering*, **2010**, *12*, 34–39.

[722] P. Eastman; M. S. Friedrichs; J. D. Chodera; R. J. Radmer; C. M. Bruns; J. P. Ku; K. A. Beauchamp; T. J. Lane; L. Wang; D. Shukla; T. Tye; M. Houston; T. Stich; C. Klein; M. R. Shirts; V. S. Pande. OpenMM 4: A Reusable, Extensible, Hardware Independent Library for High Performance Molecular Simulation. *J. Chem. Theory Comput.*, **2013**, *9*, 461–469.

[723] J. M. Swails. *Free Energy Simulations of Complex Biological Systems at Constant pH*. PhD thesis, University of Florida, 2013.

[724] C. N. Nguyen; T. Kurtzman Young; M. K. Gilson. Grid Inhomogeneous solvation theory: Hydration structure and thermodynamics of the miniature receptor cucurbit[7]uril. *J. Chem. Phys.*, **2012**, *137*, 044101–044118.

[725] X. Wu; S. Subramaniam; D. A. Case; K. Wu; B. R. Brooks. Targeted conformational search with map-restrained self-guided langevin dynamics: application to flexible fitting into electron microscopic density maps. *J. Struct. Biology*, **2013**, *183*, 429–440.

[726] C. Bergonzo; N. M. Henriksen; D. R. Roe; J. M. Swails; A. E. Roitberg; T. E. Cheatham III. Multidimensional Replica Exchange Molecular Dynamics Yields a Converged Ensemble of an RNA Tetranucleotide. *J. Chem. Theory Comput.*, **2013**, *10*, 492–499.

[727] A. Bakan; L. M. Meireles; I. Bahar. ProDy: Protein Dynamics Inferred from Theory and Experiments. *Bioinformatics*, **2011**, *27*, 1575–1577.

[728] X. Wu; M. Hodoscek; B. R. Brooks. Replica exchanging self-guided Langevin dynamics for efficient and accurate conformational sampling. *J. Chem. Phys.*, **2012**, *137*, 044106.

[729] N. Bernstein; C. Várnai; I. Solt; S. A. Winfield; M. C. Payne; I. Simon; M. Fuxreiter; G. Csányi. *Phys. Chem. Chem. Phys.*, **2011**, *14*, 646–656.

[730] C. Várnai; N. Bernstein; L. Mones; G. Csányi. Tests of an adaptive qm/mm calculation on free energy profiles of chemical reactions in solution. *J. Phys. Chem. B*, **2013**, *117*, 12202–12211.

[731] G. Csányi; T. Albaret; G. Moras; M. C. Payne; A. D. Vita. Multiscale hybrid simulation methods for material systems. *J. Phys. Condens. Matt.*, **2005**, *17*, R691.

[732] N. Bernstein; J. R. Kermode; G. Csányi. Hybrid atomistic simulation methods for materials systems. *Rep. Prog. Phys.*, **2009**, *72*, 026501.

[733] A. Jones; B. Leimkuhler. Adaptive stochastic methods for sampling driven molecular systems. *J. Chem. Phys.*, **2011**, *135*, 084125.

[734] T. Kerdcharoen; B. M. Rode. A QM/MM simulation method applied to the solution of Li+ in liquid ammonia. *Chem. Phys.*, **1996**, *211*, 313–323.

[735] N. Homeyer; H. Gohlke. FEW - A workflow tool for free energy calculations of ligand binding. *J. Comput. Chem.*, **2013**, *34*, 965–973.

[736] A. Metz. *Goethe University (Frankfurt am Main)*, **2006**.

[737] J. Åqvist; C. Medina; J. E. Samuelsson. A new method for predicting binding affinity in computer-aided drug design. *Protein Eng.*, **1994**, *7*, 385–391.

[738] J. Åqvist; V. B. Luzhkov; B. O. Brandsdal. Ligand binding affinities from MD simulations. *Acc. Chem. Res.*, **2002**, *35*, 358–365.

[739] H. G. Wallnoefer; K. R. Liedl; T. Fox. A challenging system: free energy prediction for factor Xa. *J. Comput. Chem.*, **2011**, *32*, 1743–1752.

[740] M. M. van Lipzig; A. M. ter Laak; A. Jongejan; N. P. Vermeulen; M. Wamelink; D. Geerke; J. H. Meerman. Prediction of ligand binding affinity and orientation of xenoestrogens to the estrogen receptor by molecular dynamics simulations and the linear interaction energy method. *J. Med. Chem.*, **2004**, *47*, 1018–1030.

[741] B. O. Brandsdal; F. Österberg; M. Almlöf; I. Feierberg; V. B. Luzhkov; Åqvist, J. Free energy calculations and ligand binding. *Adv. Protein Chem.*, **2003**, *66*, 123–158.

[742] W. Wang; J. Wang; P. A. Kollman. What determines the van der Waals coefficient beta in the LIE (linear interaction energy) method to estimate binding free energies using molecular dynamics simulations? *Proteins: Struct., Funct., Genet.*, **1999**, *34*, 395–402.

[743] D. K. Jones-Hertzog; W. L. Jorgensen. Binding affinities for sulfonamide inhibitors with human thrombin using Monte Carlo simulations with a linear response method. *J. Med. Chem.*, **1997**, *40*, 1539–1549.

[744] M. L. Lamb; J. Tirado-Rives; W. L. Jorgensen. Estimation of the binding affinities of FKBP12 inhibitors using a linear response method. *Bioorg. Med. Chem.*, **1999**, *7*, 851–860.

[745] W. Yang; R. Bitetti-Putzer; K. M. Free energy simulations: Use of reverse cumulative averaging to determine the equilibrated region and the time required for convergence. *J. Chem. Phys.*, **2004**, *120*, 2618–2628.

[746] J. B. Kruskal. On the shortest spanning subtree of a graph and the traveling salesman problem. *Proc. Amer. Math. Soc.*, **1956**, *7*, 48–50.

[747] *ROCS, OpenEye Scientific Software, Santa Fe*, *http://www.eyesopen.com*.

[748] P. C. D. Hawkins; A. G. Skillman; A. Nicholls. Comparison of shape-matching and docking as virtual screening tools. *J. Med. Chem.*, **2007**, *50*, 74–82.

[749] T. E. Cheatham; D. A. Case. Twenty-five years of nucleic acid simulations. *Biopolymers*, **2013**, *99*, 969–977.

[750] C. J. Cramer. *Essentials of Computational Chemistry: Theories and Models*. John Wiley & Sons, New York, 2002.

[751] T. Lazaridis. Inhomogeneous Fluid Approach to Solvation Thermodynamics. 1 Theory. *J. Phys. Chem. B*, **1998**, *102*, 3531–3541.

[752] C. N. Nguyen; T. Kurtzman Young; M. K. Gilson. Grid Inhomogeneous Solvation Theory: Hydration Structure and Thermodynamics of the Miniature Receptor cucurbit[7]uril. *J. Chem. Phys.*, **2012**, *137*, 044101.

[753] S. Chatterjee; P. G. Debenedetti; F. H. Stillinger; R. M. Lynden-Bell. A Computational Investigation of Thermodynamics, Structure, Dynamics and Solvation Behavior in Modified Water Models. *J. Chem. Phys.*, **2008**, *128*, 124511.

[754] W. Humphrey; A. Dalke; K. Schulten. VMD Visual Molecular Dynamics. *J. Molec. Graph.*, **1996**, *14*, 33–38.

[755] D. J. Sindhikara; N. Yoshida; F. Hirata. Placevent: An Algorithm for Prediction of Explicit Solvent Atom Distribution-Application to HIV-1 Protease and F-ATP Synthase. *J. Comput. Chem.*, **2012**, *33*, 1536–1543.

[756] C. J. Dickson; B. D. Madej; A. A. Skjevik; R. M. Betz; K. Teigen; I. R. Gould; R. C. Walker. Lipid14: The Amber Lipid Force Field. *J. Chem. Theory Comput.*, **2014**, *10*, 865–879.

[757] R. Konecny; N. A. Baker; J. A. McCammon. iAPBS: a programming interface to the adaptive Poisson–Boltzmann solver. *Comput. Sci. Disc.*, **2012**, *5*, 15005–15013.

[758] H. Nguyen; D. R. Roe; C. Simmerling. Improved Generalized Born Solvent Model Parameters for Protein Simulations. *J. Chem. Theory Comput.*, **2013**, *9*, 2020–2034.

[759] D. P. Fernandez; A. R. H. Goodwin; E. W. Lemmon; J. M. H. Levelt Sengers; R. C. Williams. A formulation for the static permittivity of water and steam at temperatures from 238 k to 873 k at pressures up to 1200 mpa, including derivatives and debye huckel coefficients. *J. Phys. Chem. Ref. Data*, **1997**, *26*, 1125–1166.

[760] R. Mills. Self-diffusion in normal and heavy water in the range 1-45. deg. *J. Phys. Chem.*, **1973**, *77*, 685–688.

[761] W. Wagner; A. Pruss. The iapws formulation 1995 for the thermodynamic properties of ordinary water substance for general and scientific use. *J. Phys. Chem. Ref. Data*, **2002**, *31*, 387–535.

[762] L. B. Skinner; C. Huang; D. Schlesinger; L. G. M. Pettersson; A. Nilsson; C. J. Benmore. Benchmark oxygen-oxygen pair-distribution function of ambient water from x-ray diffraction measurements with a wide q-range. *J. Chem. Phys.*, **2013**, *138*, 074506+.

[763] G. S. Kell. Precise representation of volume properties of water at one atmosphere. *J. Chem. Eng. Data*, **1967**, *12*, 66–69.

[764] S. Niu; M. L. Tan; T. Ichiye. The large quadrupole of water molecules. *J. Chem. Phys.*, **2011**, *134*, 134501+.

[765] S. Izadi; R. Anandakrishnan; A. V. Onufriev. Building Water Models: A Different Approach. *J. Phys. Chem. Lett.*, **2014**, *5*, 3863–3871.

[766] A. Mukhopadhyay; A. T. Fenley; I. S. Tolokh; A. V. Onufriev. Charge hydration asymmetry: the basic principle and how to use it to test and improve water models. *J. Phys. Chem. B*, **2012**, *116*, 9776–9783.

[767] B. Aguilar; R. Shadrach; A. V. Onufriev. Reducing the secondary structure bias in the generalized born model via r6 effective radii. *J. Chem. Theory Comput.*, **2010**, *6*, 3613–3630.

[768] B. Aguilar; A. V. Onufriev. Efficient computation of the total solvation energy of small molecules via the r6 generalized born model. *J. Chem. Theory Comput.*, **2012**, *8*, 2404–2411.

[769] A. Mukhopadhyay; B. H. Aguilar; I. S. Tolokh; A. V. Onufriev. Introducing charge hydration asymmetry into the generalized born model. *J Chem. Theory Comput.*, **2014**, *10*, 1788–1794.

[770] B. Schneider; S. Neidle; H. M. Berman. Conformations of the sugar-phosphate backbone in helical dna crystal structures. *Biopolymers*, **1997**, *42*, 113–124.

[771] B. Schneider; Z. Moravek; H. M. Berman. Rna conformational classes. *Nucleic Acids Res.*, **2004**, *32*, 1666–1677.

[772] P. A. Janowski; D. S. Cerutti; J. M. Holton; D. A. Case. Peptide crystal simulations reveal hidden dynamics. *J. Am. Chem. Soc.*, **2013**, *135*, 7938–7948.

[773] G. Monard; M. I. Bernal-Uruchurtu; A. Van Der Vaart; K. M. Merz, Jr.; M. F. Ruiz-López. Simulation of liquid water using semiempirical Hamiltonians and the divide and conquer approach. *J. Phys. Chem. A*, **2005**, *109*, 3425–3432.

[774] A. Marion; G. Monard; M. F. Ruiz-López; F. Ingrosso. Water interactions with hydrophobic groups: assessment and recalibration of semiempirical molecular orbital methods. *J. Chem. Phys.*, **2014**, *141*, 034106.

[775] A. Marion; H. Gockan; G. Monard. SemiEmpirical Born-Oppenheimer Molecular Dynamics (SEBOMD) Within the Amber Biomolecular Package. *J. Chem. Inf. Model.*, **2019**, *59*, 206–214.

[776] E. Thiriot; G. Monard. Combining a genetic algorithm with a linear scaling semiempirical method for protein-ligand docking. *J. Mol. Struct. Theochem*, **2009**, *898*, 31–41.

[777] W. Harb; M. I. Bernal-Uruchurtu; M. F. Ruiz-López. An improved semiempirical method for hydrated systems. *Theor. Chem. Acc.*, **2004**, *112*, 204–216.

[778] M. I. Bernal-Uruchurtu; M. T. C. Martins-costa; C. Millot; M. F. Ruiz-López. Improving Description of Hydrogen Bonds at the Semiempirical Level : Water - Water Interactions as Test Case. *J. Comput. Chem.*, **2000**, *21*, 572–581.

[779] O. Ludwig; H. Schinke; W. Brandt. Reparametrisation of Force Constants in MOPAC 6.0/7.0 for Better Description of the Activation Barrier of Peptide Bond Rotations. *J. Molec. Model.*, **1996**, *2*, 341–350.

[780] M. Zgarbová; F. J. Luque; J. Šponer; T. E. C. III; M. Otyepka; P. Jurečka. Toward improved description of dna backbone: Revisiting epsilon and zeta torsion force field parameters. *J. Chem. Theory Comput.*, **2013**, *9*, 2339–2354.

[781] I. Omelyan; A. Kovalenko. Generalized canonical-isokinetic ensemble: Speeding up multiscale molecular dynamics and coupling with 3d molecular theory of solvation. *Mol. Sim.*, **2013**, *39*, 25–48.

[782] I. Omelyan; A. Kovalenko. Multiple time step molecular dynamics in the optimized isokinetic ensemble steered with the molecular theory of solvation: Accelerating with advanced extrapolation of effective solvation forces. *J. Chem. Phys.*, **2013**, *139*, 244106.

[783] A. Onufriev. in *Modeling Solvent Environments*, M. Feig, Ed., (Wiley, USA). pp 127–165. 2010.

[784] D. S. Cerutti; W. C. Swope; J. E. Rice; D. A. Case. ff14ipq: A Self-Consistent Force Field for Condensed-Phase Simulations of Proteins. *J. Chem. Theory Comput.*, **2014**, *10*, 4515–4534.

[785] B. D. Madej; I. R. Gould; R. C. Walker. A Parameterization of Cholesterol for Mixed Lipid Bilayer Simulation within the Amber Lipid14 Force Field. *J Phys Chem B*, **2015**, *119*, 12424–12435.

[786] C. Vega; J. L. F. Abascal. Simulating water with rigid non-polarizable models: a general perspective. *Phys Chem Chem Phys*, **2011**, *13*, 19663–19688.

[787] R. Anandakrishnan; A. Drozdetski; R. C. Walker; A. V. Onufriev. Speed of Conformational Change: Comparing Explicit and Implicit Solvent Molecular Dynamics Simulations. *Biophysical Journal*, **2015**, *108*, 1153–1164.

[788] Y. M. Rhee; V. S. Pande. Solvent viscosity dependence of the protein folding dynamics. *J. Phys. Chem. B*, **2008**, *112*, 6221–6227. PMID: 18229911.

[789] L. David; R. Luo; M. K. Gilson. Comparison of generalized born and poisson models: Energetics and dynamics of hiv protease. *J. Comput. Chem.*, **2000**, *21*, 295–309.

[790] M. Feig. Kinetics from Implicit Solvent Simulations of Biomolecules as a Function of Viscosity. *J. Chem. Theory Comput.*, **2007**, *3*, 1734–1748.

[791] R. E. Amaro; X. Cheng; I. Ivanov; D. Xu; A. J. Mccammon. Characterizing Loop Dynamics and Ligand Recognition in Human- and Avian-Type Influenza Neuraminidases via Generalized Born Molecular Dynamics and End-Point Free Energy Calculations. *J. Am. Chem. Soc.*, **2009**, *131*, 4702–4709.

[792] B. Zagrovic; V. Pande. Solvent viscosity dependence of the folding rate of a small protein: Distributed computing study. *J. Comput. Chem.*, **2003**, *24*, 1432–1436.

[793] P. H. Hunenberger; A. E. Mark; W. F. van Gunsteren. Fluctuation and Cross-correlation Analysis of Protein Motions Observed in Nanosecond Molecular Dynamics Simulations. *J. Mol. Biol.*, **1995**, *252*, 492–503.

[794] R. Galindo-Murillo; D. R. Roe; T. E. Cheatham, III. Convergence and reproducibility in molecular dynamics simulations of the DNA duplex d(GCACGAACGAACGAACGC). *Biochim. Biophys. Acta*, **2015**, *1850*, 1041–1058.

[795] G. M. Giambasu; T. Luchko; D. Herschlag; D. M. York; D. A. Case. Ion counting from explicit-solvent simulations and 3d-RISM. *Biophys J*, **2014**, *106*, 883–894.

[796] I. S. Joung; T. Luchko; D. A. Case. Simple electrolyte solutions: Comparison of DRISM and molecular dynamics results for alkali halide solutions. *J Chem Phys*, **2013**, *138*, 044103.

[797] J. Domanski; P. Stansfeld; M. S. P. Sansom; O. Beckstein. Lipidbook: A Public Repository for Force Field Parameters Used in Membrane Simulations. *J. Membrane Biol.*, **2010**, *236*, 255–258.

[798] S. Jo; T. Kim; W. Im. Automated builder and database of protein/membrane complexes for molecular dynamics simulations. *PLoS One*, **2007**, *2*, e880.

[799] S. Jo; T. Kim; V. G. Iyer; I. W. CHARMM-GUI: a web-based graphical user interface for CHARMM. *J. Comput. Chem.*, **2008**, *29*, 1859–1865.

[800] S. Jo; J. B. Lim; J. B. Klauda; W. Im. CHARMM-GUI Membrane Builder for mixed bilayers and its application to yeast membranes. *Biophys. J.*, **2009**, *97*, 50–58.

[801] E. L. Wu; X. Cheng; S. Jo; H. Rui; K. C. Song; E. M. Davila-Contreras; Y. Qi; J. Lee; V. Monje-Galvan; R. M. Venable; J. B. Klauda; I. W. CHARMM-GUI Membrane Builder toward realistic biological membrane simulations. *J. Comput. Chem.*, **2014**, *35*, 1997–2004.

[802] N. A. Baker; D. Sept; J. Simpson; M. J. Holst; M. J. A. Electrostatics of nanosystems: application to microtubules and the ribosome. *Proc. Natl. Acad. Sci. U. S. A.*, **2001**, *98*, 10037–10041.

[803] M. Holst; F. Saied. Multigrid solution of the Poisson-Boltzmann equation. *J. Comput. Chem.*, **1993**, *14*, 105–113.

[804] M. Holst; F. Saied. Numerical solution of the nonlinear Poisson-Boltzmann equation: Developing more robust and efficient methods. *J. Comput. Chem.*, **1995**, *16*, 337–364.

[805] M. Holst. Adaptive numerical treatment of elliptic systems on manifolds. *Adv. Comput. Math.*, **2001**, *15*, 139–191.

[806] R. Bank; M. Holst. A New Paradigm for Parallel Adaptive Meshing Algorithms. *SIAM Review*, **2003**, *45*, 291–323.

[807] K. M. Callenberg; O. P. Choudhary; G. L. de Forest; D. W. Gohara; N. A. Baker; M. Grabe. APBSmem: A graphical interface for electrostatic calculations at the membrane. *PLoS One*, **2010**, *5*, e12722.

[808] H. Nymeyer; H. X. Zhou. A method to determine dielectric constants in nonhomogeneous systems: application to biological membranes. *Biophys. J.*, **2008**, *94*, 1185–1193.

[809] H. A. Stern; S. E. Feller. Calculation of the dielectric permittivity profile for a nonuniform system: application to a lipid bilayer simulation. *J. Chem. Phys.*, **2003**, *118*, 3401–3412.

[810] N. Homeyer; H. Gohlke. Extension of the free energy workflow FEW towards implicit solvent/implicit membrane MM-PBSA calculations. *BBA - Gen. Subjects*, **2015**, *1850*, 972–982.

[811] L. Waeschenbach; C. G. W. Gertzen; V. Keitel; H. Gohlke. Dimerization energetics of the G-protein coupled bile acid receptor TGR5 from all-atom simulations. *J. Comput. Chem.*, **2019**, *41*.

[812] J. Z. Ruscio; D. Kumar; M. Shukla; M. G. Prisant; T. M. Murali; A. V. Onufriev. Atomic level computational identification of ligand migration pathways between solvent and binding site in myoglobin. *Proc. Nat. Acad. Sci. USA*, **2008**, *105*, 9204–9209.

[813] C. W. Hopkins; S. Le Grand; R. C. Walker; A. E. Roitberg. Long-Time-Step Molecular Dynamics through Hydrogen Mass Repartitioning. *J. Chem. Theory Comput.*, **2015**, *11*, 1864–1874.

[814] N. Homeyer; A. H. C. Horn; H. Lanig; H. Sticht. AMBER force-field parameters for phosphorylated amino acids in different protonation states: phosphoserine, phosphothreonine, phosphotyrosine, and phosphohistidine. *J. Mol. Model.*, **2006**, *12*, 281–289.

[815] M. Grabe; H. Lecar; Y. N. Jan; J. L. Y. A quantitative assessment of models for voltage-dependent gating of ion channels. *Proc. Natl. Acad. Sci. U. S. A.*, **2004**, *101*, 17640–17645.

[816] J. A. Maier; C. Martinez; K. Kasavajhala; L. Wickstrom; K. E. Hauser; C. Simmerling. ff14SB: Improving the Accuracy of Protein Side Chain and Backbone Parameters from ff99SB. *J. Chem. Theory Comput.*, **2015**, *11*, 3696–3713.

[817] H. Nguyen; A. Pérez; S. Bermeo; C. Simmerling. Refinement of Generalized Born Implicit Solvation Parameters for Nucleic Acids and Their Complexes with Proteins. *J. Chem. Theory Comput.*, **2015**, *11*, 3714–3728.

[818] K. Takemura; A. Kitao. Water Model Tuning for Improved Reproduction of Rotational Diffusion and NMR Spectral Density. *J. Phys. Chem. B*, **2012**, *116*, 6279–6287.

[819] L.-P. Wang; T. J. Martinez; V. S. Pande. Building force fields: An automatic, systematic and reproducible approach. *J. Phys. Chem. Lett.*, **2014**, *5*, 1885–1891.

[820] B. Leimkuhler; D. T. Margul; M. E. Tuckerman. Stochastic, Resonance-Free Multiple Time-Step Algorithm for Molecular Dynamics with Very Large Time Steps. *Mol. Phys.*, **2013**, *111*, 3579–3594.

[821] I. Omelyan; A. Kovalenko. MTS-MD of Biomolecules Steered with 3D-RISM-KH Mean Solvation Forces Accelerated with Generalized Solvation Force Extrapolation. *J. Chem. Theor. and Comp.*, **2014**, *11*, 1875–1895.

[822] H. Nguyen; J. Maier; H. Huang; V. Perrone; C. Simmerling. Folding simulations for proteins with diverse topologies are accessible in days with a physics-based force field and implicit solvent. *J. Am. Chem. Soc.*, **2014**, *136*, 13959–13962. PMID: 25255057.

[823] H. Nguyen; D. R. Roe; J. M. Swails; D. A. Case. PYTRAJ: Interactive data analysis for molecular dynamics simulations. *Manuscript in preparation*, **2016**.

[824] D. L. Blood; A. M. Rosnik; B. P. Krueger. Molecular dynamics parameters for the gfp chromophore and some of its analogues. *Manuscript in preparation*, **2016**.

[825] I. Ivani; P. D. Dans; A. Noy; A. Pérez; I. Faustino; A. Hopsital; J. Walther; P. Andrió; R. Goni; A. Balaceanu; G. Portella; F. Battistini; J. L. GelpÃ; C. González; M. Vendruscolo; C. A. Laughton; S. Harris; D. A. Case; M. Orozco. Parmbsc1: A refined force field for DNA simulations. *Nature Meth.*, **2016**, *13*, 55–58.

[826] M. Zgarbová; J. Sponer; M. Otyepka; T. E. Cheatham, III; R. Galindo-Murillo; P. Jurečka. Refinement of the Sugar-Phosphate Backbone Torsion Beta for AMBER Force Fields Improves the Description of Z- and B-DNA. *J. Chem. Theor. and Comp.*, **2015**, *12*, 5723–5736.

[827] Y. Miao; V. A. Feher; J. A. McCammon. Gaussian Accelerated Molecular Dynamics: Unconstrained Enhanced Sampling and Free Energy Calculation. *J. Chem. Theory Comput.*, **2015**, *11*, 3584–3595.

[828] Y. Miao; W. Sinko; L. Pierce; D. Bucher; R. C. Walker; J. A. McCammon. Improved Reweighting of Accelerated Molecular Dynamics Simulations for Free Energy Calculation. *J. Chem. Theory Comput.*, **2014**, *10*, 2677–2689.

[829] C. Bergonzo; T. E. C. III. Improved force field parameters lead to a better description of rna structure. *J. of Chem. Theory Comput.*, **2015**, *11*, 3969–3972.

[830] K. Gao; J. Yin; N. M. Henriksen; A. T. Fenley; M. K. Gilson. Binding enthalpy calculations for a neutral host-guest pair yield widely divergent salt effects across water models. *J. of Chem. Theory Comput.*, **2015**, *11*, 4555–4564.

[831] S. Izadi; B. Aguilar; A. V. Onufriev. Protein-ligand electrostatic binding free energies from explicit and implicit solvation. *J. Chem. Theory Comput.*, **2015**, *11*, 4450–4459.

[832] C. Torrence; G. P. Compo. A practical guide to wavelet analysis. *Bull. Am. Meteorol. Soc.*, **1998**, *79*, 61–78.

[833] N. C. Benson; V. Dagget. Wavelet analysis of protein motion. *Int. J. Wavelets Multi.*, **2012**, *10*.

[834] A. Rodriguez; A. Laio. Clustering by fast search and find of density peaks. *Science*, **2014**, *344*, 1492–1496.

[835] D. R. Roe; C. Bergonzo; T. E. C. III. Evaluation of enhanced sampling provided by accelerated molecular dynamics with hamiltonian replica exchange methods. *J. Phys. Chem. B*, **2014**, *118*, 3543–3552.

[836] M. A. E. Hassan; C. R. Calladine. Two distinct modes of protein-induced bending in dna. *J. Mol. Biol.*, **1998**, *282*, 331–343.

[837] V. Babin; C. Roland; T. A. Darden; C. Sagui. The free energy landscape of small peptides as obtained from metadynamics with umbrella sampling corrections. *J. Chem. Phys.*, **2006**, *125*, 2049096.

[838] V. Babin; V. Karpusenka; M. Moradi; C. Roland; C. Sagui. Adaptively biased molecular dynamics: an umbrella sampling method with a time dependent potential. *Inter. J. Quantum Chem.*, **2009**, *109*, 3666–3678.

[839] M. Moradi; V. Babin; C. Roland; T. Darden; C. Sagui. Conformations and free energy landscapes of polyproline peptides. *Proc. Natl. Aca. Sci. USA*, **2009**, *106*, 20746.

[840] M. Moradi; V. Babin; C. Roland; C. Sagui. A classical molecular dynamics investigation of the free energy and structure of short polyproline conformers. *J. Chem. Phys.*, **2010**, *133*, 125104.

[841] M. Moradi; J.-G. Lee; V. Babin; C. Roland; C. Sagui. Free energy and structure of polyproline peptides: an ab initio and classical molecular dynamics investigation. *Int. J. Quantum Chem.*, **2010**, *110*, 2865–2879.

[842] V. Babin; C. Roland; C. Sagui. The alpha-sheet: A missing-in-action secondary structure? *Proteins –Structure Function and Bioinformatics*, **2011**, *79*, 937–946.

[843] M. Moradi; V. Babin; C. Sagui; C. Roland. A statistical analysis of the PPII propensity of amino acid guests in proline-rich peptides. *Biophysical J.*, **2011**, *100*, 1083 – 1093.

[844] M. Moradi; V. Babin; C. Sagui; C. Roland. PPII propensity of multiple-guest amino acids in a proline-rich environment. *J. Phys. Chem. B.*, **2011**, *115*, 8645–8656.

[845] M. Moradi; C. Sagui; C. Roland. Calculating relative transition rates with driven nonequilibrium simulations. *Chem. Phys. Lett.*, **2011**, *518*, 109.

[846] M. Moradi; V. Babin; C. Roland; C. Sagui. Are long-range structural correlations behind the aggregation phenomena of polyglutamine diseases? *PLoS Comput. Biol.*, **2012**, *8*, e1002501.

[847] M. Moradi; V. Babin; C. Roland; C. Sagui. Reaction path ensemble of the B-Z-DNA transition: a comprehensive atomistic study. *Nucleic Acids Research*, **2013**, *41*, 33–43.

[848] M. Moradi; V. Babin; C. Sagui; C. Roland. in *Proline: Biosynthesis, Regulation and Health Benefits*, B. Nedjimi, Ed., pp 67–110. Nova Publishers, 2013.

[849] M. Moradi; E. Tajkorshid. Driven Metadynamics: Reconstructing equilibrium free energies from driven adaptive-bias simulations. *J. Phys. Chem. Lett.*, **2013**, *4*, 1882.

[850] M. Moradi; C. Sagui; C. Roland. Investigating rare events with nonequilibrium work measurements: I. Nonequilibrium transition paths. *J. Chem. Phys.*, **2014**, *140*, 034114.

[851] M. Moradi; C. Sagui; C. Roland. Investigating rare events with nonequilibrium work measurements: II. Transition and reaction rates. *J. Chem. Phys.*, **2014**, *140*, 034115.

[852] A. C. Pan; D. Sezer; B. Roux. Finding transition pathways using the string method with swarms of trajectories. *J. Phys. Chem. B*, **2008**, *112*, 3432–3440.

[853] A. Barducci and G. Bussi and M. Parrinello. Well-tempered metadynamics: a smoothly converging and tunable free energy method. *Phys. Rev. Lett.*, **2008**, *100*, 020603.

[854] K. Minoukadeh and Ch. Chipot and T. Lelievre. Potential of Mean Force Calculations: A multiple-walker adaptive biasing force technique. *J. Chem. Theor. and Comput.*, **2010**, *6*, 1008.

[855] K. T. Debiec; D. S. Cerutti; L. R. Baker; A. M. Gronenborn; D. A. Case; L. T. Chong. Further along the Road Less Traveled: AMBER ff15ipq, an Original Protein Force Field Built on a Self-Consistent Physical Model. *J. Chem. Theory Comput.*, **2016**, *12*, 3926–3947.

[856] A. T. Bogetti; H. E. Piston; J. M. G. Leung; C. C. Cabalteja; D. T. Yang; A. J. Degrave; K. T. Debiec; D. S. Cerutti; W. S. Case, D. A. Horne; L. T. Chong. A twist in the road less traveled: The AMBER ff15ipq-m force field for protein mimetics. *J. Chem. Phys.*, **2020**, *153*, 064101.

[857] D. T. Yang; A. M. Gronenborn; L. T. Chong. Development and Validation of Fluorinated, Aromatic Amino Acid Parameters for Use with the AMBER ff15ipq Protein Force Field. *J. Phys. Chem. A*, **2022**, *126*, 2286–2297.

[858] R. Galindo-Murillo; J. C. Robertson; M. Zgarbovic; J. Sponer; M. Otyepka; P. Jureska; T. E. Cheatham. Assessing the Current State of Amber Force Field Modifications for DNA. *J. Chem. Theory Comput.*, **2016**, *12*, 4114–4127.

[859] S. Izadi; A. V. Onufriev. Accuracy limit of rigid 3-point water models. *J. Chem. Phys.*, **2016**, *145*, 074501.

[860] A. H. Aytenfisu; A. Spasic; A. Grossfield; H. A. Stern; D. H. Mathews. Revised RNA Dihedral Parameters for the Amber Force Field Improve RNA Molecular Dynamics. *J. Chem. Theory Comput.*, **2017**, *13*, 900–915.

[861] L. Maragliano; A. Fischer; E. Vanden-Eijnden; G. Ciccotti. String method in collective variables: Minimum free energy paths and isocommittor surfaces. *J. Chem. Phys.*, **2006**, *125*, 024106.

[862] T. Luchko; N. Blinov; G. C. Linon; K. P. Joyce; A. Kovalenko. SAMPL5: 3D-RISM partition coefficient calculations with partial molar volume corrections and solute conformational sampling. *J. Comput. Aided Mol. Design*, **2016**, *30*, 1115–1127.

[863] Z. Heidari; D. R. Roe; R. Galindo-Murillo; J. B. Ghasemi; T. E. Cheatham, III. Using Wavelet Analysis To Assist in Identification of Significant Events in Molecular Dynamics Simulations. *J. Chem. Inf. Model.*, **2016**, *56*, 1282–1291.

[864] G. Cui; J. M. Swails; E. S. Manas. SPAM: A Simple Approach for Profiling Bound Water Molecules. *J. Chem. Theory Comput.*, **2013**, *9*, 5539–5549.

[865] L. Wang; K. A. McKiernan; J. Gomes; K. A. Beauchamp; T. Head-Gordon; J. E. Rice; W. C. Swope; T. J. MartÃnez; V. S. Pande. Building a More Predictive Protein Force Field: A Systematic and Reproducible Route to AMBER-FB15. *J. Phys. Chem. B*, **2017**, *121*, 4023–4039.

[866] N. Forouzesh; S. Izadi; A. V. Onufriev. Grid-Based Surface Generalized Born Model for Calculation of Electrostatic Binding Free Energies. *J. Chem. Inf. Model.*, **2017**, *57*, 2505–2513.

[867] D. S. Cerutti; K. T. Debiec; D. A. Case; L. T. Chong. Links between the charge model and bonded parameter force constants in biomolecular force fields. *J. Chem. Phys.*, **2017**, *147*, 161730.

[868] V. W. D. Cruzeiro; M. S. Amaral; A. E. Roitberg. Redox Potential Replica Exchange Molecular Dynamics at constant pH in AMBER: Implementation, Validation and Application. *J. Chem. Phys.*, **2018**, *149*, 072338.

[869] V. W. D. Cruzeiro; A. E. Roitberg. Multidimensional Replica Exchange Simulations for Efficient Constant pH and Redox Potential Molecular Dynamics. *J. Chem. Theory Comput.*, **2019**.

[870] J. Khandogin; C. L. Brooks, III. Constant pH molecular dynamics with proton tautomerism. *Biophys. J.*, **2005**, *89*, 141–157.

[871] J. Khandogin; C. L. Brooks, III. Toward the accurate first-principles prediction of ionization equilibria in proteins. *Biochemistry*, **2006**, *45*, 9363–9373.

[872] J. A. Wallace; J. K. Shen. Continuous constant pH molecular dynamics in explicit solvent with pH-based replica exchange. *J. Chem. Theory Comput.*, **2011**, *7*, 2617–2629.

[873] J. A. Wallace; J. K. Shen. Charge-leveling and proper treatment of long-range electrostatics in all-atom molecular dynamics at constant pH. *J. Chem. Phys.*, **2012**, *137*, 184105.

[874] W. Chen; J. A. Wallace; Z. Yue; J. K. Shen. Introducing titratable water to all-atom molecular dynamics at constant pH. *Biophys. J.*, **2013**, *105*, L15–L17.

[875] Y. Huang; W. Chen; J. A. Wallace; J. Shen. All-Atom continuous constant pH molecular dynamics with particle mesh Ewald and titratable water. *J. Chem. Theory Comput.*, **2016**, *12*, 5411–5421.

[876] Y. Huang; R. C. Harris; J. Shen. Generalized Born based continuous constant pH molecular dynamics in Amber: implementation, benchmarking, and analysis. *J. Chem. Inform. Model.*, **2018**, *58*, 1372–1383.

[877] R. C. Harris; J. Shen. GPU-Accelerated Implementation of Continuous Constant pH Molecular Dynamics in Amber: pKa Predictions with Single-pH Simulations. *J. Chem. Inform. Model.*, **2019**, *59*, 4821–4832.

[878] O. N. Starovoytov; H. Torabifard; G. A. Cisneros. Development of amoeba force field for 1,3-dimethylimidazolium based ionic liquids. *J. Phys. Chem. B*, **2014**, *118*, 7156–7166.

[879] Y.-J. Tu; Z. Lin; M. J. Allen; G. A. Cisneros. Molecular dynamics investigation of water-exchange reactions on lanthanide ions in water/1-ethyl-3-methylimidazolium trifluoromethylsufate ([emim][otf]). *J. Chem. Phys.*, **2018**, *148*, 024503.

[880] Y.-J. Tu; M. J. Allen; G. A. Cisneros. Simulations of the water exchange dynamics of lanthanide ions in 1-ethyl-3-methylimidazolium ethyl sulfate ([emim][etso4]) and water. *Phys. Chem. Chem. Phys.*, **2016**, *18*, 30323–30333.

[881] H. Torabifard; O. N. Starovoytov; P. Ren; G. A. Cisneros. Development of an amoeba water model using gem distributed multipoles. *Theo. Chem. Acc.*, **2015**, *134*, 1–10.

[882] H. Torabifard; L. Reed; M. T. Berry; J. E. Hein; E. Menke; G. A. Cisneros. Computational and experimental characterization of a pyrrolidinium-based ionic liquid for electrolyte applications. *J. Chem. Phys.*, **2017**, *147*, 161731.

[883] G. A. Cisneros. Application of gaussian electrostatic model (gem) distributed multipoles in the amoeba force field. *J. Chem. Theo. Comput.*, **2012**, *12*, 5072–5080.

[884] G. A. Cisneros; J.-P. Piquemal; T. A. Darden. Generalization of the gaussian electrostatic model: extension to arbitrary angular momentum, distributed multipoles and computational speedup with reciprocal space methods. *J. Chem. Phys.*, **2006**, *125*, 184101.

[885] J.-P. Piquemal; G. A. Cisneros; P. Reinhardt; N. Gresh; T. A. Darden. Towards a force field based on density fitting. *J. Chem. Phys.*, **2006**, *124*, 104101.

[886] J.-P. Piquemal; G. Cisneros. in *Many-body effects and electrostatics in multi-scale computations of Biomolecules*, Q. Cui; P. Ren; M. Meuwly, Eds., pp 269–300. Pan Stanford Publishing, 2015.

[887] R. E. Duke; O. N. Starovoytov; J.-. Piquemal; G. A. Cisneros. Gem*: A molecular electronic density-based force field for molecular dynamics simulations. *J. Chem. Theo. Comput.*, **2014**, *10*, 1361–1365.

[888] Z. Zhang; X. Liu; K. Yan; M. Tuckerman; J. Liu. Unified efficient thermostat scheme for the canonical ensemble with holonomic or isokinetic constraints via molecular dynamics. *J. Phys. Chem. A*, **2019**, *123*, 6056–6079.

[889] Z. Zhang; K. Yan; X. Liu; J. Liu. A leap-frog algorithm-based efficient unified thermostat scheme for molecular dynamics. *Chinese Science Bulletin*, **2018**, *63*, 3467–3483.

[890] J. Liu; D. Li; X. Liu. A simple and accurate algorithm for path integral molecular dynamics with the Langevin thermostat. *J. Chem. Phys.*, **2016**, *145*, 024103.

[891] Z. Sun; P. Kalhor; Y. Xu; J. Liu. Extensive numerical tests of leapfrog integrator in middle thermostat scheme in molecular simulations. *Chinese Journal of Chemical Physics*, **2021**, *34*, 932–948.

[892] Z. Zhang; X. Liu; Z. Chen; H. Zheng; K. Yan; J. Liu. A unified thermostat scheme for efficient configurational sampling for classical/quantum canonical ensembles via molecular dynamics. *J. Chem. Phys.*, **2017**, *147*, 034109.

[893] D. Li; X. Han; Y. Chai; C. Wang; Z. Zhang; Z. Chen; J. Liu; J. Shao. Stationary state distribution and efficiency analysis of the Langevin equation via real or virtual dynamics. *J. Chem. Phys.*, **2017**, *147*, 184104.

[894] D. Li; Z. Chen; Z. Zhang; J. Liu. Understanding molecular dynamics with stochastic processes via real or virtual dynamics. *Chinese Journal of Chemical Physics*, **2017**, *30*, 735–760.

[895] B. Leimkuhler; C. Matthews. Rational construction of stochastic numerical methods for molecular sampling. *Appl. Math. Res. eXpress*, **2013**, *2013*, 34–56.

[896] J.-P. Ryckaert; G. Ciccotti; H. J. Berendsen. Numerical integration of the cartesian equations of motion of a system with constraints: molecular dynamics of n-alkanes. *J. of Computat. Phys.*, **1977**, *23*, 327 – 341.

[897] S. Myamoto; P. A. Kollman. Settle: An analytical version of the SHAKE and RATTLE algorithm for rigid water models. *J. Computat. Chem.*, **1992**, *13*, 952–962.

[898] H. C. Andersen. RATTLE: A "velocity" version of the shake algorithm for molecular dynamics calculations. *J. Computat. Phys.*, **1983**, *52*, 24 – 34.

[899] N. Gr"ønbech-Jensen; O. Farago. A simple and effective Verlet-type algorithm for simulating Langevin dynamics. *Mol. Phys.*, **2013**, *111*, 983–991.

[900] T. Nugent; D. T. Jones. Membrane protein orientation and refinement using a knowledge-based statistical potential. *BMC Bioinformatics*, **2013**, *14*, 276.

[901] S. Schott-Verdugo; H. Gohlke. PACKMOL-Memgen: A simple-to-use generalized workflow for membrane-protein/lipid-bilayer system building. *J. Chem. Inf. Model.*, **2019**, *59*, 2522–2528.

[902] L. Martínez; R. Andrade; E. G. Birgin; J. M. Martínez. PACKMOL: A package for building initial configurations for molecular dynamics simulations. *J. Comput. Chem.*, **2009**, *30*, 2157–2164.

[903] J. M. Martínez; L. Martínez. Packing optimization for automated generation of complex system's initial configurations for molecular dynamics and docking. *J. Computat. Chem.*, **2003**, *24*, 819–825.

[904] B. Ho. pdbremix. https://github.com/boscoh/pdbremix, 2018.

[905] X. Liu; J. Liu. Critical role of quantum dynamical effects in the Raman spectroscopy of liquid water. *Mol. Phys.*, **2018**, *116*, 755–779.

[906] H. C. Andersen. Molecular dynamics simulations at constant pressure and/or temperature. *J. Chem. Phys.*, **1980**, *72*, 2384–2393.

[907] F. Pan; V. H. Man; C. Roland; C. Sagui. Structure and Dynamics of DNA and RNA Double Helices of CAG and GAC Trinucleotide Repeats. *Biophys. J.*, **2017**, *113*, 19–36.

[908] F. Pan; Y. Zhang; V. H. Man; C. Roland; C. Sagui. E-motif formed by extrahelical cytosine bases in DNA homoduplexes of trinucleotide and hexanucleotide repeats. *Nucl. Acids Res.*, **2018**, *46*, 942–955.

[909] F. Pan; V. H. Man; C. Roland; C. Sagui. Structure and Dynamics of DNA and RNA Double Helices Obtained From the CCG and GGC Trinucleotide Repeats. *J. Phys. Chem. B*, **2018**, *122*, 4491–4512.

[910] P. Xu; F. Pan; C. Roland; C. Sagui; K. Weninger. Dynamics of strand slippage in DNA hairpins formed by CAG repeats: roles of sequence parity and trinucleotide interrupts. *Nucl. Acids Res.*, **2020**, *48*, 2232–2245.

[911] C.-E. Chang; W. Chen; M. K. Gilson. Evaluating the Accuracy of the Quasiharmonic Approximation. *J. Chem. Theory Computat*, **2005**, *1*, 1017–1028. PMID: 26641917.

[912] D. A. McQuarrie. *Statistical Thermodynamics*. Harper and Row, New York, 1973.

[913] S. Izadi; R. C. Harris; M. O. Fenley; A. V. Onufriev. Accuracy comparison of generalized born models in the calculation of electrostatic binding free energies. *J. Chem. Theory Computat.*, **2018**, *14*, 1656–1670.

[914] H. Nguyen; D. A. Case; A. S. Rose. Nglview–interactive molecular graphics for jupyter notebooks. *Bioinformatics*, **2017**, *34*, 1241–1242.

[915] D. R. Roe; T. E. Cheatham III. Parallelization of CPPTRAJ enables large scale analysis of molecular dynamics trajectory data. *J. Computat. Chem.*, **2018**, *39*, 2110–2117.

[916] H. A. Boateng; R. Krasny. Comparison of treecodes for computing electrostatic potentials in charged particle systems with disjoint targets and sources. *J. Computat. Chem.*, **2013**, *34*, 2159–2167.

[917] Z.-H. Duan; R. Krasny. An adaptive treecode for computing nonbonded potential energy in classical molecular systems. *J. Computat. Chem.*, **2001**, *22*, 184–195.

[918] P. Li; H. Johnston; R. Krasny. A Cartesian treecode for screened Coulomb interactions. *J. Computat. Phys.*, **2009**, *228*, 3858–3868.

[919] A. V. Onufriev; D. A. Case. Generalized Born implicit solvent models for biomolecules. *Annu. Rev. Biophys.*, **2019**, *48*, 275–296.

[920] D. S. Cerutti; D. A. Case. Molecular dynamics simulations of macromolecular crystals. *Wires Comput. Mol. Sci.*, **2018**, *8*, e1402.

[921] T. Graen; M. Hoefling; H. Grubmueller. Amber-dyes: Characterization of charge fluctuations and force field parameterization of fluorescent dyes for molecular dynamics simulations. *Journal of Chemical Theory and Computation*, **2014**, *10*, 5505–5512.

[922] B. Schepers; H. Gohlke. Amber-dyes in amber: Implementation of fluorophore and linker parameters into ambertools. *Journal of Chemical Physics*, **2020**, *152*.

[923] S. Kalinin; T. Peulen; S. Sindbert; P. J. Rothwell; S. Berger; T. Restle; R. S. Goody; H. Gohlke; C. A. Seidel. A toolkit and benchmark study for fret-restrained high-precision structural modeling. *Nature Methods*, **2012**, *9*, 1218–1225.

[924] M. Dimura; T. O. Peulen; C. A. Hanke; A. Prakash; H. Gohlke; C. A. Seidel. Quantitative fret studies and integrative modeling unravel the structure and dynamics of biomolecular systems. *Curr. Opin. Struct. Biol.*, **2016**, *40*, 163–185.

[925] M. Dimura; T. O. Peulen; H. Sanabria; D. Rodnin; K. Hemmen; C. A. Seidel; H. Gohlke. Automated and optimally fret-assisted structural modeling. **2019**.

[926] R. T. McGibbon; K. A. Beauchamp; M. P. Harrigan; C. Klein; J. M. Swails; C. X. Hernandez; C. R. Schwantes; L.-P. Wang; T. J. Lane; V. S. Pande. Mdtraj: A modern open library for the analysis of molecular dynamics trajectories. *Biophys. J.*, **2015**, *109*, 1528–1532.

[927] A. Patriksson; D. van der Spoel. A temperature predictor for parallel tempering simulations. *Phys. Chem. Chem. Phys.*, **2008**, *10*, 2073–2077.

[928] P. S. Shabane; S. Izadi; A. V. Onufriev. General purpose water model can improve atomistic simulations of intrinsically disordered proteins. *Journal of Chemical Theory and Computation*, **2019**, *15*, 2620–2634.

[929] D. Pantoja-Uceda; J. L. Neira; L. M. Contreras; C. A. Manton; D. R. Welch; B. Rizzuti. The isolated C-terminal nuclear localization sequence of the breast cancer metastasis suppressor 1 is disordered. *Arch. Biochem. Biophys.*, **2019**, *664*, 95 – 101.

[930] D. Dans; D. Gallego; A. Balaceanu; L. Darre; H. Gomez; M. Orozco. Modeling, simulations, and bioinformatics at the service of rna structure. *Chem*, **2019**, *5*, 51 – 73.

[931] P. Kuhrova; V. Mlynsky; M. Zgarbova; M. Krepl; G. Bussi; R. B. Best; M. Otyepka; J. Sponer; P. Banas. Improving the performance of the Amber RNA force field by tuning the hydrogen-bonding interactions. *bioRxiv*, **2019**.

[932] A. Bochicchio; M. Krepl; F. Yang; G. Varani; J. Sponer; P. Carloni. Molecular basis for the increased affinity of an RNA recognition motif with re-engineered specificity: A molecular dynamics and enhanced sampling simulations study. *PLOS Computat. Biol.*, **2018**, *14*, 1–27.

[933] N. M. Kumbhar; J. S. Gopal. Structural significance of hypermodified nucleoside 5-carboxymethylaminomethyluridine (cmnm5U) from wobble (34th) position of mitochondrial tRNAs: Molecular modeling and Markov state model studies. *J. Molec. Graph. Model.*, **2019**, *86*, 66 – 83.

[934] F. Leonarski; M. Jasinski; J. Trylska. Thermodynamics of the fourU RNA thermal switch derived from molecular dynamics simulations and spectroscopic techniques. *Biochimie*, **2019**, *156*, 22 – 32.

[935] M. Havrila; M. Otyepka; P. Stadlbauer; J. Sponer; J. L. Mergny; P. Banas; P. Kuhrova. Structural dynamics of propeller loop: towards folding of RNA G-quadruplex. *Nucl. Acids Res.*, **2018**, *46*, 8754–8771.

[936] C. Yang; M. Kulkarni; M. Lim; Y. Pak. Insilico direct folding of thrombin-binding aptamer G-quadruplex at all-atom level. *Nucl. Acids Res.*, **2017**, *45*, 12648–12656.

[937] M. Javanainen; A. Lamberg; L. Cwiklik; I. Vattulainen; O. H. S. Ollila. Atomistic model for nearly quantitative simulations of langmuir monolayers. *Langmuir*, **2018**, *34*, 2565–2572. PMID: 28945973.

[938] O. H. S. Ollila; H. A. Heikkinen; H. IwaÃ¯. Rotational dynamics of proteins from spin relaxation times and molecular dynamics simulations. *The Journal of Physical Chemistry B*, **2018**, *122*, 6559–6569. PMID: 29812937.

[939] M. Kulkarni; C. Yang; Y. Pak. Refined alkali metal ion parameters for the opc water model. *Bulletin of the Korean Chemical Society*, **2018**, *39*, 931–935.

[940] R. G. FernÃ¡ndez; J. L. F. Abascal; C. Vega. The melting point of ice Ih for common water models calculated from direct coexistence of the solid-liquid interface. *The Journal of Chemical Physics*, **2006**, *124*, 144506.

[941] G. M. Giambasu; M. K. Gebala; M. T. Panteva; T. Luchko; D. A. Case; D. M. York. Competitive Interaction of Monovalent Cations with DNA from 3D-RISM. *Nucleic Acids Res.*, **2015**, *43*, 8405–8415.

[942] G. M. Giambasu; D. A. Case; D. M. York. Predicting Site-Binding Modes of Ions and Water to Nucleic Acids Using Molecular Solvation Theory. *J. Am. Chem. Soc.*, **2019**, *141*, 2435–2445.

[943] C. Nguyen; T. Yamazaki; A. Kovalenko; D. A. Case; M. K. Gilson; T. Kurtzman; T. Luchko. A molecular reconstruction approach to site-based 3D-RISM and comparison to GIST hydration thermodynamic maps in an enzyme active site. *PLoS One*, **2019**, *14*, e0219743.

[944] G. Bussi; D. Donadio; M. Parrinello. Canonical sampling through velocity rescaling. *The Journal of chemical physics*, **2007**, *126*, 014101.

[945] M. R. Machado; E. E. Barrera; F. Klein; M. Sonora; S. Silva; S. Pantano. The SIRAH 2.0 Force Field: Altius, Fortius, Citius. *J. Chem. Theory Comput.*, **2019**, *15*, 2719–2733. PMID: 30810317.

[946] P. D. Dans; A. Zeida; M. R. Machado; S. Pantano. A coarse grained model for atomic-detailed dna simulations with explicit electrostatics. *J. Chem. Theory Comput.*, **2010**, *6*, 1711–1725. PMID: 26615701.

[947] E. E. Barrera; M. R. Machado; S. Pantano. Fat sirah: Coarse-grained phospholipids to explore membrane-protein dynamics. *J. Chem. Theory Comput.*, **2019**, *15*, 5674–5688. PMID: 31433946.

[948] P. G. Garay; E. E. Barrera; S. Pantano. Post-translational modifications at the coarse-grained level with the sirah force field. *J. Chem. Inform. Model.*, **2020**, *60*, 964–973. PMID: 31840995.

[949] F. Klein; D. Cáceres; M. A. Carrasco; J. C. Tapia; J. Caballero; J. Alzate-Morales; S. Pantano. Coarse-Grained Parameters for Divalent Cations within the SIRAH Force Field. *J. Chem. Inf. Model.*, **2020**, *60*, 3935–3943.

[950] L. Darré; M. R. Machado; P. D. Dans; F. E. Herrera; S. Pantano. Another coarse grain model for aqueous solvation: Wat four? *J. Chem. Theory Comput.*, **2010**, *6*, 3793–3807.

[951] M. R. Machado; S. Pantano. SIRAH tools: mapping, backmapping and visualization of coarse-grained models. *Bioinformatics*, **2016**, *32*, 1568–1570.

[952] A. Zeida; M. R. Machado; P. D. Dans; S. Pantano. Breathing, bubbling, and bending: DNA flexibility from multimicrosecond simulations. *Phys. Rev. E*, **2012**, *86*, 021903.

[953] M. R. Machado; H. C. González; S. Pantano. Md simulations of viruslike particles with supra cg solvation affordable to desktop computers. *J. Chem. Theory Comput.*, **2017**, *13*, 5106–5116. PMID: 28876928.

[954] H. C. Gonzalez; L. Darré; S. Pantano. Transferable mixing of atomistic and coarse-grained water models. *J. Phys. Chem. B*, **2013**, *117*, 14438–14448. PMID: 24219057.

[955] M. R. Machado; P. D. Dans; S. Pantano. A hybrid all-atom/coarse grain model for multiscale simulations of dna. *Phys. Chem. Chem. Phys.*, **2011**, *13*, 18134–18144.

[956] M. R. Machado; S. Pantano. Exploring LacI–DNA Dynamics by Multiscale Simulations Using the SIRAH Force Field. *J. Chem. Theory Comput.*, **2015**, *11*, 5012–5023. PMID: 26574286.

[957] M. R. Machado; A. Zeida; L. Darré; S. Pantano. From quantum to subcellular scales: multi-scale simulation approaches and the sirah force field. *Interface Focus*, **2019**, *9*.

[958] N. Moriarty; P. Janowski; J. Swails; H. Nguyen; J. Richardson; D. Case; P. Adams. Improved chemistry restraints for crystallographic refinement by integrating the Amber force field into Phenix. *Acta Cryst. D*, **2020**, *76*, 51–62.

[959] P. Afonine; A. Urzhumtsev. On a fast calculation of structure factors at a subatomic resolution. *Acta Cryst. A*, **2004**, *60*, 19–32.

[960] A. Fokine; A. Urzhumtsev. Flat bulk-solvent model: obtaining optimal parameters. *Acta Cryst. D*, **2002**, *58*, 1387–1392.

[961] P. Afonine; R. Grosse-Kunstleve; P. Adams; A. Urzhumtsev. Bulk-solvent and overall scaling revisited: faster calculations, improved results. *Acta Cryst. D*, **2013**, *69*, 625–634.

[962] J. Jiang; A. Brünger. Protein hydration observed by X-ray diffraction: solvation properties of penicillopepsin and neuraminidase crystal structures. *J. Mol. Biol.*, **1994**, *243*, 100–115.

[963] R. Grosse-Kunstleve; N. Sauter; N. Moriarty; P. Adams. The Computational Crystallography Toolbox: crystallographic algorithms in a reusable software framework. *J. Appl. Crystallogr.*, **2002**, *35*, 126–136.

[964] Y. Xue; N. Skrynnikov. Ensemble MD simulations restrained via crystallographic data: accurate structure leads to accurate dynamics. *Prot. Sci.*, **2014**, *23*, 488–507.

[965] A. Raval; S. Piana; M. Eastwood; R. Dror; D. Shaw. Refinement of protein structure homology models via long, all-atom molecular dynamics simulations. *Proteins*, **2012**, *80*, 2071–2079.

[966] V. Lunin; T. Skovoroda. R-free likelihood-based estimates of errors for phases calculated from atomic models. *Acta Cryst. A*, **1995**, *51*, 880–887.

[967] R. Read; A. McCoy. A log-likelihood-gain intensity target for crystallographic phasing that accounts for experimental error. *Acta Cryst. D*, **2016**, *72*, 375–387.

[968] S. Meisburger; D. Case; N. Ando. Correlated motions in a protein crystal. *Nature Commun.*, **2020**, *11*, 1271.

[969] S. Meisburger; N. Ando. Correlated Motions from Crystallography beyond Diffraction. *Acc. Chem. Res.*, **2017**, *50*, 580–583.

[970] S. Boresch; M. Karplus. The role of bonded terms in free energy simulations. 1. theoretical analysis. *J. Phys. Chem. A*, **1999**, *103*, 103–118.

[971] S. Boresch; M. Karplus. The role of bonded terms in free energy simulations. 2. calculation of their influence on free energy differences of solvation. *J. Phys. Chem. A*, **1999**, *103*, 119–136.

[972] S. Boresch. The role of bonded energy terms in free energy simulations - insights from analytical results. *Mol. Simul.*, **2002**, *28*, 13–37.

[973] T.-S. Lee; Y. Hu; B. Sherborne; Z. Guo; D. M. York. Toward fast and accurate binding affinity prediction with pmemdgti: An efficient implementation of GPU-accelerated thermodynamic integration. *J. Chem. Theory Comput.*, **2017**, *13*, 3077–3084.

[974] T.-S. Lee; D. S. Cerutti; D. Mermelstein; C. Lin; S. LeGrand; T. J. Giese; A. Roitberg; D. A. Case; R. C. Walker; D. M. York. Gpu-accelerated molecular dynamics and free energy methods in amber18: Performance enhancements and new features. *J. Chem. Inf. Model.*, **2018**, *58*, 2043–2050.

[975] L. F. Song; T.-S. Lee; C. Zhu; D. M. York; K. M. Merz Jr. Using AMBER18 for Relative Free Energy Calculations. *J. Chem. Inf. Model.*, **2019**, *59*, 3128–3135.

[976] T. J. Giese; D. M. York. A GPU-Accelerated Parameter Interpolation Thermodynamic Integration Free Energy Method. *J. Chem. Theory Comput.*, **2018**, *14*, 1564–1582.

[977] D. Tan; S. Piana; R. Dirks; D. Shaw. RNA force field with accuracy comparable to state-of- the-art protein force fields. *Proc. Natl. Acad. Sci. USA*, **2018**, *115*, E1346–E1355.

[978] C. Tian; K. Kasavajhala; K. Belfon; L. Raguette; H. Huang; A. Migues; J. Bickel; Y. Wang; J. Pincay; Q. Wu; C. Simmerling. ff19SB: Amino-Acid-Specific Protein Backbone Parameters Trained against Quantum Mechanics Energy Surfaces in Solution. *J. Chem. Theory Comput.*, **2020**, *16*, 528–552.

[979] L. Raguette; A. Cuomo; K. Belfon; C. Tian; Q. Wu; C. Simmerling. Updated Amber force field parameters for phosphorylated amino acids for ff14SB and ff19SB. *In Prep*, **2020**.

[980] K. Belfon; C. Tian; J. Maier; L. Raguette; Q. Wu; C. Simmerling. RAGTAG: Rapid Amber Gpu Torsion pArameter Generator. . *In Prep*, **2020**.

[981] K. Belfon; L. Raguette; Q. Wu; C. Simmerling. Application of RAGTAG: modified amino acids for comparing MD simulations with FRET/EPR experiments. *In Prep*, **2020**.

[982] H. Huang; C. Simmerling. Fast Pairwise Approximation of Solvent Accessible Surface Area for Implicit Solvent Simulations of Proteins on CPUs and GPUs. *J. Chem. Theory Comput.*, **2018**, *14*, 5797–5814.

[983] Y. Miao; A. Bhattarai; J. Wang. Ligand Gaussian accelerated molecular dynamics (LiGaMD): Characterization of ligand binding thermodynamics and kinetics. *J. Chem. Theory Comput.*, **2020**, *16*, 5526–5547.

[984] J. Wang; Y. Miao. Peptide Gaussian accelerated molecular dynamics (Pep-GaMD): Enhanced sampling and free energy and kinetics calculations of peptide binding. *J. Chem. Phys.*, **2020**, *153*, 154109.

[985] J. Wang; Y. Miao. Protein-Protein Interaction-Gaussian Accelerated Molecular Dynamics (PPI-GaMD): Characterization of Protein Binding Thermodynamics and Kinetics. *J. Chem. Theory Comput.*, **2022**, *18*, 1275–1285.

[986] A. V. Onufriev; S. Izadi. Water models for biomolecular simulations. *WIREs Computational Molecular Science*, **2018**, *8*, e1347.

[987] V. N. Uversky; C. J. Oldfield; A. K. Dunker. Intrinsically disordered proteins in human diseases: Introducing the d2 concept. *Annual Review of Biophysics*, **2008**, *37*, 215–246.

[988] S. Piana; A. G. Donchev; P. Robustelli; D. E. Shaw. Water dispersion interactions strongly influence simulated structural properties of disordered protein states. *The Journal of Physical Chemistry B*, **2015**, *119*, 5113–5123.

[989] V. T. Duong; Z. Chen; M. T. Thapa; R. Luo. Computational studies of intrinsically disordered proteins. *The Journal of Physical Chemistry B*, **2018**, *122*, 10455–10469.

[990] D. Song; W. Wang; W. Ye; D. Ji; R. Luo; H.-F. Chen. ff14idps force field improving the conformation sampling of intrinsically disordered proteins. *Chemical Biology & Drug Design*, **2017**, *89*, 5–15.

[991] W. Ye; D. Ji; W. Wang; R. Luo; H.-F. Chen. Test and evaluation of ff99idps force field for intrinsically disordered proteins. *Journal of Chemical Information and Modeling*, **2015**, *55*, 1021–1029.

[992] J. Huang; S. Rauscher; G. Nawrocki; T. Ran; M. Feig; B. L. de Groot; H. Grubmuller; A. D. MacKerell Jr. Charmm36m: an improved force field for folded and intrinsically disordered proteins. *Nat Meth*, **2017**, *14*, 71–73.

[993] F. Meng; M. M. Bellaiche; J.-Y. Kim; G. H. Zerze; R. B. Best; H. S. Chung. Highly disordered amyloid-$\beta$ monomer probes by single-molecule fret and md simulation. *Biophysical Journal*, **2018**, *114*, 870–884.

[994] E. Wang; H. Sun; J. Wang; Z. Wang; H. Liu; J. Zhang; T. Hou. End-Point Binding Free Energy Calculation with MM/PBSA and MM/GBSA: Strategies and Applications in Drug Design. *Chem. Rev.*, **2019**, *119*, 9478–9508.

[995] E. W. Weisstein. Euler angles From MathWorld—A Wolfram Web Resource.

[996] D. C. Rapaport. *The Art of Molecular Dynamics Simulation*. Cambridge University Press, 2010.

[997] D. K. Coutsias EA, Seok C. Using quaternions to calculate rmsd. *J Comput Chem*, **2004 Nov 30**, *25*, 1849–57.

[998] G. Fiorin; M. L. Klein; J. Hénin. Using collective variables to drive molecular dynamics simulations. *Molecular Physics*, **2013**, *111*, 3345–3362.

[999] M. Moradi; E. Tajkhorshid. Mechanistic picture for conformational transition of a membrane transporter at atomic resolution. *Proc. Natl. Acad. Sci. U.S.A.*, **2013**, *110*, 18916–18921.

[1000] M. Moradi; E. Tajkhorshid. Computational Recipe for Efficient Description of Large-Scale Conformational Changes in Biomolecular Systems. *J Chem Theory Comput*, **2014**, *10*, 2866–2880.

[1001] M. Machado; S. Pantano. Split the Charge Difference in Two! A Rule of Thumb for Adding Proper Amounts of Ions in MD Simulations. *J. Chem. Theory Comput.*, **2020**, *16*, 1367–1372.

[1002] J. Schmit; N. Kariyawasam; V. Needham; P. Smith. SLTCAP: A Simple Method for Calculating the Number of Ions Needed for MD Simulation. *J. Chem. Theory Comput.*, **2018**, *14*, 1823–1827.

[1003] C. Gebhardt; M. Lehmann; M. M. Reif; M. Zacharias; T. Cordes. Molecular and spectroscopic characterization of green and red cyanine fluorophores from the alexa fluor and af series. *bioRxiv*, **2020**.

[1004] M. E. O'Neill. PCG: A Family of Simple Fast Space-Efficient Statistically Good Algorithms for Random Number Generation. Technical Report HMC-CS-2014-0905, Harvey Mudd College, Claremont, CA, 2014.

[1005] S. Vigna. Further scramblings of Marsaglia's xorshift generators. *J. Comput. Appl. Math.*, **2017**, *315*, 175–181.

[1006] D. R. Roe; B. R. Brooks. A protocol for preparing explicitly solvated systems for stable molecular dynamics simulations. *J. Chem. Phys.*, **2020**, *153*, 054123.

[1007] D. R. Roe; B. R. Brooks. Improving the Speed of Volumetric Density Map Generation via Cubic Spline Interpolation. *J. Mol. Graphics Model.*, **2021**, *104*, 107832.

[1008] V. W. D. Cruzeiro; G. T. Feliciano; A. E. Roitberg. Exploring Coupled Redox and pH Processes with a Force-Field-Based Approach: Applications to Five Different Systems. *J. Am. Chem. Soc.*, **2020**, *142*, 3823–3835.

[1009] V. W. D. Cruzeiro; M. Manathunga; J. Merz, Kenneth M.; A. W. Götz. Open-Source Multi-GPU-Accelerated QM/MM Simulations with AMBER and QUICK. *ChemRxiv*, **2021**. https://doi.org/10.26434/chemrxiv.13984028.v1.

[1010] M. Manathunga; C. Jin; V. W. D. Cruzeiro; J. Smith; K. Keipert; D. Pekurovsky; D. Mu; Y. Miao; X. He; K. Ayers; E. Brothers; A. W. Goetz; K. M. Merz. QUICK, version 21.03. University of California San Diego, CA and Michigan State University, East Lansing, MI. 2021.

[1011] Y. Miao; K. M. Merz. Acceleration of Electron Repulsion Integral Evaluation on Graphics Processing Units via Use of Recurrence Relations. *J. Chem. Theory Comput.*, **2013**, *9*, 965–976.

[1012] Y. Miao; K. M. Merz. Acceleration of High Angular Momentum Electron Repulsion Integrals and Integral Derivatives on Graphics Processing Units. *J. Chem. Theory Comput.*, **2015**, *11*, 1449–1462.

[1013] M. Manathunga; Y. Miao; D. Mu; A. W. Götz; K. M. Merz. Parallel Implementation of Density Functional Theory Methods in the Quantum Interaction Computational Kernel Program. *J. Chem. Theory Comput.*, **2020**, *16*, 4315–4326.

[1014] M. Manathunga; C. Jin; V. W. D. Cruzeiro; Y. Miao; D. Mu; K. Arumugam; K. Keipert; H. M. Aktulga; J. Merz, Kenneth M.; A. W. Götz. Harnessing the Power of Multi-GPU Acceleration into the Quantum Interaction Computational Kernel Program. *ChemRxiv*, **2021**. https://doi.org/10.26434/chemrxiv.13769209.v1.

[1015] H. M. Aktulga; J. C. Fogarty; S. A. Pandit; A. Y. Grama. Parallel reactive molecular dynamics: Numerical methods and algorithmic techniques. *Parallel Computing*, **2012**, *38*, 245–259.

[1016] S. B. Kylasa; H. M. Aktulga; A. Y. Grama. Puremd-gpu: A reactive molecular dynamics simulation package for gpus. *J. Comput. Phys.*, **2014**, *272*, 343–359.

[1017] A. C. Van Duin; S. Dasgupta; F. Lorant; W. A. Goddard. Reaxff: a reactive force field for hydrocarbons. *J. Phys. Chem. A*, **2001**, *105*, 9396–9409.

[1018] A. K. Rappe; W. A. Goddard III. Charge equilibration for molecular dynamics simulations. *J. Phys. Chem.*, **1991**, *95*, 3358–3363.

[1019] W. J. Mortier; S. K. Ghosh; S. Shankar. Electronegativity-equalization method for the calculation of atomic charges in molecules. *J. Am. Chem. Soc.*, **1986**, *108*, 4315–4320.

[1020] M. Samieegohar; F. Sha; A. Z. Clayborne; T. Wei. Reaxff md simulations of peptide-grafted gold nanoparticles. *Langmuir*, **2019**, *35*, 5029–5036.

[1021] S. Yang; T. Zhao; L. Zou; X. Wang; Y. Zhang. Reaxff-based molecular dynamics simulation of dna molecules destruction in cancer cells by plasma ros. *Phys. Plasmas*, **2019**, *26*, 083504.

[1022] P. O. Hubin; D. Jacquemin; L. Leherte; D. P. Vercauteren. Parameterization of the reaxff reactive force field for a proline-catalyzed aldol reaction. *J. Comput. Chem.*, **2016**, *37*, 2564–2572.

[1023] S. Monti; J. Jose; A. Sahajan; N. Kalarikkal; S. Thomas. Structure and dynamics of gold nanoparticles decorated with chitosan–gentamicin conjugates: Reaxff molecular dynamics simulations to disclose drug delivery. *Phys. Chem. Chem. Phys.*, **2019**, *21*, 13099–13108.

[1024] T. Trnka; I. Tvaroska; J. Koca. Automated training of reaxff reactive force fields for energetics of enzymatic reactions. *J. Chem. Theory Comput.*, **2018**, *14*, 291–302.

[1025] A. Rahnamoun; A. Van Duin. Reactive molecular dynamics simulation on the disintegration of kapton, poss polyimide, amorphous silica, and teflon during atomic oxygen impact using the reaxff reactive force-field method. *J. Phys. Chem. A*, **2014**, *118*, 2780–2787.

[1026] D. Raymand; A. C. van Duin; M. Baudin; K. Hermansson. A reactive force field (reaxff) for zinc oxide. *Surf. Sci.*, **2008**, *602*, 1020–1031.

[1027] K. Chenoweth; S. Cheung; A. C. Van Duin; W. A. Goddard; E. M. Kober. Simulations on the thermal decomposition of a poly (dimethylsiloxane) polymer using the reaxff reactive force field. *J. Am. Chem. Soc.*, **2005**, *127*, 7192–7202.

[1028] M. F. Russo Jr; R. Li; M. Mench; A. C. Van Duin. Molecular dynamic simulation of aluminum–water reactions using the reaxff reactive force field. *Int. J. Hydrog. Ener.*, **2011**, *36*, 5828–5835.

[1029] J. Ludwig; D. G. Vlachos; A. C. Van Duin; W. A. Goddard. Dynamics of the dissociation of hydrogen on stepped platinum surfaces using the reaxff reactive force field. *J. Phys. Chem. B*, **2006**, *110*, 4274–4282.

[1030] K. Yoon; A. Rahnamoun; J. L. Swett; V. Iberi; D. A. Cullen; I. V. Vlassiouk; A. Belianinov; S. Jesse; X. Sang; O. S. Ovchinnikova et al. Atomistic-scale simulations of defect formation in graphene under noble gas ion irradiation. *ACS nano*, **2016**, *10*, 8376–8384.

[1031] A. Rahnamoun; A. Van Duin. Study of thermal conductivity of ice clusters after impact deposition on the silica surfaces using the reaxff reactive force field. *Phys. Chem. Chem. Phys.*, **2016**, *18*, 1587–1594.

[1032] C. Zou; A. Van Duin. Investigation of complex iron surface catalytic chemistry using the reaxff reactive force field method. *Jom*, **2012**, *64*, 1426–1437.

[1033] Y. K. Shin; H. Kwak; A. V. Vasenkov; D. Sengupta; A. C. van Duin. Development of a ReaxFF reactive force field for Fe/Cr/O/S and application to oxidation of butane over a pyrite-covered Cr2O3 catalyst. *ACS Catalysis*, **2015**, *5*, 7226–7236.

[1034] T. P. Senftle; S. Hong; M. M. Islam; S. B. Kylasa; Y. Zheng; Y. K. Shin; C. Junkermeier; R. Engel-Herbert; M. J. Janik; H. M. Aktulga et al. The reaxff reactive force-field: development, applications and future directions. *npj Computational Materials*, **2016**, *2*, 1–14.

[1035] L. Chen; A. Cruz; D. R. Roe; A. C. Simmonett; L. Wickstrom; N. Deng; T. Kurtzman. Thermodynamic Decomposition of Solvation Free Energies with Particle Mesh Ewald and Long-Range Lennard-Jones Interactions in Grid Inhomogeneous Solvation Theory. *J. Chem. Theory Comput.*, **2021**, *17*, 2714–2724.

[1036] O. Mikhailovskii; Y. Xue; N. R. Skrynnikov. Modeling a unit cell: crystallographic refinement procedure using the biomolecular MD simulation platform Amber. *IUCrJ*, **2022**, *9*, 114–133.

[1037] P. V. Afonine; R. W. Grosse-Kunstleve; P. D. Adams. A robust bulk-solvent correction and anisotropic scaling procedure. *Acta Cryst. D*, **2005**, *61*, 850–855.

[1038] C. J. Dickson; R. C. Walker; I. R. Gould. Lipid21: Complex Lipid Membrane Simulations with AMBER. *J. Chem. Theory Comput.*, **2022**.

[1039] Y. Gomez; A. Natale; J. Lincoff; C. Wolgemuth; J. osenberg; M. Grabe. Taking the Monte-Carlo gamble: How not to buckle under the pressure! *J. Comput. Chem.*, **2022**, *43*, 431–434.

[1040] D. R. Roe; C. Bergonzo. PrepareForLeap: An Automated Tool for Fast PDB-to-Parameter Generation. *J. Comput. Chem.*, **2022**.

[1041] X. Wu; B. R. Brooks. Origin of pka shifts of internal lysine residues in snase studied via equal-molar vmms simulations in explicit water. *J. Phys. Chem. B*, **2017**, *121*, 3318–3330.

[1042] X. Wu; B. R. Brooks. Hydronium ions accompanying buried acidic residues lead to high apparent dielectric constants in the interior of proteins. *J. Phys. Chem. B*, **2018**, *122*, 6215–6223.

[1043] X. Wu; B. R. Brooks. The homogeneity condition: A simple way to derive isotropic periodic sum potentials for efficient calculation of long-range interactions in molecular simulation. *J. Chem. Phys.*, **2019**, *150*, 214109.

[1044] X. Wu; B. R. Brooks. A double exponential potential for van der waals interaction. *AIP Advances*, **2019**, *9*, 065304.

[1045] X. Wu; B. R. Brooks. Reformulation of the self-guided molecular simulation method. *J. Chem. Phys.*, **2020**, *153*, 094112.

[1046] V. Man; X. Wu; X. He; X.-Q. Xie; B. Brooks; J. Wang. Determination of van der waals parameters using a double exponential potential for divalent metal cations in tip3p solvent. *J. Chem. Theory Comput.*, **2021**, *17*, 1086–1097.

[1047] Y. Xiong; S. Izadi; A. Onufriev. A fast polarizable water model for atomistic simulations. *ChemRxiv*, **2022**.

[1048] J. A. Lemkul; J. Huang; B. Roux; A. D. MacKerell. An empirical polarizable force field based on the classical drude oscillator model: Development history and recent applications. *Chem. Rev.*, **2016**, *116*, 4983–5013. PMID: 26815602.

[1049] Y. Xiong; A. V. Onufriev. Exploring optimization strategies for improving explicit water models: Rigid n-point model and polarizable model based on Drude oscillator. *PLoS ONE*, **2019**, *14*.